R-06-28

Modelling in support of bedrock transport property assessment

Preliminary site description Laxemar subarea – version 1.2

James Crawford, Kemakta Konsult AB

June 2006

Svensk Kärnbränslehantering AB
Swedish Nuclear Fuel
and Waste Management Co
Box 5864
SE-102 40 Stockholm Sweden
Tel 08-459 84 00
+46 8 459 84 00
Fax 08-661 57 19
+46 8 661 57 19

ISSN 1402-3091
SKB Rapport R-06-28

Modelling in support of bedrock transport property assessment

Preliminary site description Laxemar subarea – version 1.2

James Crawford, Kemakta Konsult AB

June 2006

Keywords: Retardation model, Transport properties, Laxemar, Fracture mineralogy, Diffusivity, Porosity, Sorption, F-factor.

Abstract

This report contains a detailed account of work that has been carried out within the site descriptive modelling of the Laxemar subarea for prediction of the flow related transport properties of fractured rock in the immediate vicinity of a repository for high level waste. The modelling work is based upon a number of different, although complementary analyses to give appraisals of the transport resistance (the so-called "F-factor") from first principles and using site specific data from the Laxemar subarea. The aim of the work has been to make estimations of the F-factor, while maximising transparency and robustness. This has been achieved through using simplified models to establish an envelope of possible F-factor ranges while highlighting very clearly the similarities and differences between the various calculation approaches that have been used in the appraisal.

In addition to the modelling of flow-related transport properties, simulations have been made using a transport model that explicitly considers the impact of rock matrix microstructure and how parameterisation of the altered layers of rock adjacent to migration paths may be expected to influence solute transport. This work is intended to be a complement to the bedrock transport properties modelling that has been used as a basis for parameterisation of the retardation model within the Laxemar 1.2 site descriptive model /SKB 2006a, Byegård et al. 2006/. It has been found that alteration layers with reduced retention properties can potentially give shorter solute residence times than if the alteration layers have enhanced retention properties relative to the unaltered rock matrix. Moreover, the simulation results have also indicated coupling effects arising from the incorporation of the retardation model with flow aspects that have not been previously described in the context of solute transport from the repository.

The main goal of the transport simulations, however, has been to identify the consequences of rock matrix parameterisation for solute transport with the aim of making recommendations for areas of focus within the continued site investigation. Owing to that the material properties variability within a given rock type appears to be larger than the variability between rock types (and considering the inherent data uncertainty), a tentative conclusion is that a single rock material properties parameterisation can be considered a reasonable approximation for all rock types for both the Simpevarp and Laxemar subareas. It should be emphasised, however, that this conclusion is provisional and may need to be revised when more detailed material properties data are available.

Sammanfattning

Denna rapport innehåller en detaljerad beskrivning av arbetet som har gjorts inom platsmodelleringen för Laxemar 1.2 för uppskattningen av bergets flödesrelaterade transportegenskaperna i omgivningen runt ett eventuellt slutförvar för högaktivt kärnavfall. Modelleringsarbetet är baserat på ett antal olika, men kompletterande, beräkningsmetoder som har använts för att uppskatta transportmotståndet (den s k ”F-faktorn”) baserat på första ordningens principer och med platsspecifika data för Laxemar. Målet med arbetet har varit att erhålla transparanta och robusta uppskattningar på F-faktorn genom att använda förenklade modeller och en detaljerat skildring av likheter och skillnader mellan de olika modellerna som har använts i uppskattningen.

Som komplement till den flödesrelaterade modelleringen har simuleringar även utförts där man explicit tar hänsyn till bergmatrisens mikrostruktur och hur parameteriseringen av förändrade bergarter i anslutning till flödesvägar kan antas påverka ämnestransport. Arbetet har utförts som en kompletterande analys till modelleringsarbetet som har utförts i samband med framtagningen av modellen för bergets transportegenskaper inom Laxemar 1.2 /SKB 2006a, Byegård et al. 2006/. Skikt av förändrat bergmaterial med förminskade retentionsegenskaper vid sprickytor ger upphov till kortare transporttider jämfört med system där det förändrade berget har en förhöjd retention relativt den oförändrade bergsmatrisen. Simuleringsresultaten har även påvisat effekter vilka uppstår genom kopplingen av retentionsmodellen med flödesmodellen och som inte tidigare har beskrivits i detta sammanhang.

Huvudmålet med arbetet har varit att identifiera konsekvenserna av retentionsmodellens parameterisering för transportprocesser som har relevans för den fortsatta platsundersökningen. En preliminär slutsats är att det inte finns tillräckligt variation mellan de olika bergarterna för att motivera en separat parameterisering för varje bergart. Således behövs endast en parametrisering för transportmodelleringsändamål. Denna slutsats är dock preliminär och kan komma att ändras när mer detaljerade platsspecifika data finns tillgänglig.

Contents

1 Introduction

1.1 Background

The Swedish Nuclear Fuel and Waste Management Company (SKB) is conducting site investigations at two different locations in Sweden (the Simpevarp and Forsmark areas) for the purpose of siting a deep geological repository for spent nuclear fuel. The investigations being conducted at Simpevarp encompass two subareas. These are the Simpevarp peninsula itself and Laxemar. The results from the investigations at the sites are used as a basic input to the site descriptive modelling.

A Site Descriptive Model (SDM) is an integrated description of the site and its regional setting, covering the current state of the biosphere as well as ongoing natural processes of importance for long-term safety. The SDM shall summarise the current state of knowledge of the site as well as provide parameters and models to be used in further analyses within Safety Assessment (SA), Repository Design, and Environmental Impact Assessment. The present report is produced as part of the version 1.2 modelling of the Laxemar area (henceforth, L1.2).

In this document, material property aspects of the transport SDM are referred to as the *retention properties model* or simply the *retardation model*, while the synthesis of material property data with flow-related aspects is referred to as the *integrated transport properties model*. In this context, the terms *site modelling* and *transport properties modelling* refer to the methods and procedures used in developing these models for inclusion within the overall site description. The term *transport modelling* by itself, however, refers to the use of these models within the overall site description and for safety analysis.

The process of site descriptive modelling of transport properties is described by /Berglund and Selroos 2003/. Essentially, the description consists of three parts:

- Description of rock mass, fractures and deformation zones, including relevant processes and conditions affecting radionuclide transport; the description should express the understanding of the site and the evidence supporting the proposed model.
- Retardation model: Identification and description of “typical” rock, fracture, and deformation zone materials, including parameterisation.
- Integrated transport properties model: Synthesis of flow-related transport properties with material properties parameterisation of the 3D geological model and assessment of understanding, confidence and uncertainty.

The methods used within the transport programme produce primary data on the retardation parameters (i.e. the porosity, θ_m, the effective diffusivity, D_e, and the linear equilibrium sorption coefficient, K_d). These retardation parameters are evaluated, interpreted and presented in the form of a retardation model; the strategy for laboratory measurements, data evaluation and development of retardation models is described by /Widestrand et al. 2003/. In the three-dimensional modelling, the retardation model is used to parameterise the various geological “elements” in the site-descriptive geological model. These “elements” consist of the rock mass itself (described in terms of rock domains) containing varying proportions of different characteristic rock types, fracture types, and deformation zones. The integration of the material properties parameterisation with the flow-related properties provides a basis for flow-path averaging and scale-up of flow path retention properties.

The retardation model combines material properties data for the major rock types and their various alteration states with a description of various fracture sub-classes typical for the Laxemar site investigation area. This is intended to form a basis for the parameterisation of models used within Safety Assessment.

The major flow-related property of interest is the *flow-wetted surface to flow ratio*, which is also known as the *transport resistance* or simply, the *F-factor*. In certain situations the *water residence time* or *advective travel time*, t_w may also be important for the transport of poorly sorbing radionuclides and colloidal material. In this report, however, attention has concentrated on the F-factor and its relation to parameters and parameter groups comprising the retardation model.

1.2 Objectives and scope

This report provides a detailed account of modelling that has been performed in support of bedrock transport property assessment for the Laxemar 1.2 site descriptive model (SDM). The transport site descriptive model presented in Laxemar 1.2 incorporates both retardation parameters and flow-related transport properties. The integration of material property data and flow-related aspects of radionuclide transport was absent from the previous Simpevarp 1.2 model version.

In this report, scoping calculations using the bare minimum of necessary assumptions have been used in an attempt to bound the limits of the F-factor for solute transport. In addition, simulations have been made using a model for solute transport that explicitly considers a multilayer description of rock matrix retention properties. The site specific F-factor estimations in the present model version are obtained by "first-order" consideration of possible flow paths in the first 10–100 m surrounding a canister deposition location. It is assumed that the background network of flowing fractures and minor deformation zones (MDZ) as identified from borehole investigations and hydraulic, discrete fracture network (DFN) models are representative of the flowpaths likely to be encountered in this rock mass (Hydraulic Rock Domain, HRD). Local major and regional deformation zones are considered to comprise the Hydraulic Conductor Domain (HCD) and are taxonomically separated from MDZ. Local major and regional deformation zones outside the HRD are not currently considered to provide substantial transport resistance for the retardation of radionuclide migration.

The main objective of the report is to provide a complete description of methods and procedures used in obtaining estimates of the F-factor as well as providing a basis for a discussion of solute transport properties at the Laxemar site that includes uncertainties relating to the parameterisation of the retardation model. A detailed account of the retardation model and the acquisition of site specific transport data for Laxemar is given in the companion background report on Bedrock Transport Properties /Byegård et al. 2006/. This report summarises the data presented in the companion background report and analyses what these data mean in a transport perspective together with supporting data obtained from Hydrogeology.

1.3 State of knowledge in previous model versions

Laxemar 1.2 represents the first iteration of a site descriptive model for the Laxemar subarea. Although new, the Laxemar 1.2 model version has inherited many features from the previous model version for Simpevarp (i.e. Simpevarp 1.2 SDM) and related supporting

documents /SKB 2005a, Byegård et al. 2005/. The overall organisation and structure of the retardation model is essentially the same as that for Simpevarp 1.2, although altered to accommodate newly acquired site specific data for Laxemar.

The main uncertainty identified in both Simpevarp model versions 1.1 and 1.2 was the lack of site specific transport data. Site specific formation factors based upon laboratory resistivity measurements for all major rock-types (i.e. Ävrö granite, quartz monzodiorite, and fine-grained dioritoid) were available for inclusion in Simpevarp 1.2. Data for sorption of Cs and Sr, however, were imported from Äspö Hard Rock Laboratory (Äspö HRL) investigation data, based upon geochemical analogy between Äspö diorite and all major Simpevarp rock types.

In the absence of data for altered site specific materials, specifically in association with fractures, all altered rock types were previously assumed to have the same diffusive and sorptive properties as that of altered Äspö diorite. A limitation of the imported Äspö HRL data was that different procedural methods were used for the estimation of sorption coefficients (i.e. compared with the current experimental programme) and it was therefore necessary to use an extrapolation procedure to derive consistent K_d-values as described by /Byegård et al. 2005/. Owing to inconsistencies identified in the parameterisation of the previously established retention model within Simpevarp 1.2, no data was imported for the Laxemar 1.2 model version. Instead, a different extrapolation procedure was used, based upon assumed correlation of sorption properties with the measured surface area of mineral grains. The surface area was measured by way of the BET method using the sorption of gas molecules (typically N_2 or Ar) to a surface /Brunauer et al. 1938/. Although only semi-quantitative estimates can be made in this way, the concept is thought to be more representative of true sorption properties than the previous data import.

A decision was made early in the preparation of Simpevarp 1.2 to not integrate flow-related transport properties and material properties within the site descriptive model. This decision was based largely upon perceived difficulties in communicating the difference between the transport resistances and advective travel times obtained from large scale flow models used in the SDM to those obtained from high-resolution flow models including a repository layout developed by Safety Assessment. As a result of concerns raised during the review process of Simpevarp 1.2, the integration of these two different aspects of transport (i.e. flow-related properties and material properties) has been included in the Laxemar 1.2 SDM, although in a substantially modified form compared with that in Simpevarp 1.1 (i.e. not based on large scale hydrogeological simulations). It is noted here that this integration is only partially complete within the current site descriptive model and is meant to form a basis for further discussion and scrutiny within Safety Assessment.

1.4 Conceptual model with potential alternatives

1.4.1 Basic conceptual model

The conceptual model underlying the present descriptive model is based on a description of solute transport in discretely fractured rock. Specifically, the fractured medium is viewed as consisting of mobile zones and immobile zones. The mobile zones are regions within fractures and deformation zones where groundwater flow and advective transport take place. The immobile zones include the rock mass itself as well as stagnant regions within or immediately adjacent to fractures and deformation zones where solutes can be retained (i.e. removed temporarily or permanently from the mobile water) /Berglund and Selroos 2003/.

In the Safety Assessment framework that provides the basis for identification of retention parameters in the site descriptive models, retention is assumed to be caused by diffusion and equilibrium sorption. These processes are reversible and are here referred to as *retardation processes*. A schematic illustration of the mobile and immobile zones is depicted in Figure 1-1 below.

The conceptualisation outlined above implies that radionuclide transport takes place along flow paths consisting of connected "sub paths" in fractures and deformation zones of different sizes. The fractures and deformation zones reside in specific rock types comprising the various rock domains identified at the site (where the rock domains can contain one or more different rock types as described in Chapter 5 of the SDM and the Bedrock Transport Properties background report /Byegård et al. 2006/).

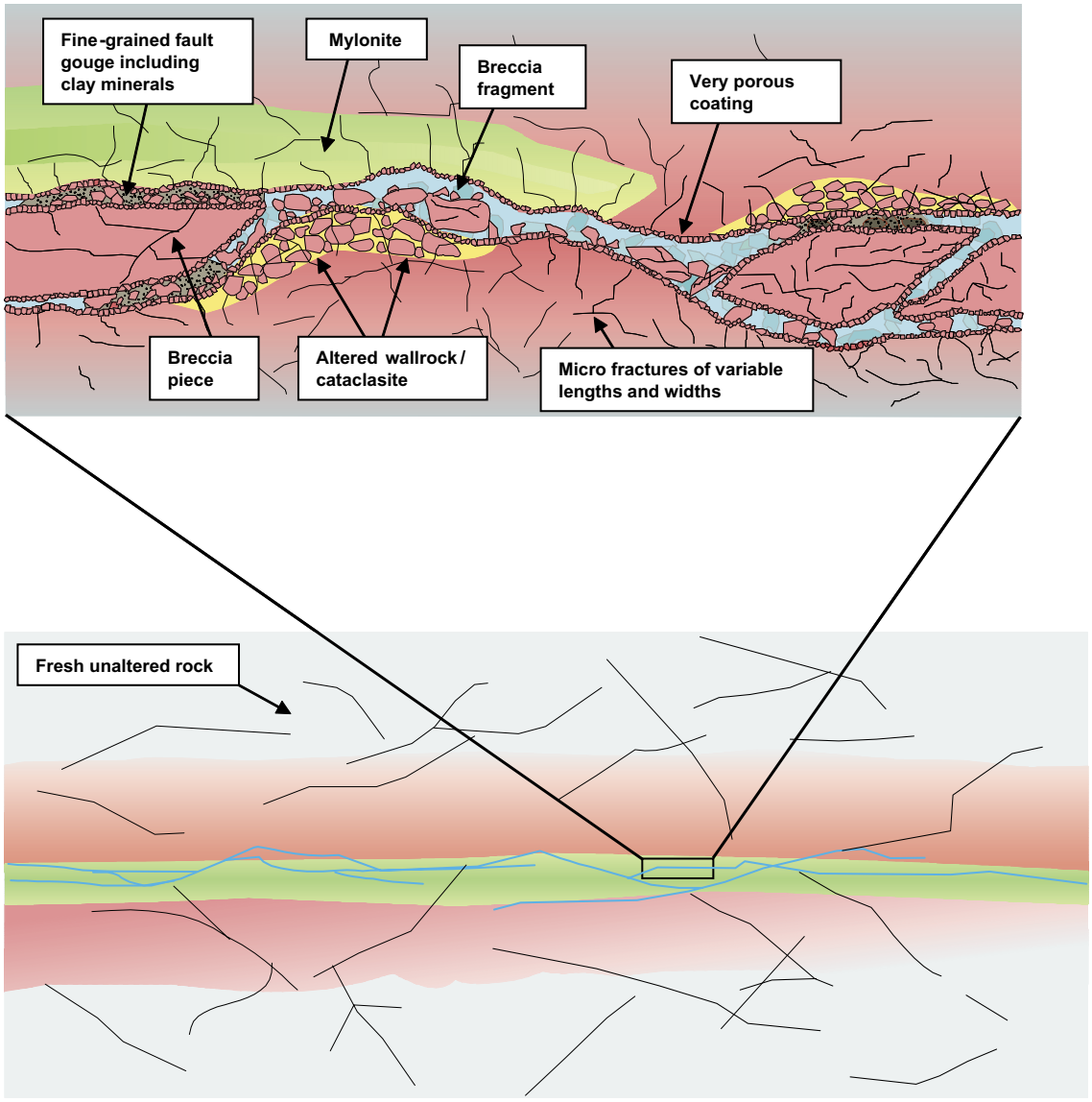

Figure 1-1. *Schematic illustration of mobile and immobile volumes in a fracture. Based on conceptual model taken from /Andersson et al. 2002a/.*

Four different, principal fracture types are currently considered within the retardation model. For the most part these differ only by type and depth of alteration, although provision is made in the conceptual model for inclusion of relations between material properties and transmissivity (or even fracture orientation) if these are subsequently shown to be relevant. For the modelling of radionuclide transport retardation, larger complex fractures and minor deformation zones constitute the link between single fractures and larger-scale zones.

Fractures are considered to have layers of hydrothermal and sometimes tectonic alteration that extend from the fracture surface to some distance within the host rock. Although no retardation model has been developed for local minor deformation zones in this model version, it is implicitly assumed that each zone is comprised of one or several types of altered wall rock. The conductive parts of the zones usually consist of multiple fractures and crush zones that can be classified as belonging to one or more of the four main fracture types mentioned above, or to a broader fault gouge classification. On the basis of this classification, four types of altered rocks have been selected for porosity, diffusion and batch-sorption measurements in the laboratory programme /Byegård et al. 2005/; these are fault gouge, chlorite, porous episyenetic wall rock, and cataclasite (with, or without mylonitic banding).

In the conceptual model, advection is the dominant process for moving the radionuclides in the transport direction, whereas the main role of diffusion is to remove the solutes from the mobile zone and transport them within the immobile zones.

It should be noted that this conceptual model, and the present methodology for site descriptive modelling in general, are to large extent based on previous experience from experiments at STRIPA /e.g. Birgersson et al. 1992/ as well as from the Äspö Hard Rock Laboratory (Äspö HRL). The conceptual model in its current form is derived primarily from the TRUE project /Winberg et al. 2000, Poteri et al. 2002/ carried out at the Äspö HRL, which may not necessarily be fully applicable to the transport conditions in the Simpevarp area including the Laxemar subarea. This means that the conceptual and methodological implications of the observations made during the site investigation must be considered. Presently, however, there are no indications that the established conceptual model is unrealistic or not applicable to the Laxemar subarea.

1.4.2 Alternative processes and process models

Alternative conceptual models could involve additional processes or more refined descriptions of the presently considered processes. Furthermore, different conceptualisations of the radionuclide transport paths could be considered. An example of this would be advective flow paths in accordance with the basic conceptual model described above in combination with, for instance, diffusive transport in the mobile zone. For radionuclide retention, consideration of more refined representations of sorption (process-based sorption models) and additional retention processes (e.g. precipitation and co-precipitation) are of particular interest. New modelling activities involving process-based sorption models were initiated during the Simpevarp 1.2 transport modelling and are ongoing. This modelling constitutes a first attempt at reactive-transport simulations in a single fracture, using data from the Äspö HRL /Dershowitz et al. 2003/.

The aims were to gain experience of this type of modelling in a transport context, and to investigate whether the process-based sorption models show qualitative differences or specific features that cannot be reproduced with K_d-based models. Although such differences and features can be observed in the preliminary results of the study, it remains

to be evaluated whether these effects occur under realistic conditions or are modelling artefacts. Hence, no conclusive results that could support, or provide alternatives to, the K_d-based model presented here are currently available. It is noted that models incorporating sophisticated process descriptions, with the aim of simulating more physically realistic conditions, should also be appropriate for the time scales considered.

1.5 A roadmap to this report

A general discussion related to the acquisition of data and material properties parameterisation is given in Chapter 2. This includes a summary of the data that is available for use in the Laxemar 1.2 SDM, a discussion of the recommended material properties data for the different rock types, and a comparison of data recommended for the Simpevarp and Laxemar sites as well as that used in the TRUE programme at the Äspö HRL. A detailed discussion concerning data uncertainty is also given in this chapter.

Chapter 3 contains a discussion of flow-related transport properties. Estimates of the F-factor are made based upon first order analyses and considering different assumptions related to flowpath channelling effects. The aim is to establish an envelope of reasonable F-factor ranges that can be considered possible for the Laxemar site under the given reference conditions. This chapter contains estimates of the F-factor and its distribution calculated using a channel network model (CNM), a stochastic multi channel model (MCM), and a porous medium approximation.

Chapter 4 contains generic modelling case studies that have been made to evaluate the impact of rock matrix alteration on transport processes in fractured rock. Owing to a lack of data for unequivocally establishing the relative retention properties of altered layers adjacent to flowpaths, a range of material property variability has been evaluated. The simulations consider transport processes along single flowpaths featuring rock matrix alteration, as well as the more general case where a range of flowpaths with differing F-factors are considered. Multi-path simulations are made for a benchmark case where F-factor distributions obtained from a typical CNM and MCM realisation are used.

Chapter 5 contains a discussion related to the synthesis of flow-related transport properties and material properties parameterisation to form an integrated transport properties model. Consequences of material properties uncertainty and different kinds of flow channelling are discussed in this section and some tentative recommendations are given for use of material properties data in Safety Assessment.

2 Description of input data

The development of the retardation model relies to a large extent on interaction with other disciplines; primarily Geology and Hydrogeochemistry. Specifically, Geology provides lithological and structural models where the rock types, fractures and deformation zones are described, as well as the mineralogical compositions of intact and altered materials. Hydrogeochemical information is used as a basis for the selection of water compositions in laboratory measurements of retardation parameters /Byegård et al. 2006/. Furthermore, hydrogeochemical data together with results from mineralogical and geochemical analyses of fracture materials are important inputs to the development of the retardation model and the description of the understanding of the retention processes at the site.

For the transport resistance, the main input is from Hydrogeology where measurement of the transmissivities of single flow-anomalies as well as hydraulic conductivities of larger rock volumes are central for the estimation of the water flowrate. In addition, data from Posiva Flow Log measurements (PFL-data) are necessary for the estimation of specific flow-wetted surface in the fractured rock. Although this parameter is only strictly needed for estimations of the F-factor in an equivalent porous medium, or stream-tube description of the system, it is still an important parameter for qualitative understanding of the site in terms of potential for solute interaction with the host rock. A high specific flow-wetted surface indicates a potential for significant advective flow through the rock volume, although at the same time the possibility of substantial solute retention owing to interaction of transported solutes with the exposed rock surfaces within flow channels in individual fractures.

Hydrogeology also provides a Hydro-DFN model for flow properties within the SDM which is used for calculations made within Safety Analysis /SKB 2006b (in prep.)/ that include estimates of the F-factor. This report, however, attempts to make more robust estimates of the F-factor with simplified approaches that preserve the essential physics of the system while giving greater transparency than sophisticated DFN modelling approaches.

2.1 Summary of available data

The input data reports used in the site specific modelling are detailed in the main report for the Laxemar 1.2 SDM (Chapter 2, Table 2-6) /SKB 2006a/.

The input data for the retardation model consist of laboratory and in situ measurements of material properties as well as supporting information from other disciplines. Many of the experiments are still in progress and thus the dataset available for use in the transport modelling is somewhat limited. The available site investigation data on transport properties at the data freeze for Laxemar 1.2 are summarised in /Börjesson and Gustavsson 2005/, /Thunehed 2005/, and /Löfgren and Neretnieks 2005/. This largely consists of numerical data from the water saturation porosity measurements, a small number of through-diffusion data, and formation factors obtained from laboratory as well as in situ electrical resistivity measurements.

Supporting descriptive data from the combined geological/hydrogeochemical interpretations of fracture mineralogy and wall rock alteration data are provided by /Drake and Tullborg, 2004, 2005, 2006ab/. Other geological, hydrogeological, and hydrogeochemical inputs were obtained from the SDM report, (i.e. from draft versions of the relevant chapters) and the hydrogeochemical modelling background reports from Simpevarp 1.2 /SKB 2004a/ and Laxemar 1.2 /Laaksoharju et al. 2006/.

No surface area or sorption data were available for the L1.2 data freeze, although a small number of preliminary data have been used as a basis for parameterisation of the retardation model. These parameters are based upon the data presented in the background report by /Byegård et al. 2006/. No PMMA porosity measurements are presented in this model version (Polymethylmethacrylate, PMMA impregnation is a method for studying the pore system, see /e.g. Hellmuth et al. 1993, 1994, Byegård et al. 1998/).

The input reports used for the development and parameterisation of the retardation model are not summarised here and the reader is directed to the appropriate background reports as described above. Data compiled in both the background report for Simpevarp 1.2 /Byegård et al. 2005/ as well as Laxemar 1.2 /Byegård et al. 2006/, however, have been used in this report for calculations and discussions related to the retardation model.

For estimations of flow-related transport properties (i.e. the F-factor), the main inputs have come from Hydrogeology. Hydrogeology provides input for the calculation of flow-related transport properties in two ways. Firstly, the data obtained from hydraulic tests carried out in boreholes can be used to characterise the transmissivity distribution of individual flowing features as well as the average hydraulic conductivity of the rock over larger borehole intervals. The methods used for obtaining these data are many and are discussed in Chapter 8 of the SDM /SKB 2006a/ and the associated background reports /e.g. Rhén et al. 2006ab, Rahm and Enachescu 2004a–f, 2005ab/.

Secondly, data obtained using the Posiva Flow Log (PFL) tool can be used to make estimates of conductive fracture frequencies (P_{10c}) down to a very fine resolution (decimetre scale) /Rouhiainen 2000, Ludvigson et al. 2002, Pollänen and Sokolnicki 2004, Rouhiainen et al. 2005, Rouhiainen and Sokolnicki 2005/. The conductive fracture frequency is necessary for the estimation of specific flow-wetted surface in the fractured rock. Both the distribution of fracture transmissivities and the conductive fracture frequency are fundamental requirements for the estimation of realistic, site-specific F-factors.

In addition to the data that is used directly for the estimation of transport resistance, hydrogeology also provides qualitative information that can be used to identify the existence or non-existence of trends or correlations between fractures and specific rock types and alteration fabrics. Such information may, in turn, provide a basis for identifying correlations between transport parameters and fracture types. This, however, is beyond the scope of this report and is discussed in more detail in the background report by /Byegård et al. 2006/.

2.2 Description of retardation model parameters

Only a brief account of the Laxemar 1.2 retardation model is given in the following sections. This consists primarily of summary tables detailing the recommended transport parameters for the major rock types and type fractures described in the main SDM report /SKB 2006a/. The details of the primary input data and the data evaluation procedure are described in the background report by /Byegård et al. 2006/ where additional comments and references are given.

The retardation model for rock domains considers the properties of the unaltered intact rock matrix, whereas that for type fractures additionally considers the material properties of alteration zones of various kinds and extents within the wall rock adjacent to fracture flow paths. No attempt has been made to parameterise the detailed microstructures of local minor and local major deformation zones owing to a lack of hard data for these structures. These, however, are not currently considered to contribute substantially to the overall transport resistance. A major improvement in the current site descriptive model is the inclusion of sorption data for a larger set of nuclides, representing a wider range of sorption properties, than was available for the previous model version.

2.2.1 Methods and parameters

The transport of radionuclides escaping from the waste repository is conceptualised to occur through a network of connected flowpaths or channels residing in fractures within the rock. Radionuclides dissolved in the water flowing in these flow channels may sorb on the surface of mineral grains on fracture surfaces or may diffuse further into the adjacent rock where they can sorb on rock matrix micro-surfaces /e.g. Neretnieks 1980/.

Intact crystalline rock is slightly porous and there are water filled pores between the crystal grains in which radionuclides can be transported by molecular diffusion. Granitic rocks of the type encountered in the site investigations typically have a porosity on the order of about 0.1 percent that in the current retention paradigm is thought to be connected over distances of many metres into the rock /Löfgren 2004, Löfgren and Neretnieks 2006 (in press)/.

The notion of sorption in the context of the SDM relates to the adsorptive interaction of radionuclides with the surfaces of geologic materials. This occurs principally by way of the association of ionic solutes with charged mineral surfaces. In the simplified approach to sorption modelling adopted within the SDM, sorption processes are considered to be linear (no concentration dependency) as well as being fast and reversible (chemical kinetics are not considered). The concept is the same as that described in the strategy report by /Widestrand et al. 2003/.

The surface area of mineral grains within the connected matrix porosity is many orders of magnitude higher than the geometric surface area of rock exposed to flow (i.e. the flow-wetted surface). In addition to matrix diffusion, this provides a very strong sink for sorbing radionuclides that significantly retards their transport along flowpaths leading to the biosphere.

The main parameters used in the retardation model are the total storage porosity, ε_p (–), the effective diffusivity, D_e (m^2/s), and the linear equilibrium sorption coefficient, K_d (m^3/kg).

The so-called, bulk sorption partitioning coefficient, K_d^* (m^3/kg) differs from the "true" partitioning coefficient, K_d (m^3/kg) in that the former also incorporates the storage capacity of the water-filled rock matrix porosity:

$$K_d^* = \frac{\varepsilon_p}{\rho_b} + K_d \qquad (2\text{-}1)$$

For strongly sorbing tracers, however, the porosity term is negligible and for all practical purposes, K_d^* and K_d are identical. It is also noted here that the product $K_d^* \rho_b$ (–) is identical to the capacity factor, α (–) obtained from through-diffusion measurements (for the particular solute concerned).

The central parameter of most Safety Assessment models for radionuclide transport within fractured rock, however, is a *material properties group* /SKB 2004b/ that incorporates the numerical product of effective diffusivity, bulk sorption partitioning coefficient, and density of the rock (actually, it is the square root of the product of these parameters that is used).The material properties group is defined as:

$$MPG = \sqrt{D_e K_d^* \rho_b} \qquad (2\text{-}2)$$

The effective diffusivity is frequently given in terms of the formation factor, F_f (–) a dimensionless number which is defined as the ratio of the effective diffusivity of a solute in the rock to that of the solute in water at infinite dilution. Theoretically, the formation factor is a geometrical factor that includes the effect of transport porosity ε_t, as well as pore tortuosity, τ^2 and constrictivity δ /e.g. Löfgren and Neretnieks 2003/. Typically, it is defined as:

$$F_f = \frac{D_e}{D_w} = \varepsilon_t \frac{\delta}{\tau^2} \qquad (2\text{-}3)$$

Although strictly a geometrical parameter, measurement of the formation factor is affected by other non-geometrical artefacts such as surface diffusion and anion-exclusion effects; operationally, however it is still defined as the ratio of effective and free diffusivity. For this reason, laboratory measurements of the formation factor are customarily carried out on materials that have been pre-equilibrated with high ionic strength water ($I \geq 1.0$ M) so as to not be excessively influenced by surface diffusion artefacts. From the formation factor, effective diffusivities can be calculated for all solutes of interest using solute-specific free diffusivities from the literature /e.g. Widestrand et al. 2003/.

Formation factors can be obtained by a variety of different methods. The main laboratory methods used within the Transport programme are through-diffusion tests on slices of rock samples and electrical resistivity measurements. Through-diffusion tests are made using a two-compartment measurement cell where a tracer (tritiated water in the current laboratory programme) is allowed to diffuse through a 1–5 cm long drill core piece from a high concentration compartment to a low concentration compartment (the measurement cell), initially free of tracer. The effective diffusivity and capacity factor are then obtained by fitting a theoretical model of diffusion to the breakthrough data for the measurement cell /e.g. Ohlsson and Neretnieks 1995/.

The through-diffusion tests also provide estimates of the total porosity by means of the "capacity factor", α calculated from the experimental results. For a non-reactive tracer the capacity factor should be identical to the total porosity. Although this is not strictly true for tritiated water (HTO) owing to hydrogen isotope exchange with surface functional groups on the mineral surfaces, due to the very small fraction of surface-bonded hydrogen compared to that in the porewater, it is close enough to provide a reasonable comparison. In previous investigations, uranine or iodide (I^-) was frequently used as a tracer. Anion exclusion effects relating to the thickness of the electrical double layer relative to the pore diameter, however, compromise the applicability of results obtained using these solutes for cation diffusion (although more so at low ionic strengths) and therefore they have not been used in the current site investigation. The choice of HTO as a reference tracer is motivated by the wish to obtain a quantification of the geometrical formation factor with a minimum of additional interacting processes that are strongly dependent on pore water chemistry /Widestrand et al. 2003/. We note, however, that both anion exclusion and surface diffusion may be important for transport processes at low ionic strength. Although these aspects are not currently included in the Bedrock Transport Properties description, it is envisaged that quantification of these effects will form part of future versions of the site descriptive model.

Laboratory electrical resistivity measurements are performed also using 1–5 cm long drill core pieces and the formation factor is obtained as the ratio between the pore water resistivity and that of the saturated rock. This is possible owing to the analogy between diffusivity and ionic mobility as defined in the Einstein relation (see e.g. /Atkins 1999/). Both alternating (AC) and direct (DC) current can be used for these measurements, although AC is frequently preferable owing to electrode polarisation effects arising when using DC methods. AC current also allows phase angle measurements to be made which can be helpful for identifying the presence of conductive minerals such as magnetite /e.g. Thunehead 2005/.

Laboratory resistivity measurement is a relatively fast method, which enables testing of large numbers of samples. Thus, the majority of the laboratory formation factor data are from resistivity measurements.

Electrical resistivity can also be measured by in situ methods using a resistivity logging tool /e.g. Löfgren and Neretnieks 2005/. In laboratory measurements of resistivity, the rock samples are firstly saturated with a solution of known salinity (1 M NaCl), whereas in situ measurements rely upon accurate characterisation of the matrix porewater. This is typically done using flowing water in fractures as a proxy, although this implicitly assumes equilibrium between the matrix porewater and that sampled in the borehole. It is possible to leach porewater from retrieved bore core samples to estimate the composition of the native porewater, although this is influenced to varying degrees by the effects of stress release and drill water imbibition. The method can only be used for parts of the borehole where sufficiently strong saline conditions prevail that surface diffusion artefacts are not an issue.

Although there are a number of difficulties related to in situ measurement, it is the opinion of the author that these measurements are more representative for use in site characterisation and transport modelling (see Chapter 10 in the main SDM report /SKB 2006a/ for a more detailed discussion of the uncertainties).

Within the laboratory programme the equilibrium sorption distribution coefficient, K_d is measured by batch sorption tests on crushed rock and fracture-filling materials. This is done in contact with different water compositions (see Appendix A) intended to cover the range of groundwater chemistries likely to be encountered by transported solutes. As the crushing of rock samples results in the formation of additional sorption surface area that is not representative of in situ rock, sorption data for different size fractions are used to extrapolate estimates for the sorption coefficient for the internal surfaces of the crushed rock material (K_d) as well as an estimate of the external surface sorption parameter (K_a). The evaluation is similar to that used for distinguishing internal and external surface area in BET-measurement data /Byegård et al. 2006/, and relates the measured solute partitioning ratio, R_d (m^3/kg) with the mass-based sorption coefficient on internal surfaces, K_d (m^3/kg) and surface area normalised sorption coefficient, K_a (m) for sorption on the external surfaces of crushed particles /Widestrand et al. 2003/:

$$R_d\left(m^3/kg\right) = K_d + \frac{6K_a}{\rho_b \mathrm{d}_p} \qquad (2\text{-}4)$$

The values of K_a and K_d and their error estimates (i.e. σ_{Kd} and σ_{Ka}) can be obtained by linear regression when data for more than one particle size fraction are available if it is assumed that different particle size fractions have essentially identical sphericity. The particle size fraction is customarily assumed to be the volumetric mean size based upon upper and lower sieve sizes bracketing the sample /e.g. Byegård and Larsson 2004/:

$$d_p = \left(\frac{d_{\min}^3 + d_{\max}^3}{2}\right)^{1/3} \qquad (2\text{-}5)$$

The laboratory programme includes measurements of the total porosity, ε_p, by the water saturation technique, and for some samples also by PMMA measurements. There is often a mismatch between the porosity as estimated from through-diffusion tests and that estimated from water saturation measurements owing to differences in evaluation procedures and measurement artefacts. We also note that there is a conceptual difference between the total accessible porosity, ε_p and the transport porosity, ε_t. The transport porosity should theoretically be lower than the total accessible porosity which also includes dead-end pores that do not contribute directly to the diffusive flux. The actual difference between the two types of porosity are not of great concern, however, as measurements of effective diffusivity or formation factor implicitly already include the transport porosity and it is therefore not necessary to evaluate this separately.

The parameterisation of the retardation model as presented in the SDM /SKB 2006a, Byegård et al. 2006/ is based on the following considerations and parameters:

- **Rock matrix porosity, θ_m (–):** The results from the water saturation porosity measurements on site-specific rock materials have been selected in this work. A lognormal distribution has been considered to describe the system somewhat better (although not perfectly) than a normal distribution, and has therefore been selected for the representation.
- **Rock matrix formation factor, F_f (–):** This parameter is used to multiply literature values of the radionuclide-specific free diffusivities in water (D_w (m^2/s); tabulated by e.g. /Ohlsson and Neretnieks 1997/) to obtain the effective diffusivities, D_e (m^2/s), for the different radionuclides. Since the results of the laboratory electrical resistivity measurements are based on a larger number of samples and have been found not to deviate significantly from the through-diffusion results, they have been selected for the retardation model. Detailed in situ measurements of formation factors are, however, forthcoming and are thought to be more relevant for model parameterisation owing to that they are obtained under prevailing formation stresses. It is anticipated that these will be used in future versions of the retardation model parameterisation. For consistency with the closely related porosity parameter, a lognormal distribution has been selected also for the formation factor representation.
- **Rock matrix sorption coefficient, K_d (m^3/kg):** All available site data are imported for use in the retardation model. Site-specific data on the BET surface areas of the different rock types are used as supporting data and are used to extrapolate K_d-values where measurement results are unavailable.

We note here that the SDM uses the term θ_m to denote matrix porosity, although it does not make a clear distinction between transport (ε_t) and total porosity (ε_p) as discussed in this report. For the purposes of the present report and the scoping calculations made herein, however, we neglect any distinction between the different kinds of porosity and also use the term θ_m in the context of the retardation model.

2.2.2 Summary of transport properties of different rock types

In this section, the recommended properties of the various rock types are presented as described in the retardation model presented in the main SDM report /SKB 2006a/. The retardation models relating to parameterisation of rock domains and fractures and deformation zones are not discussed in detail here. This is partly because they are already described in detail in the main SDM report (as well as the background report by /Byegård et al. 2006/) and partly because it would distract from the main purpose of this report; namely, to investigate the interaction between the transport resistance (F-factor) and retardation model parameterisation.

The effective diffusivity assigned to the various rock types in the retardation model is currently based largely upon electrical resistivity measurements carried out in the laboratory. These measurements give effective diffusivities that are generally larger than those obtained by in situ measurement of electrical resistivity. The differences, however, between in situ and laboratory measurements are not unequivocal when considering the data variance and overall measurement uncertainty. Although in situ measurement data have some uncertainty due to lack of knowledge concerning the true salinity of matrix porewater, at least part of the difference (if a difference indeed exists) could result from effects of tangential stress concentrations around the borehole paired with effects of stress unloading of rock samples in the case of measurements on core specimens. The net effect is that laboratory derived data are likely to be upwardly biased relative to the effective diffusivity measured in situ.

Only preliminary experimental data for sorption on Ävrö granite sampled from KLX03A (522.61–523.00 m) are available at this time. The experiments have been performed using the crushed rock in contact with both fresh groundwater and present day groundwater from repository depth (GW Type I and III, respectively – see Appendix A). The data for different size fractions (63–125 µm and 2–4 mm) have been evaluated according to Equation 2-4 in order to extrapolate an estimate of the sorption coefficient for the internal surfaces of the crushed rock material (K_d) as well as an estimate of the external surface sorption parameter (K_a). Many of these data are of a provisional nature owing to the long times required for laboratory characterisation of the samples. The preliminary sorption data are based on a rock-solute contact time of one month for the radionuclides of Cs(I), Sr(II), Ni(II), Ra(II), and three months for Am(III). Final sorption measurements will not be made until after six months contact time.

For the other major rock types and for the fracture specific materials, no site-specific experimental sorption data exist. Sorption data has been estimated for these rock types using an extrapolation procedure, assuming that the sorption K_d is linearly proportional to the BET surface area. The extrapolation procedure was based upon sorption and BET surface area data for the 63–125 µm size fraction of Ävrö granite as a reference material, scaled with respect to the BET surface area of the target rock type:

$$K_{d(x)}\left(m^3/kg\right) = R_{d(\ddot{A}G)} \times \frac{A_x}{A_{(\ddot{A}G)}} \qquad (2\text{-}6)$$

Where $K_{d(x)}$ is the extrapolated sorption partitioning ratio, $R_{d(\ddot{A}G)}$ is the measured sorption partitioning ratio for Ävrö granite, and A_x and $A_{(\ddot{A}G\ 63–125\mu m)}$ are the BET surface areas (m^2/g) of the respective materials. It should be noted that the BET surface area for the different rock types was preferentially obtained from the extrapolation of inner BET surface area where possible (see Table 3-5 and Table 3-6 in the background report by /Byegård et al. 2006/). For some rock materials (particularly fracture specific materials) only the small size fraction has been measured (i.e. 63–125 µm or < 125 µm). In these cases the measured BET surface area for the small size fraction has been used directly.

The results from these BET surface area based extrapolations of K_d-values have been used for the parameterisation of the rock types other than Ävrö granite. Very similar values are found for the different major rock types. For the fracture and fracture zone materials, however, significantly higher K_d-values are reported. This is a direct consequence of the high BET surface areas measured for these samples.

It should be emphasised that this extrapolation is only an approximate method for assigning K_d-values to rock materials where measurement data is unavailable. In /Allard et al. 1983/, for example, a far from perfect correlation was obtained for the cation exchange capacity (CEC) relative to the BET surface area, indicating a more complex and mineral-dependent

relationship between the sorption capacity and the BET surface area. More recent studies (e.g. /Bertetti et al. 1996, Jenne 1998, Prikryl et al. 2001, Davis et al. 2004/) lend strong support to the concept of BET surface area normalisation, although there do appear to be intrinsic differences between the sorption properties of specific minerals, in terms of both the density of sorption sites relative to BET surface areas, as well as different mechanisms of sorption on, for example, clay mineral edges sites as compared to basal crystal planes. Nevertheless, in the absence of sorption measurements for most of the site specific rock types in the Laxemar subarea, this concept is considered to be the best available method of assigning sorption coefficients to the various rock types. In forthcoming versions of the site description, additional sorption measurement and CEC data will be available and the possibility will exist for a more rigorous evaluation of the K_d-prediction concept.

The recommended data for the various rock types are given in Table 2-1 below.

For solutes not included in Table 2-1, K_d values from /Carbol and Engkvist 1997/ are recommended for use in transport modelling. Although not adjusted for BET surface areas of site specific materials, these data should still give order of magnitude estimates of sorption strength for different species under both non-saline and saline conditions.

Although there are no laboratory determined sorption measurements for other major rock types available at this time, BET surface area measurements indicate that relative sorption strengths (strongest to weakest sorption) should approximately follow the order Fine-grained dioritoid/Fine grained diorite-gabbro > Ävrö granite/diorite to gabbro > quartz monzodiorite. Altered Ävrö granite has a BET-surface area about twice that of the unaltered Ävrö granite. It is not currently possible to determine an accurate order of relative sorption strengths as it is not strictly robust to compare measured sorption data for Ävrö granite with extrapolated data for the other rock types. Additionally, the order of relative sorption strengths as identified from Table 2-1 is not the same for different sorbing species. It is noted, for example, that Ävrö granite in contact with non-saline groundwater (GW type I) exhibits the strongest relative sorption for Ni(II) and Ra(II), although the weakest for Cs(I) and Am(III), with Sr(II) appearing somewhere in the middle of the order (i.e. relative to the other rock types). For saline groundwater (GW type III) Ävrö granite exhibits consistently the weakest sorption for all species except for Sr(II) for which it exhibits the strongest sorption.

While there is much uncertainty in establishing a relative order of sorption strengths amongst the various rock types, it is clear that most solutes sorb more strongly under non-saline conditions than under saline conditions, at least for the groundwater compositions used in the laboratory measurements. The main exception is Am(III) which appears to be unaffected by different groundwater salinities. It is noted here that this effect is expected on the basis of the known sorption mechanisms for this radionuclide (i.e. it sorbs by way of a surface complexation mechanism which renders it less sensitive to ionic strength variations).

From the recommended data and excluding Am(III), Cs(I) appears to exhibit the smallest dependency upon salinity with only a very modest increase in sorption strength (a factor of ≤ 2) for K_d in non-saline groundwater relative to saline groundwater. This is also an expected result which is in line with the known sorption characteristics of this radionuclide.

For the other solutes, Sr(II) exhibits the largest increase (a factor of roughly 10–100), whereas Ni(II) and Ra(II) show more modest increases with factors of 6–12 and 20–35, respectively. These differences may be partly due to solution speciation effects involving HCO_3^- / SO_4^{2-}, although for Sr(II) and Ra(II) they are also related to ionic strength (specifically competition for sorption sites with other cations in solution).

Table 2-1. Suggested transport parameters for the major rock types in the Laxemar subarea. Parameter values in italics refer to K_d-values that have not been measured for that particular rock type, but instead have been obtained by extrapolation from the results for the BET surface area measurements using Equation 2-6. Values are given as mean ±σ for the considered data set where available.

Rock Type	Porosity (vol%)	Formation factor (–)	Water type	K_d (m^3/kg) Cs(I)	Sr(II)	Ni(II)	Ra(II)	Am(III)
Ävrö granite	0.27±0.09	$(1.4±1.0)×10^{-4}$	III	$< 2×10^{-2}$	$< 4×10^{-4}$	$(1.1±0.6)×10^{-2}$	$(4.0±3.6)×10^{-3}$	$(1.0±0.5)×10^{-2}$
			I	$(4.2±3.5)×10^{-2}$	$(5.8±1.4)×10^{-3}$	$(1.3±0.8)×10^{-1}$	$(1.4±1.1)×10^{-1}$	$(1.0±0.5)×10^{-2}$
Quartz monzodiorite	0.17±0.08	$(3.6±3.5)×10^{-5}$	III	*$< 9×10^{-2}$*	*$< 4×10^{-5}$*	*$< 1.5×10^{-2}$*	*$< 5×10^{-3}$*	*$< 1.4×10^{-2}$*
			I	*< 0.11*	*$< 4×10^{-3}$*	*< 0.1*	*< 0.1*	*$< 1.3×10^{-2}$*
Fine-grained dioritoid	0.14±0.14	$1.0×10^{-5}$ A	III	*$(1.0±0.9)×10^{-1}$*	*$< 10^{-4}$*	*$(1.8±0.9)×10^{-2}$*	*$(5±3)×10^{-3}$*	*$(1.7±1.0)×10^{-2}$*
			I	*$(1.4±0.7)×10^{-1}$*	*$(5±3)×10^{-3}$*	*$(1.2±0.7)×10^{-1}$*	*$(1.2±0.6)×10^{-1}$*	*$(1.7±1.0)×10^{-2}$*
Fine-grained diorite-gabbro	0.22±0.08	$(6.4±4.2)×10^{-5}$	III	*$(1.0±0.8)×10^{-1}$*	*$< 10^{-4}$*	*$(1.8±0.6)×10^{-2}$*	*$(5±2)×10^{-3}$*	*$(1.6±0.6)×10^{-2}$*
			I	*$(1.4±0.4)×10^{-1}$*	*$(5±2)×10^{-3}$*	*$(1.1±0.6)×10^{-1}$*	*$(1.1±0.3)×10^{-1}$*	*$(1.6±0.5)×10^{-2}$*
Fine-grained granite	0.22±0.0002	No data	III	No data	No data	No data	No data	No data
			I	No data	No data	No data	No data	No data
Granite	0.38	$8.0×10^{-5}$ A	III	No data	No data	No data	No data	No data
			I	No data	No data	No data	No data	No data
Diorite to gabbro	No data	No data	III	*$(7±6)×10^{-2}$*	*$< 6×10^{-5}$*	*$(1.2±0.3)×10^{-2}$*	*$(3.6±0.8)×10^{-3}$*	*$(1.1±0.3)×10^{-2}$*
			I	*$(9±2)×10^{-2}$*	*$(3.5±0.8)×10^{-3}$*	*$(8±4)×10^{-2}$*	*$(8±2)×10^{-2}$*	*$(1.1±0.3)×10^{-2}$*
Altered Ävrö granite (selected to represent all altered wall rock)	No data	No data	III	*$(1.4±1.1)×10^{-1}$*	*$< 10^{-4}$*	*$(2.5±0.7)×10^{-2}$*	*$(7±2)×10^{-3}$*	*$(2.2±0.7)×10^{-2}$*
			I	*$(1.9±0.4)×10^{-1}$*	*$(7±2)×10^{-3}$*	*$(1.6±0.7)×10^{-1}$*	*$(1.6±0.4)×10^{-1}$*	*$(2.2±0.6)×10^{-2}$*

A Data is based upon a single measurement; therefore no uncertainty interval is given.

The data obtained for most of the solutes are in line with expected values as given in recommendations by /Carbol and Engkvist 1997/ with the exception of Am(III), the measured K_d for which is some 2–4 orders of magnitude lower than typical (batch-measurement) data found in the literature /e.g. Allard et al. 1977, Allard et al. 1978, Erdal et al. 1979, Piinnioja et al. 1984, Nakayama et al. 1986, Ikeda and Amaya 1998/. Although the literature data is generally not corrected to distinguish sorption on inner and outer surfaces, this cannot by itself explain the difference and it is unclear at this time why the measured K_d values for Am(III) are so low.

It does not appear that the effect is due to diffusion or chemical kinetic effects as significantly higher K_d values have been measured for Am(III) sorption on granitic rock over much shorter contact times than the three months used as a basis for the values given in Table 2-1. The presence of carbonate (HCO_3^-) is known to reduce the sorption of Am(III) relative to that in non-carbonate containing water, owing to solution speciation effects /e.g. Alonso and Degueldre 2003/. This, however, does not appear to be the case here as the fresh groundwater used for the measurements (GW Type I) has roughly 20 times higher carbonate concentration than the saline groundwater (GW Type III) and there appears to be no significant difference between the K_d values measured for these groundwater simulants as already discussed above.

A possible artefact identified in the laboratory measurements is that there were significant Am(III) losses (up to 90%) in blank control samples, possibly the result of sorption to vessel surfaces. Although this has been corrected for in the data evaluation, it is not clear if the literature values have been corrected for such artefacts, nor if this can fully explain the observed discrepancy.

If the data are correct, this could have non-trivial consequences for Safety Assessment. Based upon the seemingly strong sorption of Am(III) as described in the literature (see above), however, it is possible that the low values could be an experimental artefact. As the sorption measurements are preliminary and additional control measurements (e.g. measurement of solid phase activity) have not been possible to perform as yet, the results for Am(III) should be considered as provisional in the current retardation model. More work will need to be done to clarify this issue in forthcoming SDM versions.

It should be noted that the differences between the rock types are typically very small (at least the extrapolated values based upon the presently available BET data) and are often less than the estimated variability and overall uncertainty in the sorption data itself. Furthermore, the results for Ävrö granite clearly indicate a strong influence of solution composition that may mask the possibly smaller differences between the data obtained for different rock types. The proposed order of sorption strengths for different rock types should therefore be treated with utmost caution.

It is difficult to give a definitive estimation of relative diffusive properties in the current SDM for Laxemar as there is a considerable inequality in sample support amongst the different rock types and measurement methods. Based upon the recommended transport parameters in Table 2-1, however, Ävrö granite appears to have the highest effective diffusivity (associated with higher retention) with a formation factor on the order of $F_f \geq 10^{-4}$. Other reported rock types appear to have essentially similar diffusive properties to each other and any relative differences are speculative owing to the inherent data uncertainty. The formation factors of these rock types are roughly 2–4 times lower than that for Ävrö granite, with the exception of fine-grained dioritoid which has a tentatively estimated

formation factor approximately 10 times lower. These observations are both quantitatively and qualitatively consistent with the data previously reported for the Simpevarp 1.2 SDM /Byegård et al. 2005, SKB 2005a/ and are discussed in more detail in the following section.

A particular uncertainty in the current model version is the unknown effective diffusivity of altered Ävrö granite which is assumed to be representative of all altered rock forms in the Laxemar subarea.

2.2.3 Comparison of Laxemar 1.2 and Simpevarp 1.2 transport properties

In the previous model version for Simpevarp 1.2 /SKB 2005a, Byegård et al. 2005/, data were imported from Äspö HRL studies for analogue rock types and extrapolated according to either Equation 2-4 or Equation 2-6 (depending upon the available data) to obtain K_d and K_a estimates. These sorption data were obtained principally from /Byegård et al. 1998/. Effective diffusivities measured for site specific rock types within the site investigation programme were then pooled with the imported sorption data. Due to a possible lack of internal consistency between the methods used for extrapolation of sorption data for altered and unaltered rock and the pooling of this data with site specific measurement data, the altered layers in the previous model were parameterised with weaker retention properties than those for the unaltered rock matrix. This, however, is now believed to be an artefact of the previous data import.

To account for the lack of data for rock types other than Ävrö granite and for altered rock in the current retardation model, data have been extrapolated by assuming the sorptive strength of the rock is linearly correlated with BET-surface area. This is thought to be a more accurate means of extrapolating data for the altered rock layers at least for solutes that sorb by way of a surface complexation mechanism. Based upon the available data and previous experience from the Äspö HRL it is believed likely that the alteration layers do, indeed, have stronger retention properties than the unaltered rock matrix. This, however, is somewhat speculative and will need to be confirmed in forthcoming versions of the SDM.

It is noted that this may not always be the case as it is the combination of sorptive and diffusive properties as described by the material properties group (MPG) for the particular rock type and solute of interest that determines retention properties. The relative retention properties of altered and unaltered rock should always be viewed in terms of the MPG given that reduced sorption strength doesn't always translate to weaker retention if it is outweighed by a corresponding, or larger increase in effective diffusivity (and vice versa).

Although the typically greater BET surface area of altered rock materials suggests increased sorption for solutes that sorb by way of a surface complexation mechanism, it is noted that solutes that sorb by way of an ion-exchange mechanism may exhibit reduced sorption on altered rock materials. In the case of Cs(I) this may be due to the alteration of biotite, which has a high affinity for Cs(I), to chlorite which sorbs Cs(I) somewhat less strongly.

In order to facilitate a comparison, however, between the Simpevarp 1.2 (S1.2) and Laxemar 1.2 (L1.2) retardation models, the recommended transport parameters for Simpevarp are reproduced in Table 2-2 below.

Table 2-2. Suggested transport parameters for the major rock types in the Simpevarp 1.2 SDM /SKB 2005a/ for GW Type III. Values are given as mean ±σ for the considered data set where available. Data given as log_{10} values are labelled as (LN).

Rock Type	Porosity (vol%)	Formation factor (–)	GW	K_d (m^3/kg) Cs(I)	Sr(II)
Ävrö granite	–0.43±0.19 (LN)	–3.85±0.66 (LN)	III	$(6±3)×10^{-2}$	$(4.2±0.8)×10^{-5}$
Quartz monzodiorite	–0.80±0.28 (LN)	–4.45±0.73 (LN)	III	$(6±3)×10^{-2}$	$(4.2±0.8)×10^{-5}$
Fine-grained dioritoid	–0.90±0.35 (LN)	–4.69±0.89 (LN)	III	$(6±3)×10^{-2}$	$(4.2±0.8)×10^{-5}$
Altered Rock (all types)	0.33	$8.0×10^{-5}$	III	$(1.3±0.6)×10^{-2}$	$(1.2±0.2)×10^{-5}$

It is difficult to make a rigorous comparison between the different subareas owing to the different levels of sample support as well as fundamental differences in the methods used for data evaluation. Moreover, for S1.2, data were only available for Cs(I) and Sr(II) which substantially reduces the possibility for comparison. Table 2-3 below summarises the recommended data for Cs(I) from the L1.2 and S1.2 SDM (for comparable rock types) as well as those used within the Äspö/TRUE programme /Dershowitz et al. 2003/.

Table 2-3. Comparison of recommended material properties data for Cs(I) transport taken from Simpevarp 1.2, Laxemar 1.2, and the TRUE programme for various rock types and saline water (GW Type III). Ratios of MPG values for altered/unaltered rock (R_{12}) are given in far right-hand column where appropriate.

Rock Type	Porosity (vol%)	Formation factor (–)	K_d Cs (m^3/kg)	MPG ($m/y^{1/2}$)	R_{12}
Laxemar 1.2					
Ävrö granite	0.27	$1.4×10^{-4}$	< 0.02	$1.80×10^{-2}$	n/a
Quartz monzodiorite	0.17	$3.6×10^{-5}$	0.09	$1.94×10^{-2}$	n/a
Fine-grained dioritoid	0.14	$1×10^{-5}$	0.1	$1.08×10^{-2}$	n/a
Altered rock[1] (all types)	n/a	n/a	0.14	n/a	
Simpevarp 1.2					
Ävrö granite	0.37	$1.4×10^{-4}$	0.06	$3.14×10^{-2}$	0.35
Quartz monzodiorite	0.16	$3.6×10^{-5}$	0.06	$1.57×10^{-2}$	0.70
Fine-grained dioritoid	0.13	$2×10^{-5}$	0.06	$1.19×10^{-2}$	0.92
Altered rock[2] (all types)	0.33	$8×10^{-5}$	0.013	$1.10×10^{-2}$	
Äspö/TRUE (Taken from Table 2-2 and Table 2-4 in /Dershowitz et al. 2003/)					
Äspö diorite	0.3	$7×10^{-5}$	0.01	$9.02×10^{-3}$	2.39
Altered Äspö diorite	0.6	$2×10^{-4}$	0.02	$2.16×10^{-2}$	

Notes: 1 Based upon data for altered Ävrö granite (selected to represent all altered rock).
2 Based on Äspö HRL imported data for altered Äspö diorite (selected to represent all altered rock).

Based upon the data contained in the retardation model for Laxemar 1.2 and Simpevarp 1.2, it appears that the same rock types from different subareas have essentially identical porosities and diffusive properties.

Similarly to the diffusive properties of the rock, the recommended sorption data suggest only small differences between the major rock types from each site, although we note that in the Laxemar 1.2 data set Ävrö granite is parameterised to sorb Cs(I) less strongly than the other rock types. This may be due to the fact that data values extrapolated according to Equation 2-4 were used for Ävrö granite in the Laxemar 1.2 dataset, whereas the values for the other Laxemar rock types were obtained by extrapolation using Equation 2-6. For the inter-comparison between sites, it is also noted that actual measurement data were used for Ävrö granite in the Laxemar 1.2 dataset, whereas the corresponding data for Simpevarp 1.2 were based upon imported Äspö data (using Äspö diorite as a proxy for all rock types). Given the mix of imported and extrapolated data upon which the recommended data values are based, it is difficult to make any meaningful comparisons between the material properties of the rocks from the different sites (i.e. comparisons of the MPG parameter group).

Bearing in mind the provisional nature of the retention properties data and the fact that a large proportion of the data are extrapolated on a tentative basis, it is not currently possible to rigorously compare the retention properties of different rock domains, nor draw specific conclusions concerning the differences between rock domains in the Laxemar subarea and those within the Simpevarp subarea. The rock types found in both the Laxemar and Simpevarp subareas, however, appear to have broadly similar retention properties based upon the current level of understanding. The reasons for any differences, however, are not of primary concern for this report. Instead, the focus here is to explore the consequences of the material properties parameterisation for Safety Assessment calculations. This is explored further in Chapter 4.

It is interesting to note that both the sorption K_d and formation factor for altered Äspö diorite (i.e. Äspö/TRUE data /Dershowitz et al. 2003/) are greater than the corresponding data for unaltered rock. The MPG value calculated for the altered rock is thereby roughly 2.4 times higher than that calculated for the unaltered rock. For Simpevarp 1.2, on the other hand, the K_d value is lower for the altered rock while the formation factor is greater relative to the unaltered rock for all rock types except Ävrö granite, where the formation factor is actually lower for the altered rock. The ratio of MPG values for the altered/unaltered rock are in the range 0.35–0.92 based upon the Simpevarp retardation properties model. It is noted that the Äspö HRL/TRUE sorption data obtained from /Dershowitz et al. 2003/ are estimated values based upon an extrapolation procedure using measured CEC values and consideration of ion-exchange equilibria (as outlined in /Andersson et al. 2002a/) and are therefore also associated with a large degree of uncertainty. The prediction of enhanced retention in the altered rock in this case is therefore dependent upon the accuracy of the extrapolated K_d values.

For Safety Assessment purposes, alteration layers with reduced retention properties relative to the unaltered rock matrix (which we refer to in this report as unfavourable retention properties) generally give shorter breakthrough times for transported solutes as compared with simulation results where the alteration layers are neglected. If the retention properties of the alteration layers are enhanced relative to the unaltered rock matrix, on the other hand, (favourable retention properties) longer breakthrough times are expected for transported solutes. In the models currently used for Safety Assessment, alteration layers are disregarded and the rock matrix is assumed to be homogeneous with material properties corresponding to those for unaltered rock.

3 Transport properties of flowpaths

In the event of deposition canister failure, radionuclides may escape and migrate to the surrounding rock through the bentonite buffer or backfilling material surrounding the canister emplacement. The radionuclides may then be transported into fractures intersecting the deposition hole, into the disturbed zone around the excavated volume, and into fractures intersecting the tunnels.

Radionuclides that reach the rock volume are transported by the groundwater flowing in fractures within the rock. Certain nuclides may sorb on the surface of the fractures through which they are transported. From the fractures they may also migrate into the rock matrix by molecular diffusion. The interior of the rock matrix contains stagnant "porewater" and micro-surfaces upon which the radionuclides can sorb. Diffusion and sorption in the rock matrix and to a lesser extent, sorption on the external fracture surfaces, are the primary mechanisms for radionuclide transport retardation.

Molecular diffusion into the rock matrix is a slow process and over the short timescales characteristic of tracer experiments very little matrix diffusion occurs. Under such conditions any retardation of solute transport is largely due to sorption on external fracture surfaces and infill materials in the fracture. At Safety Assessment (SA) timescales, however, sorption on external surfaces and infill materials can be insignificant in comparison to the retardation effect arising from diffusion into the rock matrix and sorption on internal surfaces.

In general, the greater the surface area in contact with flowing water (the so-called "flow-wetted surface", or FWS) for a given water flowrate the greater the interaction will be with both the external fracture surfaces and the rock matrix. The flow-wetted surface to flow ratio (FWS/q) is referred to variously as the "F-factor" /Andersson et al. 1998/, or "transport resistance" in different SKB reports and literature sources. The understanding and modelling of the flowpaths in the system and the assessment of the FWS to flow ratio are very important, if not central, for the prediction of radionuclide transport retardation /SKB 2004b/.

Large scale deformation zones with relatively fast water flows within the hydraulic conductor domain (HCD) are not currently considered to provide substantial transport resistance. For transport modelling, single fractures or fracture clusters constituting potential transport pathways from a canister position to the nearest major deformation zone are therefore likely to be of overwhelming importance for the solute transport retardation. A central problem in establishing a retention property model for the hydraulic rock domain (HRD) is how to identify these fractures, which are well connected and large enough to have a dominating impact on transport, but which are small enough to not be identified as substantial deformation zones and therefore part of the HCD. Although this could be seen as merely a question of nomenclature, we note that the demarcation between minor deformation zones (MDZ) within the HRD and major deformation zones making up the HCD is of some importance for the modelling of solute transport.

In the Laxemar 1.2 SDM, the bulk of the transport resistance is conceptualised to reside in the network of background fractures and minor deformation zones comprising the first 10–100 m of rock surrounding the repository. To distinguish this from transport through major deformation zones to the surface and other regional scale transport processes, this zone is referred to as the *immediate far-field* as shown schematically in Figure 3-1 below.

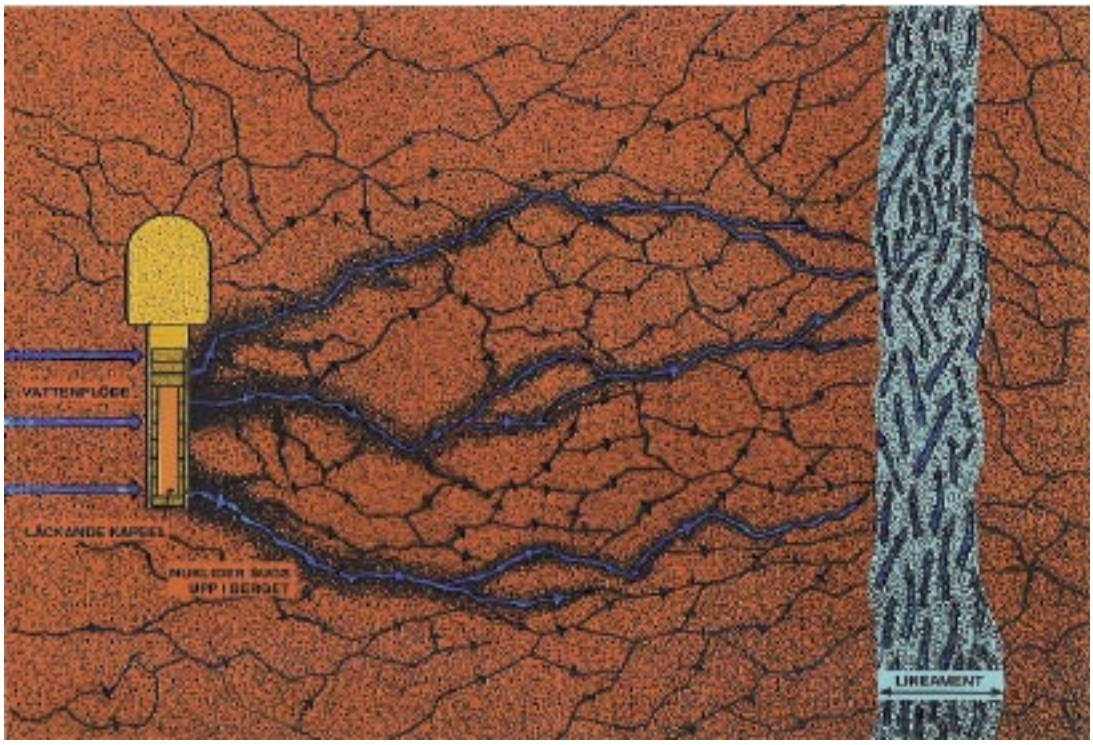

Figure 3-1. *Schematic representation of flow and transport in the "immediate far-field" conceptualised to be the first 10–100 m between any given canister hole and the nearest large scale deformation zone.*

Major deformation zones and large-scale conducting structures are, however, included within the Hydro-DFN as described in Chapter 8 of the main SDM report /SKB 2006a/.

3.1 Conceptual aspects and limitations of transport resistance estimations

The flow-wetted surface to flow ratio (F-factor) is a difficult parameter to quantify. Although being a site characteristic and a physical entity, it is neither a directly measurable quantity nor a material property in the sense of parameters such as porosity, formation factor, or the sorption K_d value. It is strongly influenced by physical features such as the aperture distribution within individual fractures as well as the orientation, geometry, and connectivity of individual fractures in the population of fractures distributed through the rock volume. At the same time, both the flow-wetted surface itself and the flow-wetted surface to flow ratio are dependent upon hydrological boundary conditions that can be expected to change throughout the lifespan of the repository.

In addition to these physical aspects, predictions of both large-scale flow fields on a sub-regional level (100–10,000 m) as well as local flow fields comprising the immediate far-field of the repository (10–100 m) are strongly dependent upon assumptions made during modelling that are, at best, only possible to verify by indirect observations and measurements. Furthermore, much of the available data can be interpreted along alternative lines of reasoning. Many postulated processes and physical qualities (such as severe flow channelling, length-transmissivity power law relations, etc) while conceptually appealing and broadly consistent with observational data, are not universally accepted owing to the difficulty of demonstrating that they actually occur on the scales of interest. This introduces

an element of measurement interpretation uncertainty into the predictions. Being model-derived parameters, there are thus limitations and uncertainties imposed upon the estimation of the flow-wetted surface and the F-factor that stem from the assumptions made during DFN analysis and flow modelling.

3.2 Generic, first order estimation of the F-factor

The repository siting concept seeks to provide a substantial buffer distance between any given canister emplacement and surrounding zones of high transmissivity that may provide fast transport paths to the biosphere. Although radionuclide transport within major deformation zones (DZ) and further on to other regional features is also subject to retardation processes, this cannot be relied upon from a design perspective owing to large uncertainties in the physical description of these features as well as their hydraulic and material properties. Owing to their high transmissivity, the transport resistance of these zones is also potentially far lower than that provided by less transmissive background and minor deformation zones. In this context, the scale of particular interest for SA transport resistance assessment is on the order of the first 10–100 m from a leaking canister to the nearest large scale deformation zone.

The network of migration paths extending through the rock volume comprising the immediate far-field is complex and spatially variable. Although useful for determining hydraulic boundary conditions, regional flow modelling with the aim of assessing transport resistance has limited value on this scale bearing in mind that the focus of these models is typically centred around structures on the 100–1,000 m scale.

Given that the estimation of the site specific transport resistance is strongly influenced by modelling assumptions that are not easily verifiable, we seek to make a prediction of this parameter from first principles using only absolutely necessary assumptions. It should be noted this does not mean that the more sophisticated Hydro-DFN models contain unnecessary assumptions, but that owing to a lack of data for fractures on the scale of interest here (i.e. 10–100 m scale) there are significant elements of expert judgement within these models that are not sufficiently indisputable nor transparent for our purposes if the aim is to calculate a reasonably defensible "envelope" of possible F-factor ranges.

One way of estimating such a range is to focus on the level of individual conductors identifiable from borehole hydraulic measurements. Here we consider what the theoretical transport resistance would be if the flow path sampled in a borehole were to extend from a deposition hole to a more distant major fracture zone in a straight line.

The transport resistance, or F-factor for a flowpath is the ratio of the fracture surface area in contact with flowing water (*FWS*), and the flowrate of the water along that path (q), or simply FWS/q. In most algorithmic representations, the transport resistance (F) is expressed as twice the product of the average width (W_p) and length (L_p) of a migration path, divided by the flow (q) /see e.g. Moreno and Neretnieks 1993, Vieno et al. 1992, SKB 2004b/:

$$F = \frac{2 W_p L_p}{q} \qquad (3\text{-}1)$$

This representation assumes, of course, that the flow within the migration path is well mixed. If the flow geometry and flow patterns within individual conductors are known in detail, this formula can be used to calculate the transport resistance distribution for different flowpaths – an approach which is used for the estimation of transport resistance in Hydro-DFN analyses. The main difference in this simple analysis is that apart from an assumed

flow-transmissivity relation (Equation 3-2), no a priori assumptions are made concerning the flowpath geometry and flow distribution between different flowpaths except that the flowpath is the shortest distance between the release and recovery locations (i.e. a straight line) and that the flow is evenly distributed within that path.

Assuming that the flow is evenly distributed across the width of the flowpath, the flow is given by:

$$q = TW_p\, i \qquad (3\text{-}2)$$

Where T (m^2/y) is the transmissivity and i (m/m) is the hydraulic gradient. Combining Equation 3-1 and 3-2 gives:

$$F = \frac{2L_p}{T\, i} \qquad (3\text{-}3)$$

Although the introduction of a transmissivity-flow relation here also constitutes an assumption, we note that we do not necessarily require the paradigm of viscous flow between parallel plates (i.e. the so-called cubic law) to use this representation of flow. Indeed, any suitable relation that describes flow as a function of applied hydraulic head differential would suffice equally well. It can be shown, for example, that for the generalised flow case where the fracture transmissivity is proportional to the fracture hydraulic aperture raised to some arbitrary exponent, n (the flow exponent), the results are largely unchanged. A flow exponent of unity, for example, corresponds to the case where fracture infill materials restrict flow so that the fracture has flow characteristics equivalent to a porous medium. A flow exponent of zero, on the other hand, indicates that the flowpath is pinched across the extent of the fracture aperture giving a flow restriction that dominates the characteristics of the system.

As can be seen from Equation 3-3 the estimate of the F-factor is, in theory, independent of the width of the migration path. This, however, assumes that the flow is proportional to the channel width which may not always be the case and it is easy to imagine situations where the flow is restricted in such a way that the flow is independent of the assumed flow channel width (i.e. flow "bottlenecks"). We also note that the estimate of the F-factor is strongly dependent upon transmissivities being correctly estimated from hydraulic test data and also does not make any consideration of flow channelling or the interconnectivity of different conducting features that make up the network of flow paths in the rock.

If the flowpath width is typically much larger than the borehole diameter this may not introduce a large error into the calculations if the assumption of cylindrical flow is approximately valid within the radius of influence of the test. Errors may be large, however, if the actual flow channels sampled in a hydraulic test are narrow (i.e. on the order of the borehole diameter or smaller). We note here that narrow flow channels radiating from a borehole would be difficult to distinguish from true cylindrical flow in a two-dimensional fracture plane if the frequency of flow channel bifurcation is sufficiently high that piecewise linear flow features are not distinguishable in a transient hydraulic test.

In fact, for randomly distributed flow channels in a two-dimensional fracture plane, we would expect a radial flow channel bifurcation frequency that is roughly proportional to the distance from the test borehole and therefore consistent with a cylindrical flow assumption (i.e. for a constant spatial density of flow channel intersections, the total number of channel intersections at a given radial distance from the borehole is proportional to the perimeter of the circle with that radius and centre at the borehole axis). In this respect, "confirmation" of 2D-cylindrical flow dimension using, for example, generalised radial flow analysis /Barker 1988, Walker and Roberts 2003/ does not necessarily rule out strongly channelled flow.

The existence of narrow channels may also influence the interpretation of hydraulic tests if the borehole only partly, or tangentially, intersects a flow channel. The strongly convergent flow at the channel-borehole intersection would then result in substantial downward biasing of the estimated transmissivity. This particular aspect of flow channelling is also discussed in the Preliminary Safety Evaluation for Forsmark /SKB 2005b/. For flow channels that are much wider than the borehole, the biasing effect still occurs although the probability of flow channels and boreholes intersecting in this manner are substantially lower and it will therefore have a consequently smaller impact upon transmissivity statistics. Flow channels that are only partly intersected by a borehole or are very narrow could give rise to strong flow convergence or divergence effects close to the borehole which may be interpreted as a "skin factor" in transient hydraulic tests.

For very narrow channels, the transmissivity could be potentially underestimated by as much as one, or more, orders of magnitude depending upon the different assumptions used in the evaluation procedure.

It is noted, however, that there are a number of uncertainties embedded in the estimation of flowpath transmissivities and Equation 3-3 may be sufficient given that reported transmissivities from, for example, PFL data may only be as accurate as an order of magnitude estimate /e.g. Ludvigson et al. 2002/. It should also be pointed out that F-factors estimated using other approaches (such as DFN-modelling) contain essentially the same uncertainties. The advantage of using the very simple approaches described in this and the following sections, however, is that the models are based upon very simple principles and are fundamentally transparent unlike the more complex models of flow and transport typically used in Safety Assessment.

The representative hydraulic gradient required to give a reasonable estimate of the F-factor under Safety Assessment conditions is also uncertain. It is influenced by surface hydraulic boundary conditions as well as distant, although strongly transmissive conductors that influence the distribution of hydraulic head at depth. In the following discussion we therefore consider a range of gradients that are likely to be representative of the hydraulic conditions at repository depth.

Assuming a path length of 100 m and a hydraulic gradient ranging from 0.1–1.0%, Equation 3-3 can be used to make generic estimates of the value of the F-factor. These data are given in Table 3-1 below.

Table 3-1. Generic transport resistance (F-factor) estimated for different fracture transmissivities, a path length of 100 m, and some representative hydraulic gradients (data is given in $\log_{10}$ units).

Transmissivity [m^2/s]	$\log_{10}$(F) [y/m]		
	0.1% (0.001 m/m)	0.5% (0.005 m/m)	1% (0.01 m/m)
10^{-4}	1.8	1.1	0.8
10^{-5}	2.8	2.1	1.8
10^{-6}	3.8	3.1	2.8
10^{-7}	4.8	4.1	3.8
10^{-8}	5.8	5.1	4.8
10^{-9}	6.8	6.1	5.8
10^{-10}	7.8	7.1	6.8

The form of Equation 3-3 implies that the F-factor scales linearly with distance and the generic estimates given in Table 3-1 can therefore be easily scaled to any other transport distance (and hydraulic gradient, for that matter) through multiplying by an appropriate factor. A migration distance of 10 m, for example, will have a characteristic F-factor that is 10 times less than that for a 100 m migration path (all other things being equal). Note that a similar table to Table 3-1 was provided in the Preliminary Safety Evaluation of the Forsmark site /SKB 2005b/.

3.3 Estimations of the F-factor using site specific data

Assessing a realistic site specific value for the transport resistance is dependent upon correctly predicting the transmissivities, extents, frequencies, and connectivity of conductive features in the rock volume being investigated. It is clear from borehole hydraulic tests that there is a broad distribution of flowrates and transmissivities that characterise different flowing features. The question for Safety Assessment is then to gauge what transmissivity is representative for the rock volume in question and what percentage of flowing features can be expected to have high transmissivities and consequently low transport resistance.

The F-factor is dependent not only on the hydraulic characteristics of individual flowing features comprising a flowpath, but also their interconnectivity in the extended network of fractures surrounding the repository. For migration from the repository within the immediate far-field, radionuclides may be transported over a number of independent flowpaths. The effective F-factor for such an ensemble of possible flowpaths therefore is best described in terms of a statistical distribution of F-factors.

There are a number of different, although complementary approaches that can be used to make estimations of site specific F-factors. As they attempt to model the same physics of flow and solute retention, however, for the same input data set and parameterisation they should give broadly comparable results. These are examined in the following sections.

Although the network of flow channels and potential migration paths is complex, it is possible to make estimates of the F-factor distribution from site specific data according to different conceptual models that represent extremes of possible behaviour. While not altogether physically realistic, they nonetheless can provide approximate bounds for the likely distribution of transport resistance to be found in the repository target volume. Moreover, they can also be used to provide a "reality check" on more sophisticated models where underlying concepts and assumptions may not be as transparent.

3.3.1 Hydraulic properties of conductive features and specific flow-wetted surface

There are a number of methods and techniques that can be used to assess the hydraulic properties of fractured rock. Typically these techniques are based upon measurements of flow within packed-off sections within a borehole. One such technique that has been used extensively in the site investigation programme is the Posiva Flow Log (PFL) /Öhberg and Rouhiainen 2000/. The probe consists of a cable deployed flow sensor device flanked by two sets of flexible rubber disks pressing outwards on the borehole wall. The rubber disks serve as packers enabling flow to be measured from the isolated borehole section between the disks. The probe is deployed in the borehole and flow measurements are made in steps where the probe is winched upwards along the borehole in discrete, although overlapping steps usually while a hydraulic drawdown is maintained in the borehole by pumping. Based on the flow data obtained from these measurements it is possible to give estimates

of hydraulic transmissivities and conductive fracture frequencies down to a resolution of 5 m in PFL-s ("section measurement") mode and on a dm-scale in PFL-f ("flow anomaly") mode (see e.g. /Rhén et al. 2006ab/ for an explanation of the different measurement modes). The flow measurement data obtained during these investigations are translated to hydraulic transmissivities using Thiem's equation (i.e. assuming steady-state radial flow).

Another means for measuring the hydraulic properties of the rock is the Pipe String System (PSS) used within the site investigation. The system consists of a static "string" of flow measurement modules separated by packers to isolate each individual section in the borehole. In the site investigations the PSS equipment has been used to measure flows with test scales of 3 m, 5 m, 20 m, and 100 m. Flow data obtained from these measurements have been evaluated according to both transient and steady-state analysis techniques in order to obtain estimates of hydraulic transmissivity and conductivity (see e.g. /Rahm and Enachescu 2004b/ and /Ludvigson et al. 2004/ for details). Additional hydraulic tests that have been employed in the site investigations include those based on wire-line based measurement equipment employed during drilling as well as pumping tests. An overview of this technique is given in the reports by /Rhén et al. 2006ab/.

Measurements made using the PSS have a higher sensitivity than those made using the PFL method and it is likely that there are flow anomalies in the boreholes that have transmissivities below the limit of detection of PFL equipment. Analysis of high resolution PSS data (i.e. packer distance 5 m) therefore can give lower central moments for the calculated log-normal transmissivity distribution and higher conductive fracture frequencies than that obtained by analysis of PFL data if allowance isn't made for data censoring in PFL measurements. High resolution PSS measurement data is presently available for boreholes KLX02, KLX04, and KLX06 /Rhén et al. 2006ab/. The high spatial resolution data is somewhat sparse, however, and no attempt has been made thus far to interpret the data to ascertain conductive fracture frequencies. The transmissivity measurements, however, are broadly consistent with the data obtained from PFL measurements.

The specific flow-wetted surface or a_R (m^2/m^3) is the estimated surface area of flowing features per unit volume of rock and is calculated from geometrical-statistical treatment of the frequency of flowing fractures identified in a borehole (assuming that the measurement data is representative of the rock volume). If the dimensions of identified flowing features are assumed to be sufficiently large relative to the borehole diameter, the specific flow-wetted surface can be shown to be roughly four times the borehole conductive fracture frequency, P_{10c} (m^{-1}) for randomly oriented fractures /e.g. Gylling et al. 1998/. The conductive fracture frequency, P_{10c} (m^{-1}) is, of course, equal to the reciprocal of the average distance separating adjacent flowing features, H (m):

$$a_R \approx a_{R0} = 4/H \qquad (3\text{-}4)$$

Here, we also note that the specific flow-wetted surface, a_{R0} as defined above is only an approximation of the "true" flow-wetted surface, a_R. We make the distinction in order to indicate that the value of a_R is additionally dependent upon assumptions concerning flow channel dimensions that are difficult to specify a priori. This is discussed in more detail in Appendix E, although for the purposes of the present discussion, we shall assume that the assumption holds for the cases examined here.

The conductive fracture frequency can be estimated from PFL flow anomaly statistics if it is assumed that the distribution of flow conductors is Poissonian. This is actually a tacit assumption in most hydro-DFN models. The conductive fracture frequency is calculated by either numerically fitting the Poisson distribution to the PFL flow anomaly data, or by estimating the Poisson frequency parameter directly from the identified number of non-conductive test sections. The data presented in this analysis have been calculated using the

latter procedure, although both should give similar results. Although the distribution of flow conductors is assumed to be Poissonian, other statistical distributions could theoretically be used if they were shown to more accurately describe the borehole data.

The approximated specific flow-wetted surface, a_R and two-sided, 95% binomial confidence intervals for the statistical uncertainty in a_R (see /Crawford et al. 2003/ and Appendix E for details) are given in Table 3-2 below for various boreholes in the Laxemar subarea.

Table 3-2. Mean specific flow-wetted surface, a_R (m^2/m^3) estimated from PFL measurements for different boreholes in the Laxemar sub-region (deterministic deformation zones excluded). Data is given for upper 450 m of rock as well as for entire borehole as indicated by the upper (Secup) and lower (Seclow) bounds of the tested section. Two-sided, 95% binomial confidence intervals are also given for the specified borehole data.

Borehole ID	Secup (m)	Seclow (m)	Test scale (m)	Sample size	H (m)	$\overline{a_R}$ (m^2/m^3)	95% conf. int.
KLX02	204.42	405.42	3	68	3.0	1.33	0.94–1.83
KLX03	101.3	992.42	5	161	25.2	0.16	0.11–0.23
	101.3	450	5	70	12.6	0.32	0.21–0.50
KLX04	100.2	986.22	5	148	12.1	0.33	0.25–0.45
	100.2	450	5	60	6.9	0.58	0.41–0.87
KAV04A	100.16	996.17	5	168	10.6	0.38	0.29–0.48
	100.16	450	5	70	11.9	0.34	0.23–0.52

The data in Table 3-2 are based upon PFL-f data binned in 3 m sections as reported in the appendices of the individual data reports (/Rouhiainen 2000, Ludvigson et al. 2002, Rouhiainen et al. 2005, Rouhiainen and Sokolnicki 2005, Sockolnicki and Rouhiainen, 2005/). Only data in borehole sections outside of deterministic deformation zones (DZ) have been included in the compiled statistics. The deformation zones are as defined in /Hermanson et al. 2005/ for KLX02, KLX03, and KLX04. Borehole KLX02 has one deformation zone extending from 748–936 m. For KLX03 there is also only one deformation zone in the lower part of the borehole (770–960 m). KLX04 has five smaller deformation zone regions in the upper 450 m and one large zone in the lower part of the borehole (873–973). The exclusion of these regions appears to have only a very minor impact upon estimated transmissivity distributions and conductive fracture frequencies.

The actual specific flow-wetted surface is sensitive to the average width of flow channels residing within fractures. The width of these channels is unknown although speculated to be in the range 0.1–0.5 m /e.g. Abelin et al. 1994, Birgersson et al. 1992, Moreno and Neretnieks 1989, SKB 2005b/. If the unknown flow channels are very narrow, on the order of 0.1 m, the actual specific flow-wetted surface may be as little as half of those values given in Table 3-2.

It is important to note that the confidence intervals given in the table only consider uncertainty related to the estimated value of the Poisson frequency parameter (see Appendix E) and do not have any relation to additional uncertainties relating to channelling effects as described above or measurement errors and bias.

The specific flow-wetted surface is a parameter of central importance for the estimation of transport resistance in fractured rock. Although this is only strictly true for a porous medium representation of flow and transport, we note that in systems where diffusive exchange with the rock matrix dominates the solute residence time distribution, the magnitude of the

surface area over which matrix diffusion takes place is a key entity governing transport. In flow and transport models based upon concepts other than a porous medium approach, the specific flow-wetted surface is not used directly as a model parameter. In DFN-modelling concepts, for example, the specific flow-wetted surface still appears implicitly in terms of the conductive fracture intensity, or P_{32c} (actually, $a_R = 2 \times P_{32c}$). For the same input data set and making allowances for basic differences in modelling assumptions, however, the various modelling approaches should reproduce the same average flow-wetted surface to flow ratio (F-factor) for the system as a whole, although not necessarily distributed the same way. The magnitude of the specific flow-wetted surface is therefore an indicator of the potential for solute-rock matrix interaction for a given flow system and has a strong qualitative significance for site understanding in this respect.

3.3.2 Evaluation of the F-factor using flow channelling models

In this section, two different conceptual models are used to make estimates of the mean F-factor and its distribution for Laxemar site specific data. These are the Channel Network Model (CNM) /Moreno and Neretnieks 1993, Gylling 1997/ and the Stochastic Multi Channel Model (MCM) /Neretnieks 2002/. Simulations have been made with both model concepts to evaluate the transport resistance distribution of the rock surrounding the repository.

The Channel Network Model (CNM)

In the CNM model concept it is assumed that fluid flow and solute transport take place in a network of interconnected channels. Using this simplification, a model is developed that does not need very detailed information.

Every channel member can connect to any number of other channel members, although an upper limit of six members intersecting at a point has been chosen in the current model version. Some of these channel members may have a conductivity that is so low that no connection is made. The use of six channel members is thus arbitrary, although partly based on the observation that both fracture intersections and channels in the fracture planes play an important role in conducting flow. For two fractures that intersect, it is assumed that there is at least one channel member in each fracture plane that may continue over the intersection line with the other fracture. In this way, up to four channel members in the fracture plane may intersect at one node if their trajectories coincide. For those intersections where the fracture intersection itself is conducting, two more members may be added, forming a six-member intersection. If there is more than one channel in a fracture, an independent intersection point will exist. This concept is illustrated in Figure 3-2 below where channels in the plane of one fracture can interconnect both with channels in the other plane as well as the flow conduit or “wormhole” along the line of plane intersection (i.e. an abutting or crossing fracture termination):

In the generic simulations prepared for this report, the conductances of individual channel members were assigned randomly from a log-normal distribution where the channel members are simply arranged in an orthogonal three-dimensional grid consisting of 101×101×101 nodes. The term “conductance” in this context is equal to the product of transmissivity and channel width. The current model, however, does not consider any correlation between channel length and conductance nor the possibility of a conduit with elevated transmissivity at the line of plane intersection. This is a weakness that will need to be addressed in due course in order to make proper comparisons with DFN model predictions (where length-transmissivity correlations are considered).

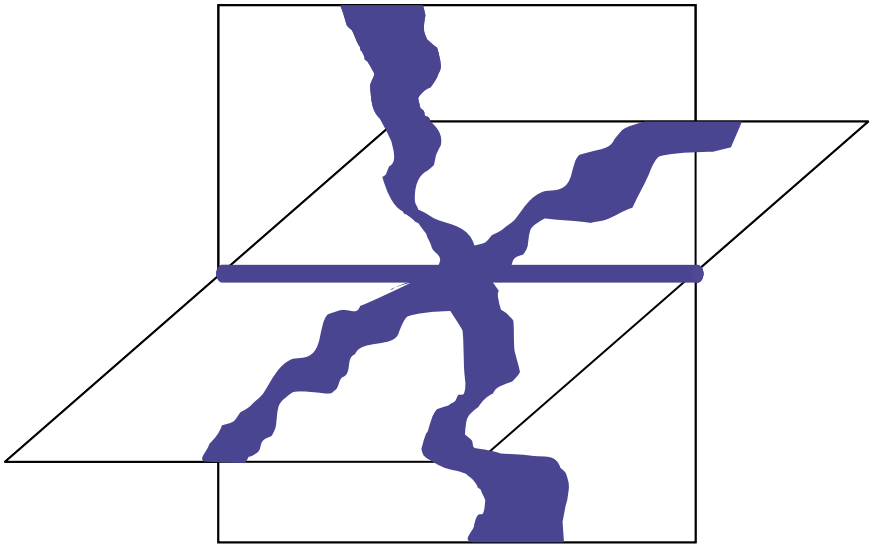

Figure 3-2. *Illustration of interconnected channels both within the fracture planes as well as at the line of fracture intersection giving at total of six channels emanating from a central "mixing node"*

Using a particle tracking technique, the F-factor distribution for an ensemble of transport paths can be calculated for different flow network realisations. Apart from the assumed distribution of flow (i.e. short and highly interconnected channels with stochastically generated transmissivities), the main assumption in this representation of transport is that full mixing is assumed at channel intersections. A detailed account of the calculation procedure is given in Appendix B.

The Stochastic Multi-Channel Model (MCM)

The Stochastic Multi-Channel Model (MCM) is essentially an extension of the first-order approximation described in Section 3.2. In this case, however, we assume that any radionuclides released from the repository instantaneously come in contact with a multitude of independent, non-mixing flow channels that extend all the way from the repository to the recovery location, here defined as the nearest deformation zone. The individual flow channels have transmissivities reflecting the measured transmissivity distribution obtained from borehole data. This is the same as estimating the F-factor using Equation 3-3, although extending the calculation to the entire transmissivity distribution.

In this case we make the same assumption as in the channel network model that all flow channels have the same length and width, although different hydraulic apertures. The main assumption for transport is that there is no mixing between channels which results in the initial variability between channels to persist along the entire transport path length.

Although the MCM represents a limiting case of extreme channelling that may not be physically realistic, it is interesting to note that it predicts a dispersion length that increases with transport distance (i.e. non-Gaussian dispersion); something that is consistent with field data obtained over a range of observation distances /e.g. Neretnieks 2002, and references therein/. The simple CNM described in the previous section, on the other hand, predicts a constant dispersion length (i.e. Gaussian dispersion) over different transport distances. It is possible to adapt the CNM to simulate non-Gaussian dispersion if channel members are used that have correlated channel length and transmissivity.

Comparison of simulation results

If the measured transmissivity distribution is assumed to be representative of individual flow channels, then the magnitude of the F-factor calculated using either the CNM or MCM approaches can be shown to be formally insensitive to flow channel width for any specified channel length. Owing to the short and highly interconnected nature of the flowpaths in the CNM, the calculated F-factor distribution tends to reflect the average flow properties of channel members making up the flowpath ensemble within the rock volume. The variance of the F-factor distribution is therefore somewhat dependent upon the number of channels and mixing nodes separating the release and recovery locations. This is contingent upon the choice of channel length, although it can be considered to be a secondary effect of flowpath discretisation. To illustrate the impact of different assumptions of average channel length, CNM simulations have been made using a range of channel lengths varying between 1–10 m.

Estimated site specific F-factor data, calculated using both the CNM and MCM approaches, are given in Table 3-3 below for a nominal path length of 100 m (i.e. straight line distance) and a representative hydraulic gradient of 0.5%.

Table 3-3. Estimated F-factor using site-specific data for various boreholes in the Laxemar subarea. Data is evaluated using a Channel Network Model (CNM) considering a range of possible channel lengths (L_c) and a Multi Channel Model (MCM). Both models consider an overall nominal path length of 100 m and a hydraulic gradient of 0.5%.

Borehole ID	Test Type	Test Scale (m)	$\log_{10}(T_m)$ (m^2/s)	L_c (m)	Model	$\text{Log}_{10}(F_{mean})$ (y/m)	$\text{Log}_{10}(F_{U10\%})$ (y/m)	$\text{Log}_{10}(F_{U1\%})$ (y/m)
KLX02	PFL-s	3	–9.32±1.27	1	CNM	6.86±0.16	6.67	6.51
				2	CNM	6.84±0.19	6.61	6.42
				5	CNM	6.80±0.25	6.50	6.25
				10	CNM	6.77±0.32	6.39	6.07
				100	MCM	6.42±1.27	4.92	3.64
	PSS	5	–10.5±2.50	1	CNM	7.94±0.30	7.59	7.29
				2	CNM	7.90±0.31	7.53	7.21
				5	CNM	7.84±0.40	7.37	6.96
				10	CNM	7.78±0.48	7.21	6.73
				100	MCM	7.60±2.50	4.64	2.13
KLX03	PFL-s	5	–10.5±2.19	1	CNM	7.97±0.27	7.65	7.38
				2	CNM	7.93±0.30	7.57	7.27
				5	CNM	7.87±0.39	7.42	7.03
				10	CNM	7.82±0.46	7.28	6.82
				100	MCM	7.60±2.19	5.01	2.81
KLX04	PFL-s	5	–8.5±1.62	1	CNM	6.01±0.20	5.78	5.57
				2	CNM	5.99±0.24	5.71	5.46
				5	CNM	5.94±0.31	5.57	5.26
				10	CNM	5.90±0.38	5.45	5.07
				100	MCM	5.60±1.62	3.68	2.05
	PSS	5	–8.5±2.00	1	CNM	5.98±0.25	5.69	5.44
				2	CNM	5.95±0.29	5.61	5.32
				5	CNM	5.90±0.37	5.46	5.10
				10	CNM	5.84±0.43	5.33	4.89
				100	MCM	5.60±2.00	3.23	1.22
KAV04A	PFL-s	5	–8.5±1.33	1	CNM	6.03±0.16	5.84	5.68
				2	CNM	6.02±0.20	5.78	5.58
				5	CNM	5.98±0.26	5.66	5.40
				10	CNM	5.94±0.33	5.55	5.22
				100	MCM	5.60±1.33	4.03	2.69

Notes: Estimates are based upon hydraulic conductivity distributions given in Table 8-8 and Table 8-9 in main SDM report /SKB 2006a/ which have been corrected for artefacts of data censoring.

Data is given in $\log_{10}$-units as the mean ± estimated standard deviation for the considered datasets.

$F_{U10\%}$ and $F_{U1\%}$ correspond to the top 10% and 1% most conductive paths based upon single-sided tolerance interval and 1,000 randomly sampled migration paths.

In Table 3-3 above, the data values $F_{U10\%}$ and $F_{U1\%}$ correspond to the F-factors where at most 10% and 1%, respectively, of randomly selected migration paths can be expected to have a lower F-factor. These are calculated using a single-sided 99% tolerance interval assuming a lognormal distribution of values and 1,000 randomly sampled migration paths (this is an arbitrary sample size although based upon the fact that 1,000 particles are used for particle tracking in the CNM simulations).

The transmissivity data given in Table 3-3 are taken from Table 8-8 and Table 8-9 in the main SDM report /SKB 2006a/ and are corrected for data censoring artefacts relating to the relatively high transmissivity cut-off ($T_{cutoff} \approx 10^{-9}$ m^2/s) of data obtained from PFL-s measurements (see the background report by /Rhén et al. 2006ab/ for more details).

These calculations also assume that the transmissivities of conductive features are not correlated in space, which may not always be accurate, particularly if multiple adjacent fractures are hydraulically well-connected. It should also be noted that the assumption of a spatially non-correlated distribution of conductive features in the rock volume is actually an implicit assumption underlying the Poisson distribution.

The mean F-factor calculated using the CNM model is slightly higher than that calculated using the MCM approach. This is at least partly due to the circuitous nature of the particle transport paths in the CNM simulations, although it is complicated by network channelling effects that give locally high flowrates along preferential flowpaths. Both the CNM and MCM models give mean F-factors that scale linearly with distance for the given set of underlying assumptions in the calculations. While the MCM model predicts a distribution with constant variance, the CNM model predicts a variance that decreases with transport distance for a given discrete channel length. As discussed previously, this is considered to be a secondary effect of flowpath discretisation, although we note that the predicted mean F-factor is for all practical purposes independent of the actual channel length used in the calculation.

A significant difference between calculations made with the CNM and MCM approaches is the magnitude of the estimated variance of the F-factor distribution and consequently also the calculated $F_{U10\%}$ and $F_{U1\%}$ values. The variance of the F-factor distribution calculated using the CNM is reduced considerably by the interconnectedness of the channel network whereas the MCM model has an F-factor variance that is the same as the original transmissivity distribution. If there is a strong positive correlation between transmissivity and characteristic fracture length, then we would expect the "actual" F-factor distribution in the rock to approach that of the MCM model for the fast migration paths. If there is no such correlation, on the other hand, we would expect the F-factor distribution to be more reminiscent of the results obtained using the CNM approach.

The large differences between the results obtained using the CNM and MCM models are not immediately obvious from the data in Table 3-3. A typical simulation result is shown in Figure 3-3 below for a hypothetical set of input data and clearly illustrates the differences between predictions made by the two modelling approaches:

For Safety Assessment the relevant issue is the spatial distribution of migration paths related to the scale of individual deposition holes rather than the ensemble of all possible migration paths as described above. The percentile of deposition holes with a low F-factor would not exactly equal the percentile of individual flow paths with this low F-factor in the rock volume as a whole, as a deposition hole could be intersected by a varying number of migration paths (varying from zero to several for each hole). Moreover, the F-factor for any given deposition hole would be dominated by the path with the lowest F-factor value intersecting the hole. DFN simulations incorporating a range of different modelling assumptions are needed to provide more quantified uncertainty ranges for application within Safety Assessment.

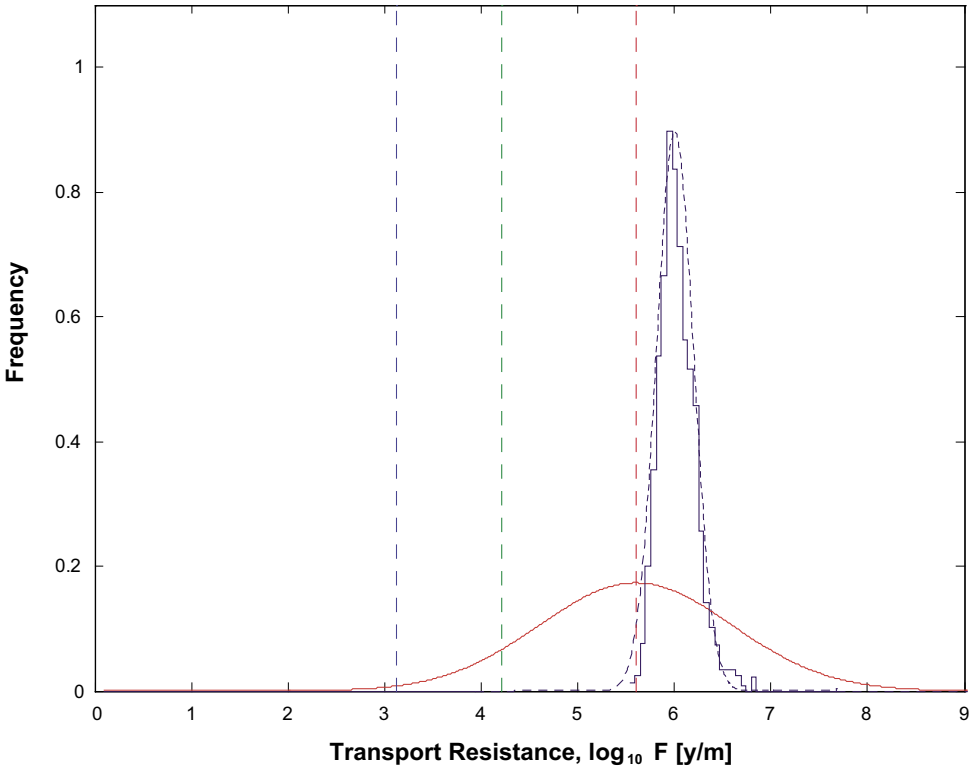

Figure 3-3. *F-factor distributions estimated using the CNM (blue curves) and MCM (red curve) modelling approaches for a mean log_{10}-transmissivity, $\mu_T = -8.5$, $\sigma_T = 1.0$, a channel length (L_c) of 3 m, and a nominal path length (L_p) of 100 m. The staircase plot contains raw CNM simulated data for one network realisation. The height of the staircase plot is rescaled to provide a better comparison with the lognormal approximation of the CNM data (broken blue curve). The vertical broken lines in the figure indicate the mean F-factor (red), $F_{U10\%}$ (green), and $F_{U1\%}$ (blue) estimated using the MCM.*

In spite of this, however, it is possible to make estimates of the consequence of this for individual deposition holes if we make some simplifying assumptions. For KLX03, for example, the distance between conductive features is estimated to be on the order of 25 m (see Table 3-2). Taken at face value, this would mean that on average 20% of the canister emplacements would be intersected by a conductive fracture (assuming a 5 m canister length and neglecting end effects). Owing to their larger diameter, however, the probability of a canister hole being intersected is greater than the frequency of conductive fractures identified from borehole statistics. For infinitely long and narrow flow channels, the relation between deposition hole intersection frequency (P_{10can}) and borehole intersection frequency (P_{10bh}) is:

$$P_{10can} = \left(\frac{d_{can}}{d_{bh}} \right) \cdot P_{10bh}$$

For a deposition hole with diameter, d_{can} = 1.5 m and borehole diameter, d_{bh} = 0.076 m, the flow channel intersection frequency for a canister emplacement is roughly 20 times greater than the borehole flowing fracture frequency. Even for more realistic channel widths in the range 0.1–0.5 m, the intersection frequency for a canister emplacement should still be 6–10 times greater than the borehole conductive fracture frequency (see Appendix C for details). It is noted that similar reasoning has been used in calculations presented in the preliminary safety evaluation (PSE) for the Forsmark site /SKB 2005b/.

For a repository containing 4,000 canister emplacements and assuming 0.1 m wide flow channels, up to 800 emplacements will be will be intersected by at least one conductive fracture with an F-factor greater than $F_{U10\%}$ and up to 80 of these emplacements will have at least one feature with an F-factor greater than $F_{U1\%}$. This estimation is based upon the borehole (KLX03) with the least number of flowing features as identified from PFL data. If the calculation was based upon data for the other boreholes, the channel intersection frequencies would be 2–3 times greater.

It should be remembered that the actual F-factor distribution for a given radionuclide release scenario is strongly dependent upon the connectivity of flowpaths leading from the deposition hole through the immediate far-field and is particularly sensitive to the number and transmissivity of flow channels initially encountered in the vicinity of a leaking canister. The "true" F-factor for transport from a leaking canister is therefore subject to a large degree of variation depending upon the probability of channels with various transmissivities intersecting a deposition hole and their connectivity with the wider fracture network. The simulation results presented in this Chpater are based upon average properties of the rock volume and do not specifically consider these stochastic aspects that are more of a Safety Assessment character.

3.3.3 Evaluation of the F-factor using a stream tube model

An alternative for making estimates of the F-factor is to use a stream tube model such as that commonly used in Safety Assessment studies (e.g. FARF31 /Norman and Kjellbert 1990, SKB 1999/). The F-factor for a stream tube is given by:

$$F = \frac{V_p a_R}{q} \qquad (3\text{-}5)$$

Where V_p (m^3) is the volume of the stream tube, a_R (m^2/m^3) is the specific flow-wetted surface, and q (m^3/y) is the flowrate. For an equivalent porous medium, the flowrate is given by:

$$q = KA_{xs}i \qquad (3\text{-}6)$$

The variable K (m/y) is the hydraulic conductivity of the rock, A_{xs} (m^2) is the average cross-sectional area of the stream tube, and i (m/m) is the hydraulic gradient used previously in Equation 3-2. Considering that the volume of the stream tube is equal to the product of its average cross-sectional area, A_{xs} (m^2) and its length, L_p (m) the F-factor can also be given as:

$$F = \frac{L_p a_R}{K\, i} \qquad (3\text{-}7)$$

For the simplified case where the stream tube is conceptualised as being made up of a "bundle" of independent flowpaths, it can be shown that Equation 3-3 and Equation 3-7 are identical (see Appendix D).

Estimates of the site specific F-factor can be made using Equation 3-7 with the specific flow-wetted surface data given in Table 3-2 and hydraulic conductivity data from Table 8-8 and Table 8-9 in the main SDM report /SKB 2006a/. These data are given in Table 3-4 below for a nominal path length of 100 m and a representative hydraulic gradient of 0.5%:

Table 3-4. Estimated F-factor using site-specific data for various boreholes in the Laxemar subarea using hydraulic conductivities given in Table 8-8 and Table 8-9. Data is evaluated using a stream tube model for a nominal path length of 100 m and a hydraulic gradient of 0.5%.

Borehole ID	Test Type	Test Scale (m)	Sample Size	$Log_{10}(K)$ (m^2/s)	a_R (m^2/m^3)	$Log_{10}(F_{mean})$ (y/m)
KLX02	PFL-s	3	398	–9.8±1.27	1.33	6.73
	PSS	5	49	–11.2±2.50	1.33	8.13
	PSS	20	48	–9.7±2.08	1.33	6.63
	PSS	100	8	–8.34±1.78	1.33	5.27
	PSS	100–300	11	–8.11±1.71	1.33	5.04
	PT	≈ 1,000	1	–7.1	1.33	4.03
KLX03	PFL-s	5	178	–11.2±2.19	0.16	7.21
	WLP	≈ 100	9	–8.0±0.69	0.16	4.01
	PT	≈ 1,000	1	–7.4	0.16	3.41
KLX04	PFL-s	5	177	–9.2±1.62	0.33	5.52
	PSS	5	77	–9.2±2.00	0.33	5.52
	PSS	20	44	–8.7±1.99	0.33	5.02
	PSS	100	9	–8.1±1.92	0.33	4.42
	PT	≈ 1,000	1	–6.8	0.33	3.12
KAV04A	PFL	5	179	–9.2±1.33	0.38	5.58
	PSS	20	42	–8.2±1.44	0.38	4.58
	PSS	100	9	–7.9±1.64	0.38	4.28
	PT	≈ 1,000	1	–7.6	0.38	3.98

Notes: Estimates are based upon hydraulic conductivity distributions given in Table 8-8 and Table 8-9 in the main SDM report /SKB 2006a/ which have been corrected for data censoring artefacts. Data for specific flow-wetted surface, however, is derived from raw PFL data set (deterministic deformation zones excluded).

Data is given in log_{10}-units as the mean ± estimated standard deviation for the considered datasets.

$F_{U10\%}$ and $F_{U1\%}$ are not calculated owing to that individual stream tubes have uniquely defined F-factors. The uncertainty in the central mean of the F-factor is, however, equal to the standard deviation of the hydraulic conductivity distribution provided the specific flow-wetted surface and the hydraulic conductivities are correctly estimated.

The results obtained using a stream tube model are strongly dependent upon the scale of measurement for the hydraulic conductivity as well as the estimated value of the specific flow-wetted surface. Generally, a larger measurement interval gives a higher hydraulic conductivity and consequently lower estimates of the F-factor. An additional uncertainty in this analysis is that Posiva Flow Log (PFL) data is used to obtain the specific flow-wetted surface, whereas the hydraulic conductivities are obtained using different methods. As methods such as the Pipe String System (PSS) and pump tests (PT) typically have higher sensitivities than the PFL method, there is a potential disparity between the data values used as a basis for the calculations.

The combination of PFL-derived flow-wetted surface estimates with more sensitive measurements of hydraulic conductivity gives F-factors that could be considered too low when taken at face value. Given that fast flowpaths will tend to dominate solute transport processes, however, this is not a major consideration as the hydraulic conductivity measured over larger scales (e.g. 20–100 m) will be mostly dominated by the major conducting flowpaths which are also the basis of the PFL data estimates of the specific flow-wetted surface.

It should be noted that if high spatial resolution, PFL transmissivity data are used directly in calculations, the appropriate scale for stream tube calculations is significantly larger than the 3–5 m packer separation given in Table 3-4 owing to the requirement that individual flow channels do not intersect the walls of the stream tube. The summation of PFL data over intervals larger than 5 m typically gives higher overall hydraulic conductivities and consequently lower F-factors than the data for the 5 m scale would otherwise suggest. The increase in effective hydraulic conductivity over increasing borehole test length-scales is supported by the transmissivity data presented in /Rhén et al. 2006ab/ where it is shown that the summation of PFL data to interval lengths corresponding to PSS measurements give consistently similar hydraulic conductivities to those obtained using PSS.

4 Modelling in support of transport property evaluation

4.1 Overview of the basic transport retardation model

The retardation model as defined by /Widestrand et al. 2003/ refers specifically to the descriptive set of material properties for typical rock types and structures at a site. Apart from numerical material property data, the model includes rock type description as well as a description of typical alteration layers associated with fractures and fracture zones. The properties of significance for the retardation model are matrix porosities, effective diffusivities, and sorption data for the different materials and target radionuclides. Sorption is assumed to be a reversible linear process and data is given in the form of sorption distribution coefficients (K_d-values).

In addition to the data for major rock types and their alteration forms, the retardation model detailed in the Bedrock Transport Properties SDM for the Laxemar subarea /Byegård et al. 2005/ considers different fracture categories to account for different kinds of fracture coatings and alteration types encountered in the site investigations. There are four specific fracture types, A–D considered in the model that are derived from core mapping observations. Fracture type A is a typical background fracture with chlorite and calcite as major fracture coating materials. The fracture coating is customarily less than 0.5 mm in thickness and overlies essentially unaltered rock. Fracture types B and C consist of a fracture coating ($\leq$ 0.5 mm) and a layer of altered rock on the order of 0.5 mm – 5 cm in thickness overlying unaltered matrix rock. The fracture coating for fracture type B is similar in composition to fracture type A. The fracture coating for fracture type C contains hematite in addition to chlorite and calcite. Fracture type D has a fracture coating of up to 1 mm in thickness and an altered layer 1 mm to $\geq$ 5 cm deep. According to the presently available data the different fracture coatings and the presence or absence of particular fracture coatings is not correlated with different major rock types or rock domains.

4.2 Generic analysis of rock transport properties

As discussed in Section 2.2.3 there is a considerable degree of uncertainty regarding the parameterisation of altered rock materials relative to unaltered rock in both the Laxemar and Simpevarp version 1.2 site descriptive models. It has furthermore been speculated that the apparently weaker retention properties of altered rock in the Simpevarp SDM may be an artefact of the data import where material properties measured for site specific materials have been pooled with imported data in only a partially consistent manner.

Based upon the data from the TRUE programme (see Table 2-3 and associated discussion) it is believed that for correctly matched data the altered layers should have enhanced retention properties relative to the unaltered rock matrix. This, however, has not yet been established for the site investigation areas using measurement data and therefore is only a tentative hypothesis. As outlined previously, the notion of retention property enhancement or reduction as discussed in this report is based upon consideration of both diffusive and sorptive properties by way of the magnitude of the material properties group, MPG.

Owing to the uncertainty concerning the material properties of altered rock materials relative to unaltered rock, generic simulations have been made using a model for solute transport where alteration layers are explicitly considered. The model is based upon an analytical solution in Laplace space with numerical inversion to obtain the solution in the time plane (see Appendix F for details). The model is generalised to handle solute transport and matrix interaction with an arbitrary number of layers of altered rock and includes the possibility of simulating mass transfer to stagnant zones in the fracture plane with additional matrix interaction as well as equilibrium or non-equilibrium mass transfer to fracture infilling material (fault gouge). It is also feasible to simulate solute transport in features with non-symmetrical matrix properties as may be appropriate for modelling complex fractures or deformation zones.

In the present report, however, we have used the model to explore the dynamics of solute transport in an idealised fracture system characterised by only two layers; an alteration layer with a thickness of 5 cm and a limited unaltered rock matrix with a depth of 0.5 m. This is mostly intended to be an illustrative exercise to demonstrate how material property parameters influence the residence time distribution (RTD) of migrating solutes (both sorbing and non-sorbing). The RTD calculated in the generic simulations in this report correspond to the cumulative recovery breakthrough curve for a Dirac pulse injection, although the curves can also be interpreted as a relative concentration breakthrough curve for a constant concentration release scenario.

The RTD of a solute is sensitive to the multilayer parameterisation of the rock matrix to varying degrees depending upon the value of the F-factor. A very small F-factor allows little time for the solute to penetrate the rock matrix and the material properties of the outermost altered layers may then dominate the solute RTD. A large F-factor, on the other hand, results in equilibration of the outer, altered layers of the rock matrix and the material properties of more deeply lying, unaltered rock layers may then be dominating. In the extreme, where solute penetrates the entire depth of the connected rock matrix, the ultimate matrix depth may be the limiting factor. In such cases, the F-factor may not even be a relevant parameter and it is the equilibrium storage capacity of the rock that governs the solute retardation.

In the following sections, we detail these effects for the simple case of a single flowpath as well as the more general case of a multiple flowpath system such as that conceptualised in the MCM and CNM models described previously in Section 3.3.2

4.2.1 Transport properties of a single flowpath

To illustrate the interdependent effects that rock matrix parameterisation and F-factor have upon the transport of solutes, simulations have been made considering typical F-factors likely to be encountered under repository conditions for three solutes with differing sorptive properties. As discussed previously in Section 2.2.3, the relation between the material properties of the altered rock layers and the underlying unaltered rock matrix is given by the ratio, R_{12} which is defined as:

$$R_{12} = \frac{MPG_{\text{altered layer}}}{MPG_{\text{matrix}}} \quad \begin{cases} R_{12} > 1 & \Rightarrow \; MPG_{\text{altered layer}} > MPG_{\text{matrix}} \\ R_{12} < 1 & \Rightarrow \; MPG_{\text{altered layer}} < MPG_{\text{matrix}} \end{cases} \qquad (4\text{-}1)$$

Values of R_{12} in the range 0.35–2.4 were predicted from the recommended data given in Table 2-3 from the Simpevarp 1.2 SDM and the Äspö/TRUE program, although these values are now considered to be extremely uncertain.

In the simulations detailed in the following sections, the impact that the altered layer has upon the transport of solute has been tested by setting the value of R_{12} at three different levels (i.e. R_{12} = 0.1, 1, 10) relative to the MPG of the unaltered rock matrix which was fixed for the simulations. This span of values is thought to cover the range of variation that is reasonably expected for the altered rock found in the site investigation areas.

For Safety Assessment purposes, alteration layers with reduced retention properties relative to the unaltered rock matrix (i.e. "unfavourable" retention properties) generally give shorter breakthrough times for transported solutes as compared with simulation results where the alteration layers are neglected or have similar material properties to the unaltered rock. If, on the other hand, the retention properties of the alteration layers are enhanced relative to the unaltered rock matrix (i.e. "favourable" retention properties), longer breakthrough times are expected for transported solutes. Altered rock having a similar MPG to the unaltered rock matrix is referred to here as having "neutral" retention properties relative to the host rock. It is noted here, however, that the notion of favourable and unfavourable retention properties depends upon the context of the transport scenario envisaged. It should also be noted that the inclusion or neglection of alteration layers has consequences for the remobilisation of radionuclides (resulting from changes in chemical or physicochemical conditions). If altered layers are incorrectly parameterised or neglected in Safety Assessment calculations then the actual amount, peak load, and release timing of a radionuclide that is remobilised may be subsequently estimated inaccurately.

For the simulations, the total diffusion accessible rock matrix was set to 0.5 m with an alteration layer assumed to be 5 cm thick. The thickness of the alteration layer is arbitrary although in concordance with the retardation model for different fracture types as presented in the SDM /SKB 2006a, Byegård et al. 2006/. As outlined in /Löfgren 2004/ the diffusion-accessible rock matrix porosity is considered to be connected over substantial distances into the rock matrix and there is no maximum penetration depth that has been corroborated by field or laboratory measurements. In Safety Assessment calculations, however, the maximum penetration depth is typically based upon half the spacing of hydraulically conductive fractures in order that the overall sorption capacity of the system is not exceeded.

Weakly sorbing solutes

Simulations of a weakly sorbing solute ($K_{dm} = 10^{-5}$ m^3/kg) were made for three different F-factors in the range $10^4 – 10^6$ y/m and R_{12} values varying from 0.1 – 10. In all simulations, the free diffusivity in water, D_w has been assumed to be 10^{-9} m^2/s and the water residence time, t_w has been arbitrarily set to 10 y. The residence time distribution (RTD) curves are shown in Figure 4-1, Figure 4-2, and Figure 4-3 below (where the subscript *m* refers to the corresponding property of the unaltered rock matrix):

The simulation results indicate very poor retardation for weakly sorbing solutes and for systems where the alteration layer is parameterised with weaker retention properties than the rock matrix itself, retardation is for all practical purposes non-existent. For F-factors on the order of 10^6 y/m or higher and with favourable retention properties, the retardation effect is more tangible. In Figure 4-2 and Figure 4-3, mauve coloured breakthrough curves are also given for the central case (i.e. R_{12} = 1.0) although with an infinite matrix. When compared with the red curve for a limited matrix, the matrix saturation effect obtained at later times is clearly illustrated. This is a consequence of the maximum penetration depth of 0.5 m assumed for the calculations. Although the solute considered in these simulations is essentially non-sorbing, the solute RTD is found to be largely independent of the water residence time given a sufficiently high F-factor (e.g. F ≥ 10^6 y/m) and for alteration layers with neutral to favourable retention properties.

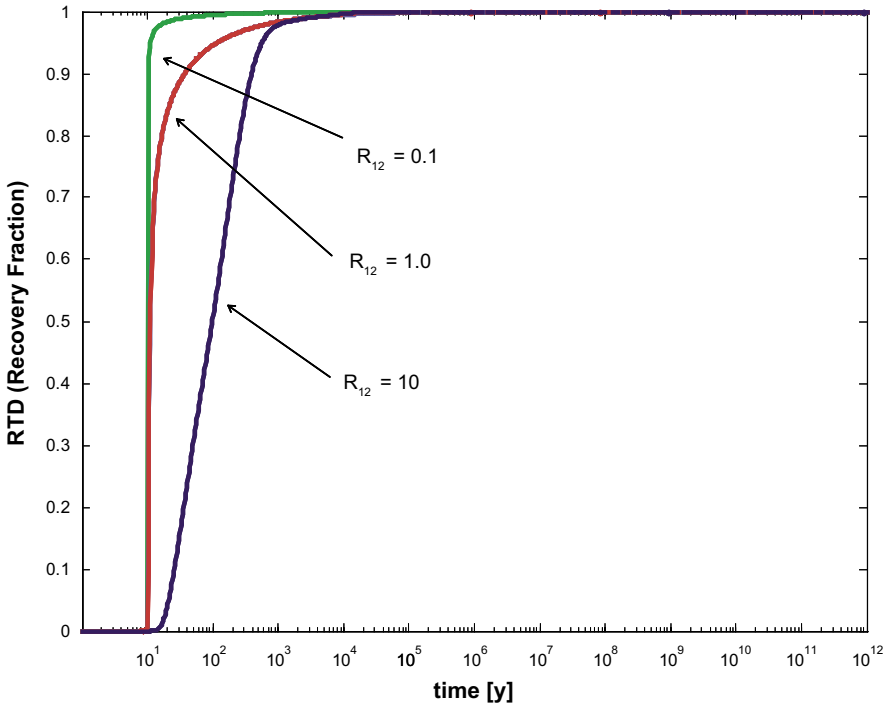

Figure 4-1. *Simulated RTD's for a weakly sorbing solute* $\mathbf{K_{dm}} = 10^{-5}$ *m³/kg in a system with a 2-layer, limited matrix. The simulations consider an altered layer thickness of 5 cm, a total matrix depth of 0.5 m, an unaltered rock formation factor of* $F_{fm} = 10^{-5}$*, an F-factor of* 10^{4} *y/m, and water residence time* $t_w = 10$ *y. Different case studies for the alteration are indicated in the figure relative to unaltered rock matrix.*

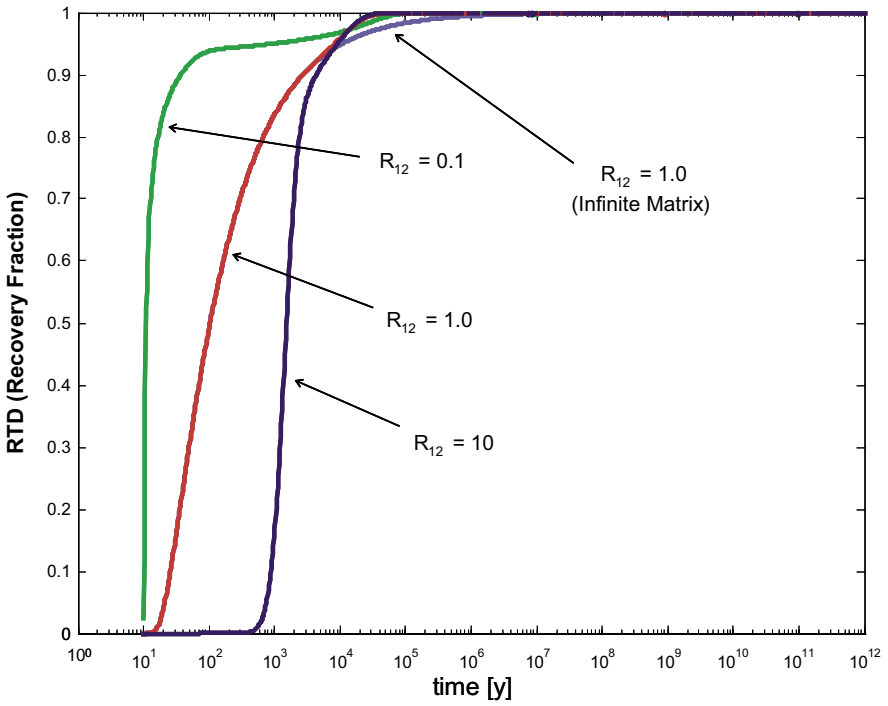

Figure 4-2. *Simulated RTD's for a weakly sorbing solute* $\mathbf{K_{dm}} = 10^{-5}$ *m³/kg in a system with a 2-layer, limited matrix. The simulations consider an altered layer thickness of 5 cm, a total matrix depth of 0.5 m, an unaltered rock formation factor of* $F_{fm} = 10^{-5}$*, an F-factor of* 10^{5} *y/m, and water residence time* $t_w = 10$ *y. Different case studies for the alteration are indicated in the figure relative to unaltered rock matrix.*

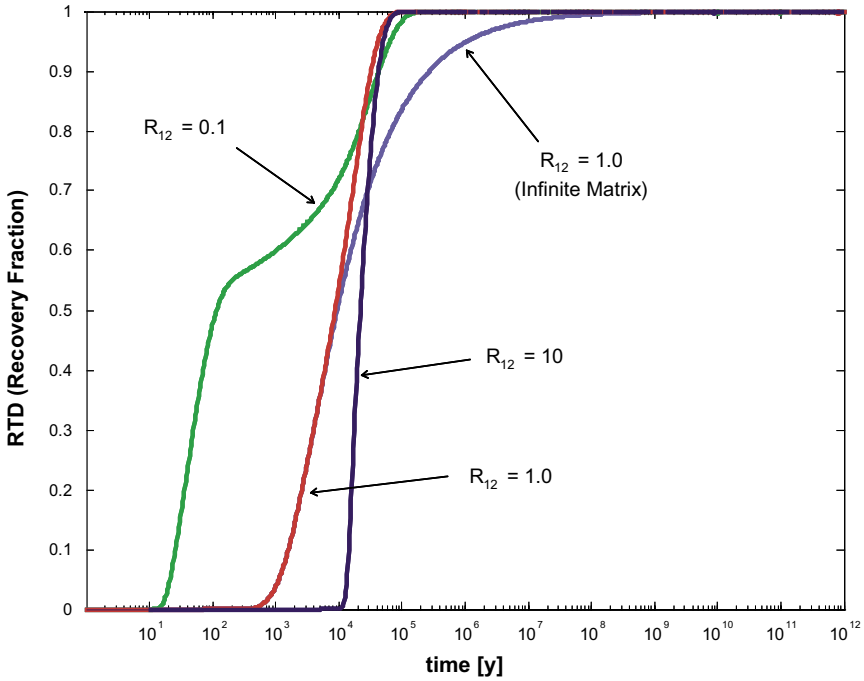

Figure 4-3. *Simulated RTD's for a weakly sorbing solute* $\boldsymbol{K_{dm}} = 10^{-5}$ *m³/kg in a system with a 2-layer, limited matrix. The simulations consider an altered layer thickness of 5 cm, a total matrix depth of 0.5 m, an unaltered rock formation factor of* $F_{fm} = 10^{-5}$*, an F-factor of* 10^6 *y/m, and water residence time* $t_w = 10$ *y. Different case studies for the alteration are indicated in the figure relative to unaltered rock matrix.*

Moderately sorbing solutes

Simulated residence time distribution (RTD) curves are shown in Figure 4-4, Figure 4-5, and Figure 4-6 below for a typical, moderately sorbing solute (K_d = 0.01 m³/kg). The same F-factor, R_{12} and matrix depth parameter values were used for these simulations as for the previously defined case studies.

It was found in the simulations for the moderately sorbing solute that the method used for numerical inversion of the Laplace space solution occasionally could not find a solution for certain parameter combinations. This was identified to be due to floating point overflow involving exponential functions native to the Laplace space solution and was typically a problem at short times when the solute would not have had sufficient time to penetrate the alteration layer to reach the underlying rock matrix. In these situations it was found that the analytical solution given by /Tang et al. 1981/ for a single matrix layer parameterised with the material properties of the altered rock could give the missing part of the breakthrough curve with negligible error. The breakthrough curve segments approximated in this manner are indicated in the figures as broken lines. It should be noted that the agreement between the approximated part of the RTD and that calculated using the full multilayer solution was exceptionally good and essentially identical curve slopes are obtained at the point of intersection of the curves.

The simulation results indicate a substantial solute retardation effect that scales approximately with the square of the F-factor if comparing recovery times for 50% of the released solute (i.e. t_{50}) in the central case. For F = 10^4 y/m, for example, the $t_{50\%}$ recovery time is on the order of 10^3 y. For F = 10^5 y/m we have a corresponding recovery time of 10^5 y and for F = 10^6 y/m the recovery time increases to as much as 10^7 y. The RTD of the solute is for all practical purposes independent of the water residence time over the entire range of F-factors

tested, with the possible exception of the extreme case of unfavourable retention properties and F $\leq 10^5$ y/m. Similarly to the results obtained for the weakly sorbing solute, a matrix saturation effect is seen for higher F-factor values and late breakthrough times.

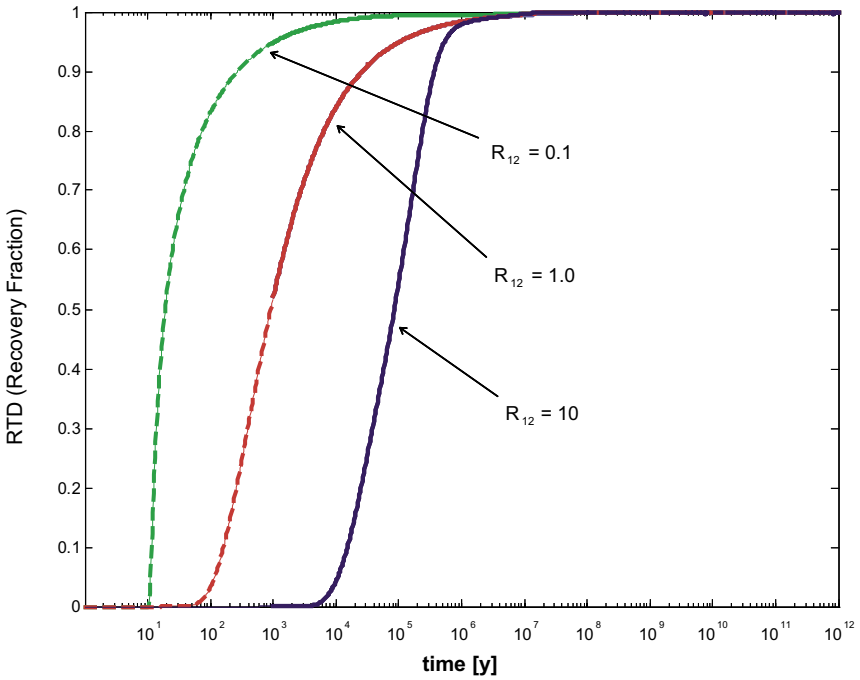

Figure 4-4. *Simulated RTD's for a moderately sorbing solute* $\boldsymbol{K_{dm}}$ *= 0.01 m³/kg in a system with a 2-layer, limited matrix. The simulations consider an altered layer thickness of 5 cm, a total matrix depth of 0.5 m, an unaltered rock formation factor of* $F_{fm} = 10^{-5}$*, an F-factor of* 10^4 *y/m, and water residence time* $t_w = 10$ *y. Different case studies for the alteration are indicated in the figure relative to unaltered rock matrix.*

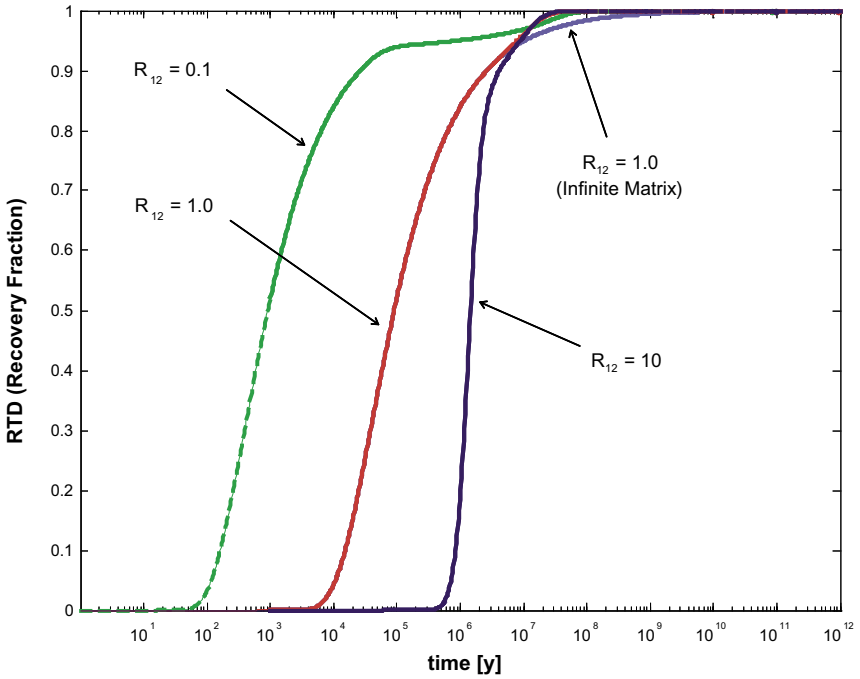

Figure 4-5. *Simulated RTD's for a moderately sorbing solute* $\boldsymbol{K_{dm}}$ *= 0.01 m³/kg in a system with a 2-layer, limited matrix. The simulations consider an altered layer thickness of 5 cm, a total matrix depth of 0.5 m, an unaltered rock formation factor of* $F_{fm} = 10^{-5}$*, an F-factor of* 10^5 *y/m, and water residence time* $t_w = 10$ *y. Different case studies for the alteration are indicated in the figure relative to unaltered rock matrix.*

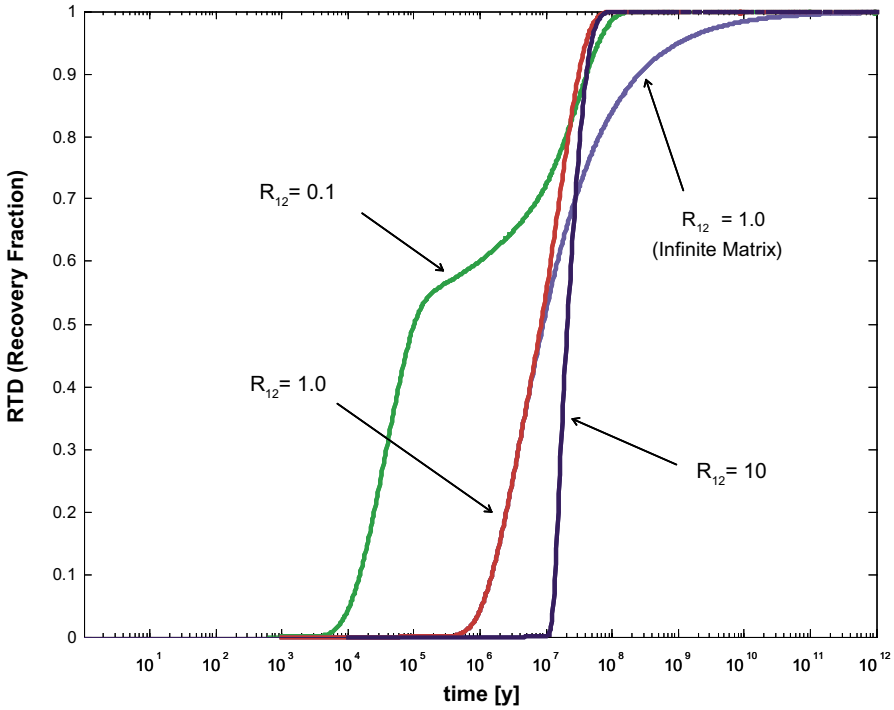

Figure 4-6. *Simulated RTD's for a moderately sorbing solute* $\mathbf{K_{dm}}$ *= 0.01 m³/kg in a system with a 2-layer, limited matrix. The simulations consider an altered layer thickness of 5 cm, a total matrix depth of 0.5 m, an unaltered rock formation factor of* $F_{fm} = 10^{-5}$*, an F-factor of* 10^6 *y/m, and water residence time* t_w *= 10 y. Different case studies for the alteration are indicated in the figure relative to unaltered rock matrix.*

Strongly sorbing solutes

Simulated residence time distribution (RTD) curves are shown in Figure 4-7, Figure 4-8, and Figure 4-9 below for a typical, strongly sorbing solute (K_d = 1.0 m³/kg). The same F-factor, R_{12} and matrix depth parameter values were used for these simulations as for the previously defined case studies.

As described previously, it was found that the method used for numerical inversion of the Laplace space solution occasionally could not find a solution for certain parameter combinations. In these simulations, the missing part of the breakthrough curve segments were approximated using the analytical solution given by /Tang et al. 1981/ and are indicated in the figures as broken lines.

Once again, the simulation results give clear indications of solute retardation that scales with the square of the F-factor if comparing recovery times for 50% of the released solute (i.e. $t_{50\%}$) in the central case. For F = 10^4 y/m, the $t_{50\%}$ recovery time is on the order of 10^5 y. For F = 10^5 y/m we have a corresponding recovery time of 10^7 y and for F = 10^5 y/m the recovery time is on the order of 10^9 y. The RTD of the solute is for all practical purposes independent of the water residence time over the entire range of F-factors tested. Similarly to the results obtained for the other simulated solutes, a matrix saturation effect is seen for higher F-factor values and late breakthrough times. It should be noted that the matrix saturation effect appears to be identical for weakly, moderately, and strongly sorbing solutes which is highly suggestive of commensurate solute penetration in each case.

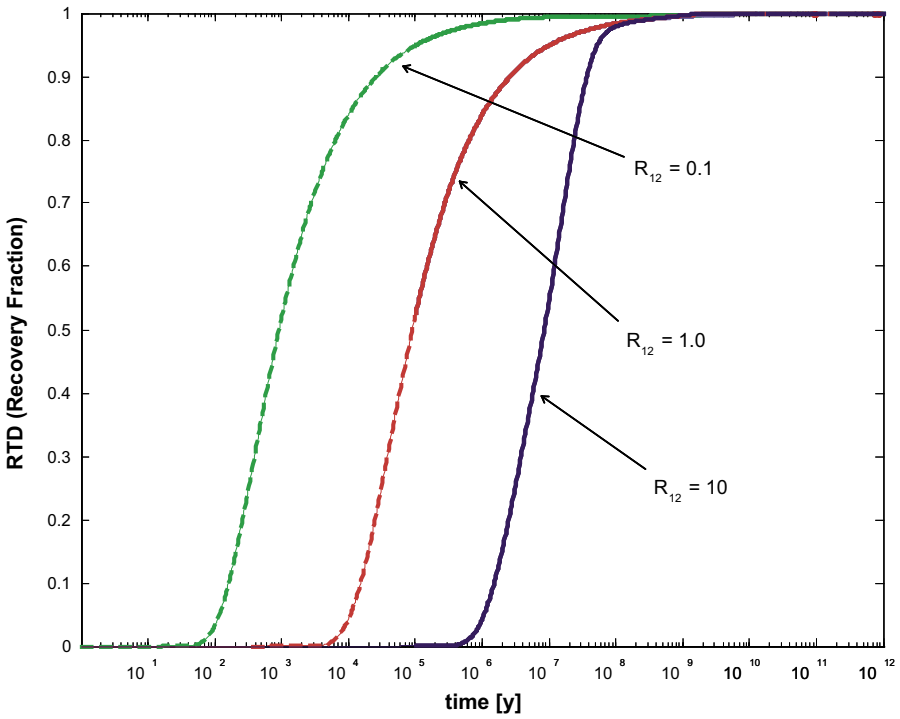

Figure 4-7. *Simulated RTD's for a strongly sorbing solute* $\boldsymbol{K_{dm}}$ *= 1.0 m³/kg in a system with a 2-layer, limited matrix. The simulations consider an altered layer thickness of 5 cm, a total matrix depth of 0.5 m, an unaltered rock formation factor of* $F_{fm} = 10^{-5}$*, an F-factor of* 10^{4} *y/m, and water residence time* $t_w = 10$ *y. Different case studies for the alteration are indicated in the figure relative to unaltered rock matrix.*

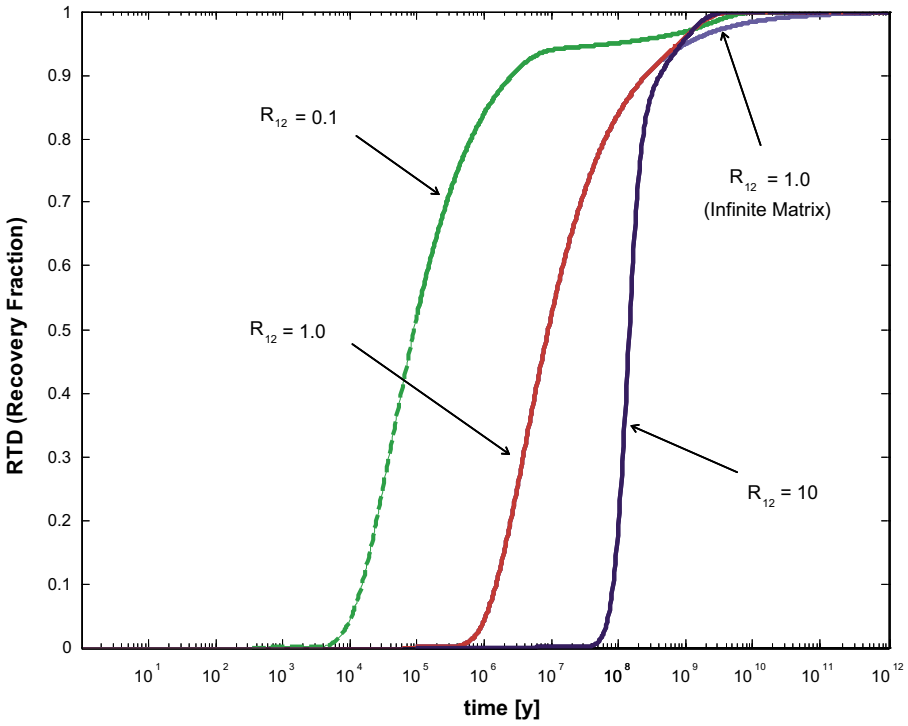

Figure 4-8. *Simulated RTD's for a strongly sorbing solute* $\boldsymbol{K_{dm}}$ *= 1.0 m³/kg in a system with a 2-layer, limited matrix. The simulations consider an altered layer thickness of 5 cm, a total matrix depth of 0.5 m, an unaltered rock formation factor of* $F_{fm} = 10^{-5}$*, an F-factor of* 10^{5} *y/m, and water residence time* $t_w = 10$ *y. Different case studies for the alteration are indicated in the figure relative to unaltered rock matrix.*

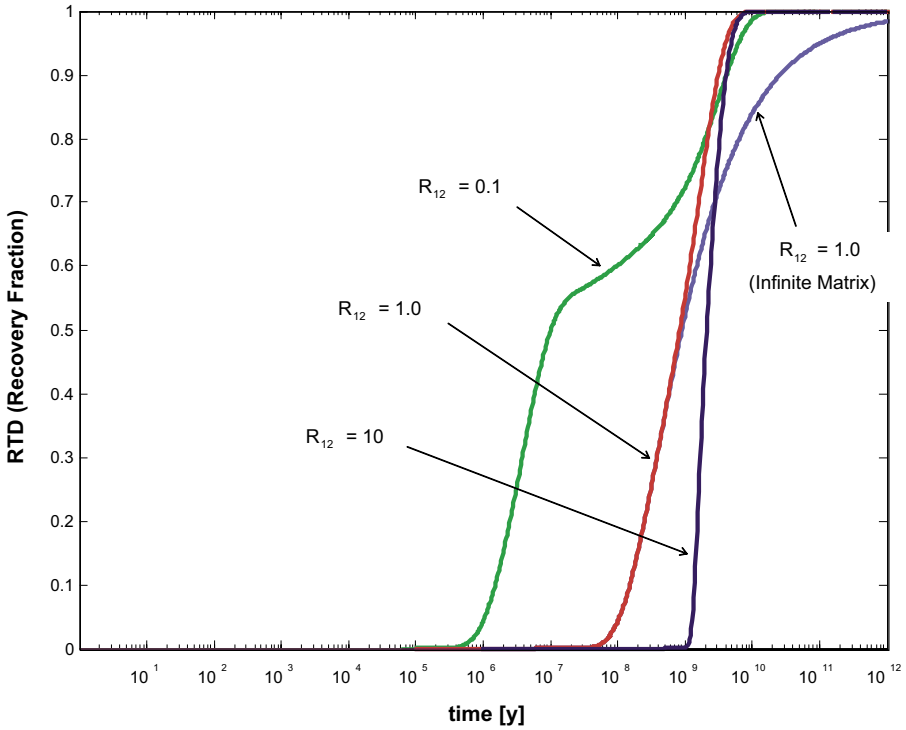

Figure 4-9. *Simulated RTD's for a strongly sorbing solute* $\boldsymbol{K_{dm}}$ *= 1.0 m³/kg in a system with a 2-layer, limited matrix. The simulations consider an altered layer thickness of 5 cm, a total matrix depth of 0.5 m, an unaltered rock formation factor of* $F_{fm} = 10^{-5}$*, an F-factor of* 10^6 *y/m, and water residence time* t_w *= 10 y. Different case studies for the alteration are indicated in the figure relative to unaltered rock matrix.*

The material properties group (MPG) as a key parameter

In simple calculations of solute transport involving a single matrix layer, the analytical solution for solute residence time distribution, $C(t)/C_0$ for a constant concentration boundary condition can be shown to be /Tang et al. 1981/:

$$\frac{C(t)}{C_0} = \begin{cases} 0 & \text{for } t \le R_* t_w \\ erfc\left[\dfrac{W_c L_p}{q}\sqrt{\dfrac{D_e K_d^* \rho_b}{t - R_* t_w}}\right] & \text{for } t > R_* t_w \end{cases} \qquad (4\text{-}2)$$

The term R_* is a retardation factor that describes instantaneous equilibrium sorption on the external fracture surface. If we neglect the role of equilibrium sorption on fracture coatings, the strength of matrix interaction for a given solute is then determined by the material properties group, or MPG (m/y^{½}), which has previously been defined in Section 2.2.1 as:

$$MPG = \sqrt{D_e K_d^* \rho_b} \qquad (4\text{-}3)$$

For more complex representations of solute transport, however, which may involve multiple layers of altered rock with differing material properties, the Laplace space solution (see Appendix F) does not exclusively use the MPG as the only variable describing the material

properties of the rock. Indeed, the Laplace space solution typically includes a recursive set of equations incorporating both the MPG terms as well as the terms, A_i ($y^{½}$/m) for each rock layer which are defined as:

$$A_i = \sqrt{\frac{K_d^{*(i)}\rho_b^{(i)}}{D_e^{(i)}}} = \frac{1}{\sqrt{D_a^{(i)}}} = \frac{MPG_i}{D_e^{(i)}} \qquad (4\text{-}4)$$

The term D_a in Equation 4-4 is the so-called solute apparent diffusivity. Although we can say with certainty that the relevant material properties variable in Equation 4-2 is the MPG, it is not entirely clear in more complex, layered systems whether this is always the case, nor if this in addition to the ratio of MPG values (i.e. R_{12} as defined in Equation 4-1) uniquely describes the relative transport properties of the system.

To answer this question, simulations were performed where the formation factor, F_{fs} and sorption K_{ds} for the altered layer were independently varied over a range of two orders of magnitude relative to the unaltered rock matrix. The resulting response surfaces comparing the recovery times for 10% of the recovered solute are shown in Figure 4-10 for three different solutes with differing sorption strengths (i.e. weakly, moderately, and strongly sorbing as previously). For clarity, in the figure the subscript *s* refers to the alteration layer (or fracture "skin") and the subscript *m* refers to the unaltered rock matrix:

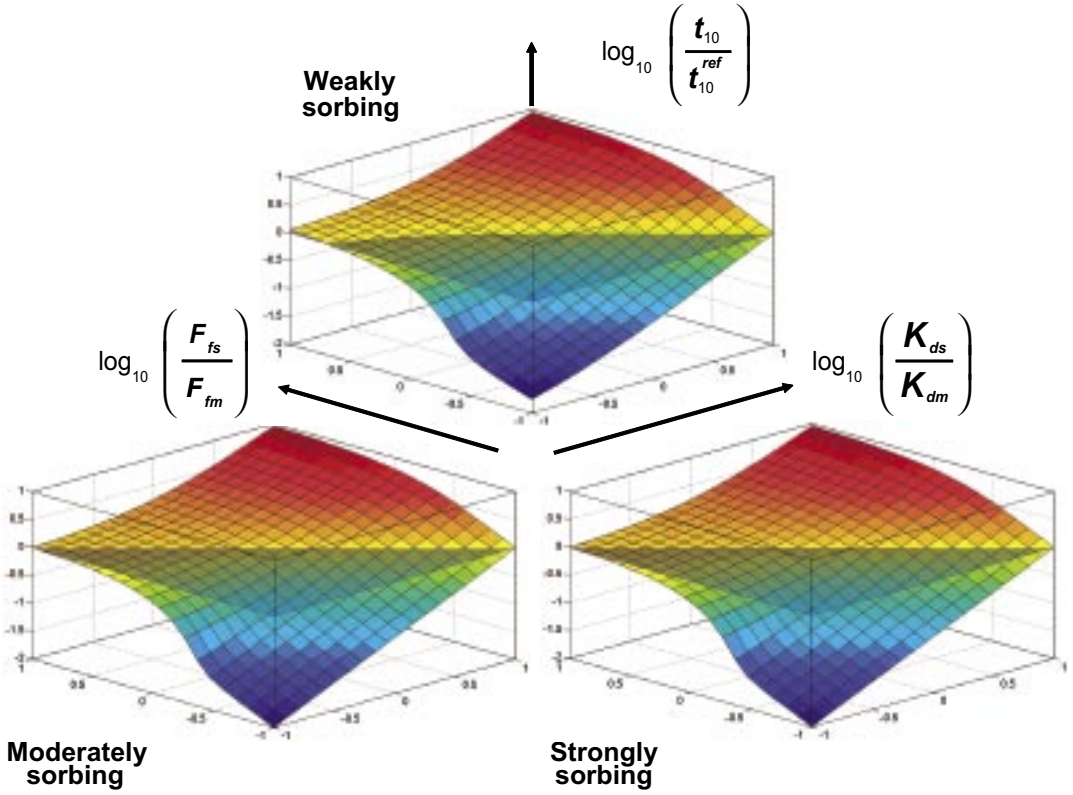

Figure 4-10. *Typical response surface for breakthrough of solute corresponding to 10% recovery and variable surface layer retention properties relative to 1-layer, unaltered rock matrix. Simulations consider the same solutes as for the previous figures in a system with a 2-layer, limited matrix (altered layer thickness of 5 cm, total matrix depth of 0.5 m, unaltered rock formation factor of $F_f = 10^{-5}$, an F-factor of 10^5 y/m, and water residence time $t_w = 10$ y).*

If the MPG value for the unaltered rock and the ratio of MPG values (R_{12}) for the altered and unaltered rock uniquely describe the transport properties of the two-layer system, we would expect the response surface to intersect the zero-level plane for (t_{10}/t_{10}^{ref}) along the diagonal corresponding to a constant MPG (i.e. where the altered rock layer has an identical MPG to that of the unaltered rock matrix). The grey feature in the foreground of the figure images is the zero level plane and, as can be seen for both moderately and strongly sorbing tracers, this is indeed the case. In practical terms this means that the case of enhanced sorption coupled with reduced effective diffusivity is indistinguishable from reduced sorption and enhanced effective diffusivity provided both cases are characterised by identical MPG values.

There is some deviation from this behaviour in the case of a weakly sorbing solute when K_{ds} is very low and F_{fs} is large (see centre top image in Figure 4-10). This is due to the fact that for such low sorption K_{ds} values, which correspond to essentially zero surface sorption, the storage capacity of the water filled pores becomes dominating. As the storage porosity and effective diffusivity are partially correlated, the sorption coefficient for the altered layer (K_{ds}) ceases to be a meaningful parameter for sorption and a deviation occurs. This, however, can be considered to be a secondary effect and not directly related to the applicability of the MPG concept.

Although we have not tested systems containing stagnant regions, nor complex systems with more than two alteration layers, the form of the solute flux term in the Laplace space solution is analogous to that for solute uptake from the main flow channel to the bi-laminar rock matrix and therefore the same result should hold for such systems as well.

4.2.2 Transport properties of a multiple flowpath system

In this section, generic simulations are made using the same material properties data and matrix parameterisation as discussed previously in Section 4.2.1. Here, however, the calculations have been extended to incorporate multiple flowpaths based upon data obtained from the F-factor estimations detailed in Section 3.3.2. As a calculation "benchmark", we have elected to use the F-factor distributions given in Figure 3-3 as a basis for the simulations. The estimated F-factor distributions were based upon a mean $\log_{10}$-transmissivity, $\mu_T = -8.5$, $\sigma_T = 1.0$, a hydraulic gradient of 0.5%, a nominal path length $L_p = 100$ m, and a channel length, $L_c = 3$ m in the case of the CNM data.

To simplify the calculations, the F-factor distributions for both the CNM and MCM models were plotted as a cumulative distribution and stochastically resampled 1,000 times. Figure 4-11 below shows the cumulative probability data for the F-factor distributions calculated using both the MCM and CNM modelling approaches:

Each of the 1,000 F-factor values sampled in this way was taken to represent an individual solute flowpath. An RTD curve was calculated for each F-factor by numerically inverting the Laplace-space model for solute transport. The RTD for the system was then determined by taking the ensemble average over all flowpaths.

Weakly sorbing solutes

Simulations of a weakly sorbing solute ($K_{dm} = 10^{-5}$ m^3/kg) were made for resampled F-factor distributions obtained from the CNM and MCM data as described above and considering R_{12} values in the range 0.1 – 10. The residence time distribution (RTD) curves are shown in Figure 4-12 (MCM data) and Figure 4-13 (CNM data) below (where the subscript *m* refers to the corresponding property of the unaltered rock matrix):

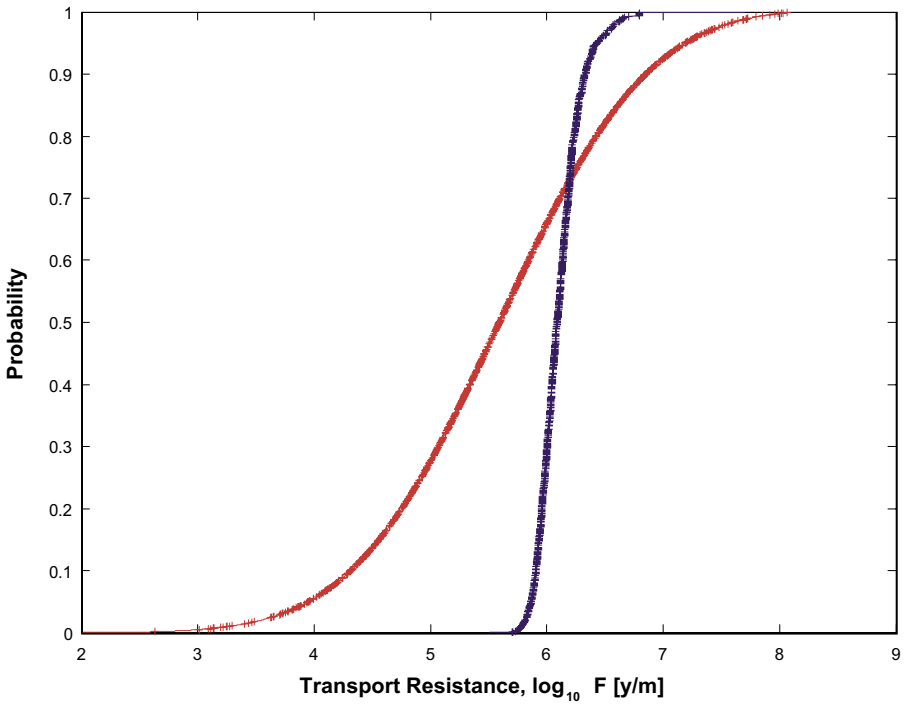

Figure 4-11. *Cumulative probability density function for F-factor distribution. Red curve indicates data for MCM model; Blue curve indicates data for CNM model (coloured symbols indicate resampled data).*

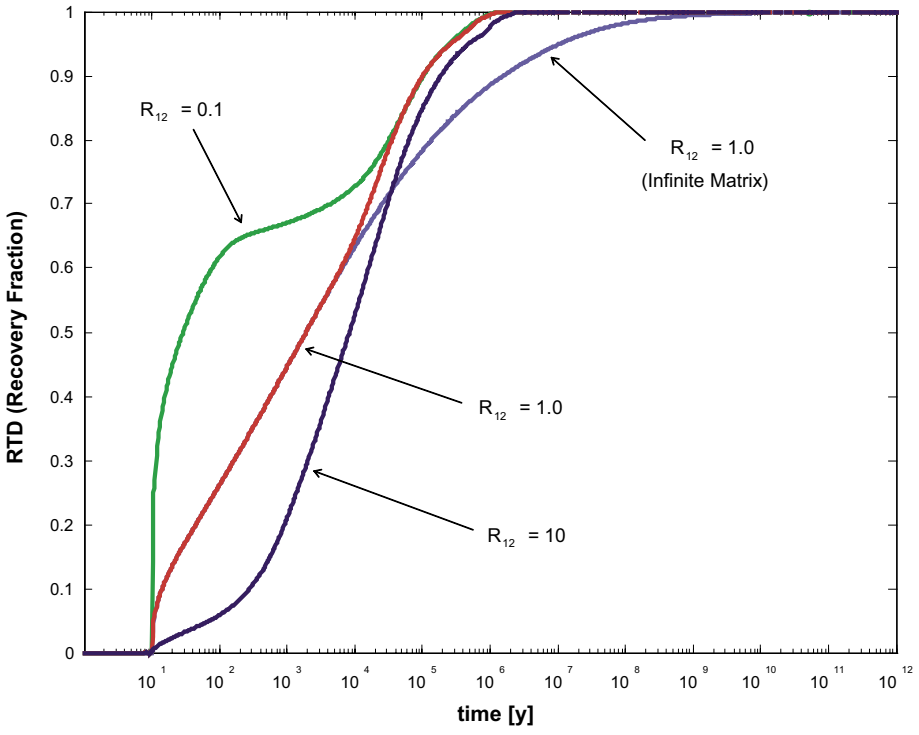

Figure 4-12. *Simulated RTD's for a weakly sorbing solute* $\mathbf{K_{dm}} = 10^{-5}$ *m³/kg in a system with a 2-layer, limited matrix and multiple flowpaths based upon MCM F-factor distribution. Matrix parameterisation is the same as used previously for single flowpath simulations. Different case studies for the alteration are indicated in the figure relative to unaltered rock matrix.*

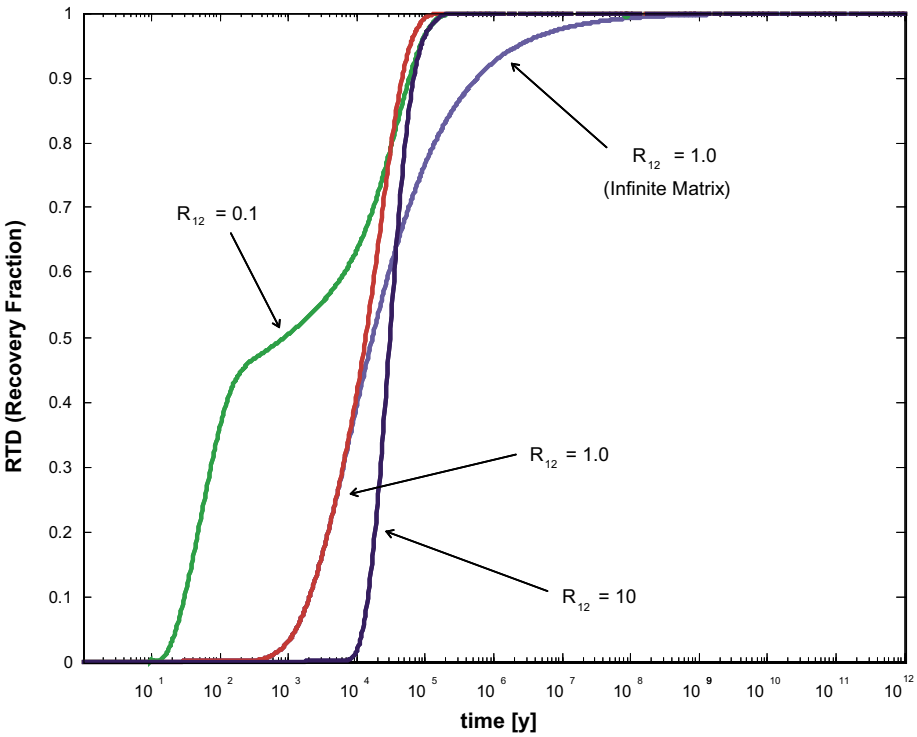

Figure 4-13. *Simulated RTD's for a weakly sorbing solute* $K_{dm} = 10^{-5}$ *m³/kg in a system with a 2-layer, limited matrix and multiple flowpaths based upon CNM F-factor distribution. Matrix parameterisation is the same as used previously for single flowpath simulations. Different case studies for the alteration are indicated in the figure relative to unaltered rock matrix.*

Similarly to the simulations performed for single flowpaths, the results for a multiple flowpath simulation demonstrate poor retention for weakly sorbing solutes which is particularly apparent for systems with unfavourable retention properties. As the ensemble RTD is essentially a linear combination of RTD curves for a broad range of F-factors, the underlying F-factor distribution strongly determines the retardation of solute in the system. Not unexpectedly, the broad distribution of F-factors predicted by the MCM model gives rise to a substantially poorer retardation effect for the leading edge of the RTD than the F-factor distribution predicted by the CNM model (i.e. there are a larger proportion of paths with low F-factors in the MCM model prediction). For the central case with neutral retention properties (i.e. $R_{12} = 1.0$), a matrix saturation effect is clearly apparent when comparing with the result obtained for an infinite matrix (mauve coloured curve).

Moderately sorbing solutes

Simulated RTD curves are shown in Figure 4-14 (MCM data) and Figure 4-15 (CNM data) below for a typical, moderately sorbing solute ($K_{dm} = 0.01$ m³/kg) and the same range of R_{12} parameters used previously:

The simulation results for a moderately sorbing solute indicate improved solute retardation relative to the weakly sorbing solute, although the RTD calculated for the MCM F-factor distribution performs significantly worse than that for the CNM derived data. Similarly to the previous results, a clear matrix saturation effect can be seen.

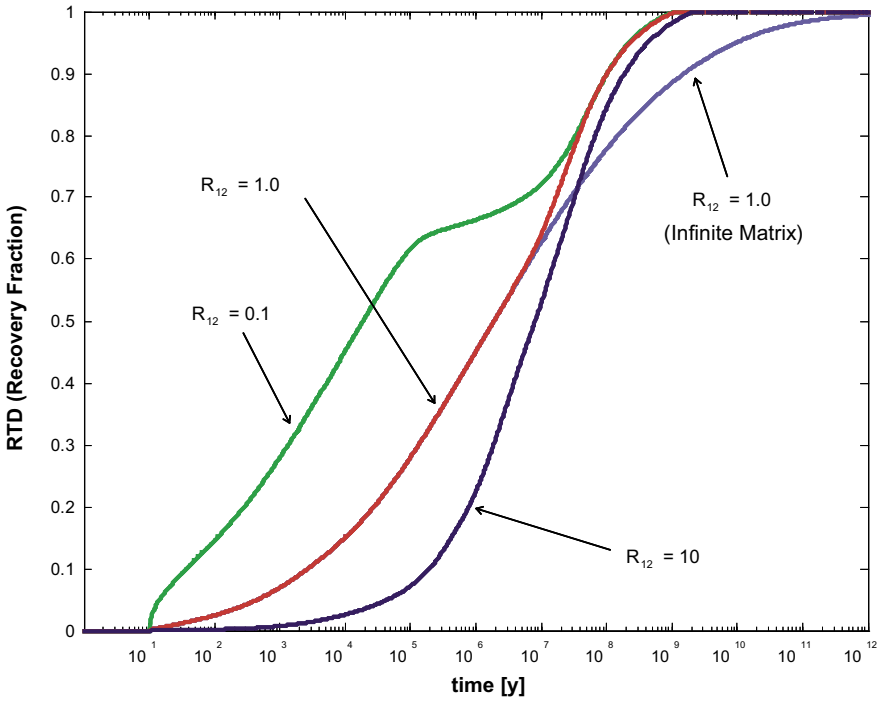

Figure 4-14. *Simulated RTD's for a moderately sorbing solute* K_{dm} *= 0.01 m³/kg in a system with a 2-layer, limited matrix and multiple flowpaths based upon MCM F-factor distribution. Matrix parameterisation is the same as used previously for single flowpath simulations. Different case studies for the alteration are indicated in the figure relative to unaltered rock matrix.*

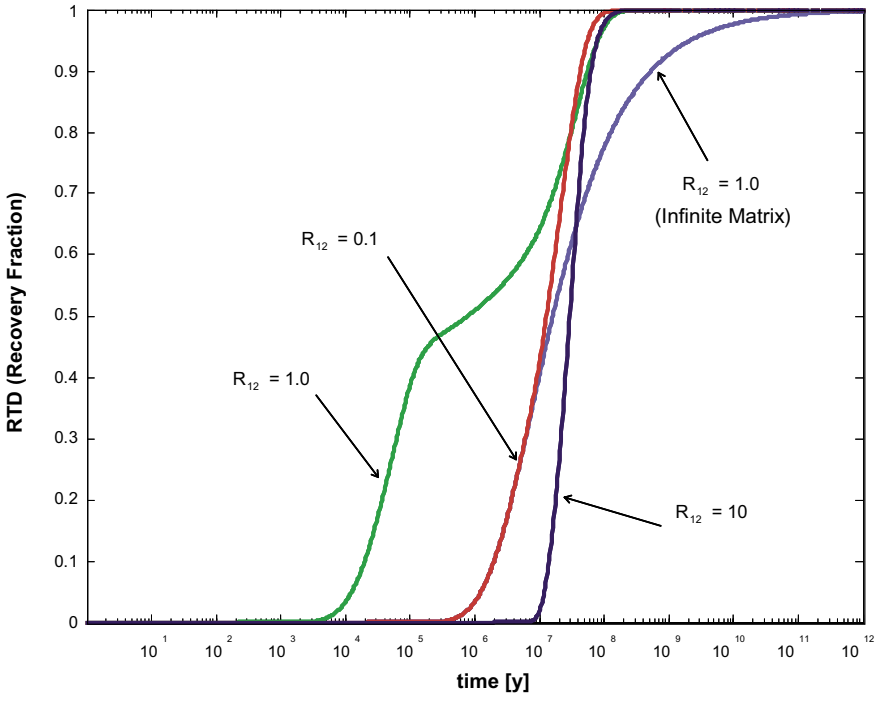

Figure 4-15. *Simulated RTD's for a moderately sorbing solute* K_{dm} *= 0.01 m³/kg in a system with a 2-layer, limited matrix and multiple flowpaths based upon CNM F-factor distribution. Matrix parameterisation is the same as used previously for single flowpath simulations. Different case studies for the alteration are indicated in the figure relative to unaltered rock matrix.*

Strongly sorbing solutes

Simulated RTD curves are shown in Figure 4-16 (MCM data) and Figure 4-17 (CNM data) below for a typical, strongly sorbing solute (K_{dm} = 1.0 m^3/kg) and the same range of R_{12} parameters used previously:

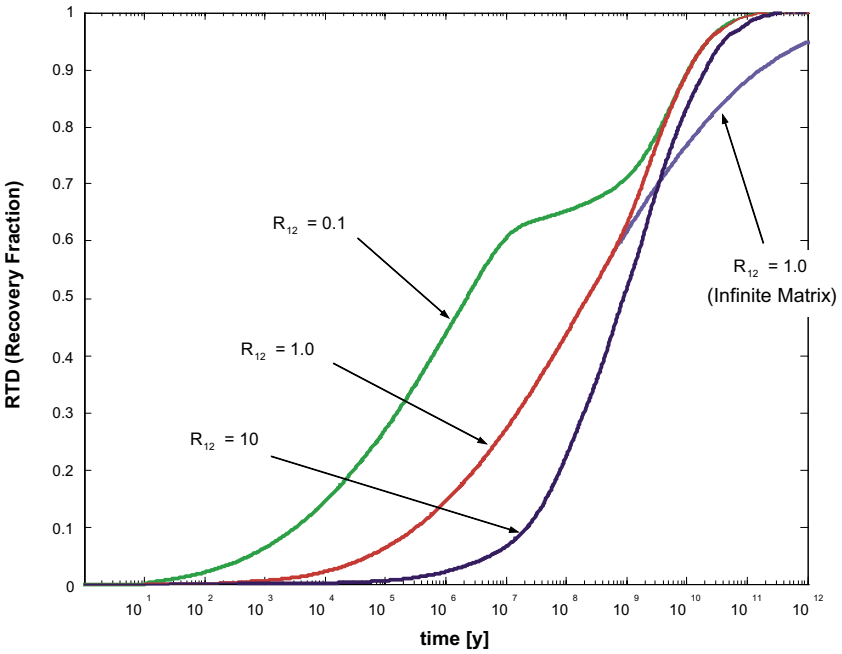

Figure 4-16. *Simulated RTD's for a strongly sorbing solute* $\mathbf{K_{dm}}$ *= 1.0 m^3/kg in a system with a 2-layer, limited matrix and multiple flowpaths based upon MCM F-factor distribution. Matrix parameterisation is the same as used previously for single flowpath simulations. Different case studies for the alteration are indicated in the figure relative to unaltered rock matrix.*

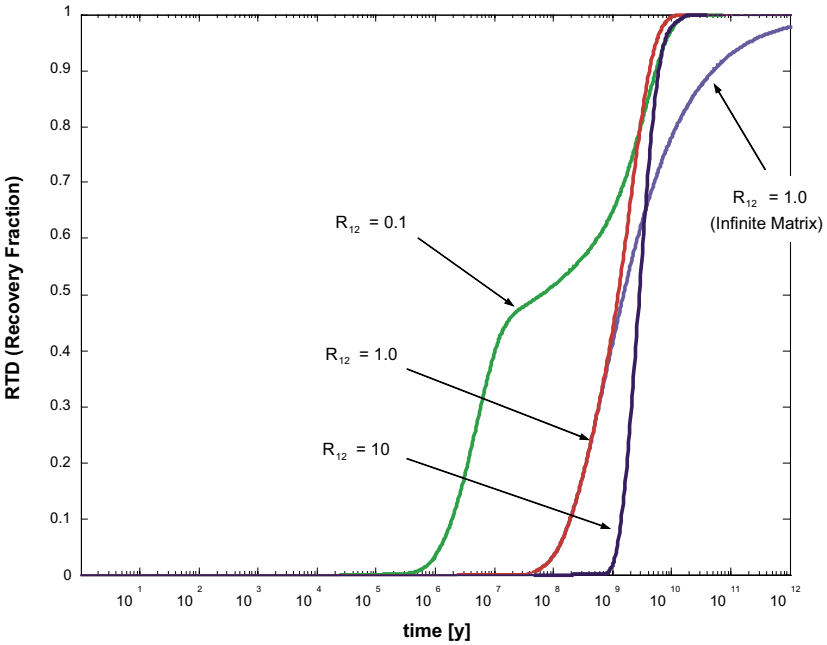

Figure 4-17. *Simulated RTD's for a strongly sorbing solute* $\mathbf{K_{dm}}$ *= 1.0 m^3/kg in a system with a 2-layer, limited matrix and multiple flowpaths based upon CNM F-factor distribution. Matrix parameterisation is the same as used previously for single flowpath simulations. Different case studies for the alteration are indicated in the figure relative to unaltered rock matrix.*

The simulation results for the strongly sorbing solute show strong retention particularly in the case of the CNM derived data. The results obtained using the MCM derived F-factor distribution, on the other hand, are characterised by a significant early solute breakthrough owing to the presence of fast flowpaths with poor retardation properties. Similarly to the results seen for the other solutes, a matrix saturation effect can be discerned and the similar locations of the point of divergence for the limited and infinite matrix cases indicates a similar penetration depth characteristic for all three solutes.

4.3 Main findings of transport data assessment

The impact of material properties including rock matrix alteration on solute retardation has been investigated in the simplified generic simulations presented in Section 4.2. In the absence of reliable data describing the material properties of hydrothermally altered rock materials in the vicinity of flowing fractures, the primary intent of these calculations was to identify common features of these systems over a broad range of possible alteration classes ranging from strongly enhanced to strongly diminished retention relative to unaltered matrix rock. Particular emphasis has been given to the material properties parameterisation in the context of its relation to the transport resistance (the so-called "F-factor") of potential migration paths through the rock.

Generally speaking, larger F-factors correspond to longer travel times for transported solutes. This has been clearly demonstrated for all solute types (i.e. weakly, moderately, and strongly sorbing solutes) and alteration classes investigated. As mentioned in Section 4.2, however, the F-factor approach is not strictly applicable for situations where the solute (typically non-sorbing) penetrates the entire, diffusion-accessible depth of the rock matrix. In such situations, it is the equilibrium storage capacity of the rock matrix that determines the solute retardation and the F-factor is not a significant entity. This was not the case for any of the scenarios envisaged in this study and will not be discussed further here.

To understand the minutiae of the individual simulation results it is illustrative to consider the analytical solution given by /Tang et al. 1981/ for the simple case of a step change in concentration at the inlet of a single flowpath and a rock matrix of infinite extent with constant material properties (Equation 4-2). This equation can be rearranged to obtain the residence time for the solute explicitly:

$$t = R_* t_w + \frac{D_e K_d^* \rho_b}{4\left[erfc^{-1}\left(C/C_0\right)\right]^2}\left(\frac{FWS}{q}\right)^2 \qquad (4\text{-}5)$$

The term *FWS/q* is used here in lieu of "F-factor" for reasons of transparency to emphasise its physical significance as the *flow-wetted surface to flow ratio* for the flowpath. If we consider instantaneous equilibrium with a thin fracture coating having different properties to the rest of the rock matrix, the retardation factor R_* is given by:

$$R_* = 1 + \frac{2K_a}{\delta_c} \qquad (4\text{-}6)$$

The parameter K_a (m) is a surface area normalised sorption partitioning coefficient and δ_c (m) is the aperture of the flow channel. The water residence time, t_w (y) is related to both the flow-wetted surface to flow ratio and the fracture aperture in the following way:

$$t_w = \frac{\delta_c}{2} \times \frac{FWS}{q} \qquad (4\text{-}7)$$

Equation 4-5 can then be written in the form:

$$t = \frac{\delta_c}{2}\left(\frac{FWS}{q}\right) + K_a\left(\frac{FWS}{q}\right) + \frac{D_e K_d^* \rho_b}{4\left[erfc^{-1}\left(C/C_0\right)\right]^2}\left(\frac{FWS}{q}\right)^2 \qquad (4\text{-}8)$$

Conceptually, this can be expressed in the form:

$$\begin{pmatrix}\text{total}\\ \text{residence}\\ \text{time, } t\end{pmatrix} = \begin{pmatrix}\text{water}\\ \text{residence}\\ \text{time, } t_w\end{pmatrix} + \begin{pmatrix}\text{residence time due to}\\ \text{sorption on external}\\ \text{fracture surfaces, } t_s\end{pmatrix} + \begin{pmatrix}\text{residence time due to}\\ \text{diffusion and sorption}\\ \text{in rock matrix, } t_m\end{pmatrix} \qquad (4\text{-}9)$$

For a sufficiently strongly sorbing solute (i.e. $K_a >> \delta_c/2$) it can be shown using Equation 4-8 that the total residence time will be independent of the fracture aperture and only depend on the *FWS/q* ratio for the flowpath (for a given K_a and MPG). Even in the case of a non-sorbing tracer, if the *FWS/q* term is sufficiently high the water residence time will be insignificant compared to the residence time in the rock matrix and therefore can be neglected.

If we neglect the water residence time and surface sorption on fracture coatings, it can be demonstrated that the solute residence time is directly proportional (for any value of C/C_0) to the individual parameters comprising the material properties group (i.e. D_e and $K_d^* \rho_b$) and the square of *FWS/q*:

$$t \propto \left(D_e K_d^* \rho_b\right)\left(\frac{FWS}{q}\right)^2 \qquad (4\text{-}10)$$

Given these assumptions, the uncertainty in arrival time for a given solute can be shown to be proportional to the uncertainty in individual retardation parameters (noting that the bulk sorption coefficient, $K_d^* \rho_b$ implicitly includes the storage capacity of the water-filled porosity of the rock matrix). As the arrival time is proportional to the square of *FWS/q*, on the other hand, a similar level of uncertainty in this parameter has a disproportionately larger impact upon estimated solute residence times.

Although this simple analysis is not strictly applicable to a complex rock matrix micro-structure, the quadratic scaling of solute residence times with increasing F-factor (*FWS/q*) is clearly quantifiable in the residence time distributions presented in Section 4.2.1. This observation along with the form of the matrix flux terms for the more complex cases detailed in Appendix F suggest that the general principle enshrined in Equation 4-10 is commonly applicable to analogous systems containing multilayered matrix microstructures (i.e. with an arbitrary number of alteration layers).

In the residence time distribution curves calculated for the different sub cases (both for a single path and multiple pathways) it was observed that the partial matrix saturation effect was similar for the different solutes modelled. This is an important result as it suggests that the "effective" penetration depth for a fully recovered solute pulse is the same for all solutes independent of their sorption K_d value. To understand why this should be the case, we can make a first order analysis of the solute penetration depth.

If we consider an infinite rock matrix, the solute penetration depth can be obtained from the solution to the diffusion equation and is given by /Neretnieks 1980/ as:

$$\eta = \zeta\sqrt{D_a t} = \zeta\sqrt{\frac{D_e t}{K_d^* \rho_b}} \qquad (4\text{-}11)$$

Where, t is the contact time and the term ζ is a parameter that depends on the part of the solute diffusion profile in the rock matrix upon which the calculation is based. If, for example, we want to know the penetration depth in the matrix corresponding to the leading edge of the diffusion front where the concentration is 1% of the equilibrium concentration at the fracture surface, we would have:

$$\eta_{0.01} = 3.64\sqrt{\frac{D_e t}{K_d^* \rho_b}} \tag{4-12}$$

For the 50% concentration point, on the other hand, we would have:

$$\eta_{0.5} = 0.954\sqrt{\frac{D_e t}{K_d^* \rho_b}} \tag{4-13}$$

It is also possible to define a hypothetical "average penetration depth" based upon the concept of a saturation isotherm (i.e. a rectangular concentration profile), where the solute would be sorbed at the equilibrium concentration corresponding to that at the fracture surface:

$$\overline{\eta} = \frac{2}{\sqrt{\pi}}\sqrt{\frac{D_e t}{K_d^* \rho_b}} \tag{4-14}$$

It should be noted that this hypothetical, average penetration depth is not physically significant, but merely "helps to visualise the depth of rock, which on average, will be reached by the solute" /Neretnieks 1980/.

The appropriate contact time, t for this calculation should ideally based upon the residence time of the solute along the migration pathway to give the depth of rock matrix actually associated with the retardation effect. If we take the estimate of residence time as defined in Equation 4-10 and substitute it into Equation 4-11, we obtain:

$$\overline{\eta} \propto \sqrt{\frac{D_e t}{K_d^* \rho_b}\left(D_e K_d^* \rho_b\right)\left(\frac{FWS}{q}\right)^2} = D_e \times \frac{FWS}{q} \tag{4-15}$$

This means that the "effective" penetration depth for a transported solute is a function of the effective diffusivity and F-factor, and is independent of the sorption K_d value. It is interesting to note that Equation 4-15 also predicts that solute transported along flowpaths with high F-factors will be associated with greater effective penetration depths than flowpaths with low F-factors. For an F-factor of 10^6 y/m, for example, we would expect the effective penetration depth for a transported solute pulse to be 100 times greater than for a flowpath with an F-factor of 10^4 y/m. We use the term "effective penetration depth" to emphasise that this relates to the depth of rock matrix which gives rise to the observed retardation effect in the RTD rather than the actual depth of solute penetration. For a constant concentration or extended pulse release scenario, for example, the actual depth of penetration may be greater than that given by Equation 4-15 and, in general, the actual penetration depth will be dependent on the sorptive properties of the solute (i.e. weakly or non-sorbing solutes can be expected to diffuse to a greater distance in the rock than strongly sorbing solutes).

To numerically calculate the effective penetration depth for a solute transported in a fracture, we need to specify the part of the RTD that we want to compare with as earlier parts of the solute breakthrough curve are influenced by the deeper lying layers of the rock matrix to a lesser extent than later arriving solute. If we neglect the water residence time and sorption on the fracture outer surface, by combining Equation 4-8 and 4-11 we can write for the penetration depth:

$$\overline{\eta} \approx \zeta \times \frac{D_e}{2\,erfc^{-1}\left(C/C_0\right)}\left(\frac{FWS}{q}\right) \tag{4-16}$$

Figure 4-18 below shows some values for the penetration depth at different times corresponding to different recovery fractions (C/C_0) obtained in the solute RTD

From the simulations described in Section 4.2.1 it was observed that the deviation of the infinite matrix solution and that for the limited matrix only became apparent after a recovery fraction of about 40–50%. As can be seen from Figure 4-18, the concentration profile in the rock matrix as described by the penetration depth effectively does not "sense" the presence of the limited matrix for small recovery fractions, and it is only after a recovery fraction of about 30–50% that the solute diffusion profile would seem to be affected appreciably by the boundary at 0.5 m.

The main observation in the simulations insofar as partial matrix saturation is concerned, was that the effect occurred at roughly the same part of the RTD for each of the solutes tested independent of their sorption K_d value. This is fully consistent with the prediction made by Equation 4-15. It should be noted, however, that it is difficult to make rigorous comparisons between the simple infinite matrix case and the limited matrix depth cases simulated in Section 4.2.1 and the numerical exercise shown below in Figure 4-18 should be seen as merely illustrative in showing that the previous simulation results are consistent with what would be expected when considering the magnitude of the solute penetration depth at various times.

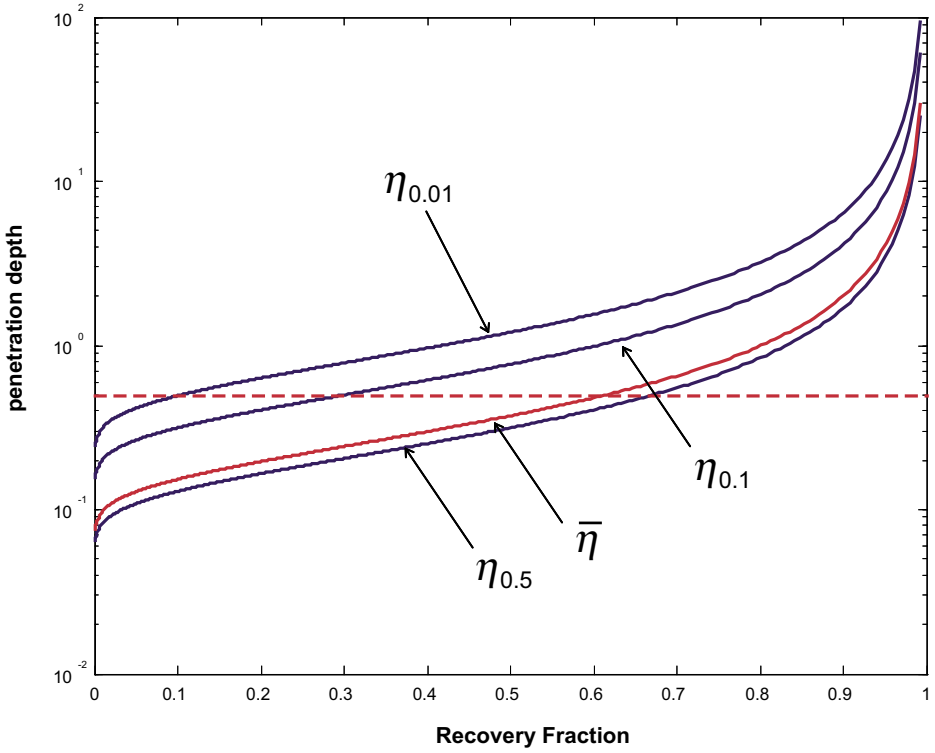

Figure 4-18. *Effective penetration depth as a function of recovery fraction from the solute RTD for a rock matrix formation factor of $F_f = 10^{-5}$ and an F-factor of 10^6 y/m (assuming an infinite, simple matrix). Different penetration cases are indicated in the diagram for 1%, 10%, and 50% concentration locations in the matrix solute diffusion front. The red curve corresponds to the hypothetical average penetration depth as defined in Equation 4-14. The red broken line indicates a depth of 0.5 m used as a maximum matrix depth in the simulations described in previous sections.*

Another feature of solute transport in systems with a complex matrix microstructure that is of relevance for Safety Assessment is the phenomenon of RTD front "sharpening" and front "broadening" (RTD-S/B). This should occur in two principal ways, which we will refer to as primary and secondary RTD-S/B, although both phenomena are directly related to the notion of penetration depth as discussed above.

Primary RTD-S/B occurs by way of the fact that early arriving solute does not "sample" the deeper lying layers of the rock matrix and its retardation tends to be associated primarily with the shallow layers of the rock matrix adjacent to the migration path. For late arriving solute, on the other hand, the solute retardation is more strongly influenced by the deeper lying layers of rock matrix if the penetration depth is sufficiently high that the altered layers can be neglected. This means that for a system with favourable retention properties, the net result may be a sharpening of the solute RTD along a migration path. This occurs because the altered layers which are associated with early solute breakthrough give stronger retention than the deeper lying unaltered matrix rock which exhibits weaker retention. The overall effect is then that the later arriving solute "catches up" with the early part of the solute RTD resulting in a narrower breakthrough RTD than that which would be obtained if the alteration layer is neglected. For a system with unfavourable retention properties, the effect would be the opposite and a broadening of the solute RTD should be obtained.

Conceptually, the idea of secondary RTD-S/B can be explained in the following way:

Transport paths with high flow rates and low F-factors will provide solutes with little time to diffuse into the rock matrix and alteration layers will have a stronger influence upon the transport time along these paths. For transport paths with low flow rates and high F-factors, solutes will have time to diffuse more deeply into the rock matrix and will consequently be less affected by the alteration layers. For systems with unfavourable retention properties, this has the effect of exaggerating the impact of material property uncertainty (i.e. fast transport paths experience reduced retention relative to slow transport paths which experience the enhanced retention of the deeper lying unaltered rock matrix). This gives rise to the secondary RTD front broadening effect. The converse is true for systems with favourable retention properties. In these cases there is a secondary RTD front sharpening effect and the uncertainty introduced by altered layer parameterisation is diminished. The overall effect of this is, of course, complicated by the additional presence of primary RTD-S/B, although the general principle still holds.

The effect of primary RTD-S/B is difficult to discern in the simulations described in Section 4.2.1 owing to the partial matrix saturation. This occurs because a limited rock matrix will also give an RTD front sharpening effect (albeit for a different physical reason – matrix saturation) and to observe the phenomenon unambiguously it is necessary to compare RTD curves for systems with an infinite matrix. In Figure 4-19 below, a set of simulations have been made to demonstrate front sharpening and broadening for an F-factor of 10^6 y/m. All MPG values for the unaltered rock matrix are related to a reference material property group, MPG_{ref} as indicated in the figure. The reference material property group is based upon a solute with a K_d of 0.01 m^3/kg and a formation factor of 10^{-5}. For the 2-layer systems, an additional R_{12} parameter is specified to define the properties of the altered rock layers as appropriate:

As can be seen from the figure, the case (broken blue curve) where we consider a two-layer system for an unaltered rock matrix with the reference material properties (i.e. MPG_{ref}) and an alteration layer having 10 times enhanced retention falls someway in between the two bounding cases for a single layered rock matrix (i.e. the red and blue solid curves). The lower bounding case corresponds to the single layer solution where we consider the entire rock matrix to have the properties of the reference rock matrix (MPG_{ref}). The

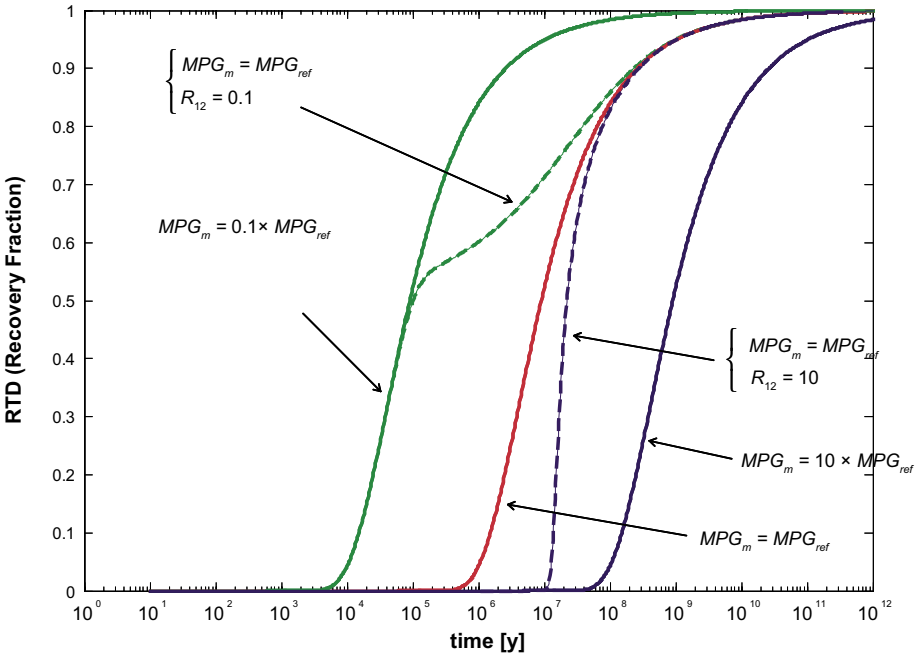

Figure 4-19. *RTD curves for different case studies of matrix microstructure parameterisation for an F-factor of 10^6 y/m and a water residence time t_w = 10 y (All RTD curves consider an infinite matrix). The broken curves correspond to a 2-layer microstructure with favourable (blue) and unfavourable (green) retention properties as indicated in the figure (MPG_m and R_{12}); green, red, and blue RTD curves represent single layer microstructure with properties as indicated (MPG_m only).*

upper bounding case, on the other hand, considers the entire rock matrix to have the same properties as the alteration layer. The 2-layer system exhibits a considerably steeper RTD front as expected for an alteration layer with favourable retention properties. The opposite is seen for the 2-layer system (broken green curve) with unfavourable retention properties (10 times reduced retention in the alteration layer) where a clear peak broadening effect is seen as compared with the bounding cases (i.e. the green and red solid curves). Incidentally, inspection of the RTD curves for the bounding cases shows clearly that the difference between the various cases is directly related to the magnitude of the migration parameters incorporated in the definition of the MPG as suggested by Equation 4-5. As can be seen in the figure, an increase in the MPG by a factor 10 gives a 100 times increase in the recovery time (all other things being equal). For a decrease in the MPG by a factor 10, the recovery time is reduced by a factor of 100.

Although the front sharpening and broadening effect is clearly demonstrated above, it is noted that the extent to which this will affect the shape of the RTD in a two-layer system depends to a large extent upon the magnitude of the F-factor in relation to the thickness of the alteration layer. Figure 4-20 below shows the impact of the effect for an F-factor of 10^5 y/m:

Comparing the solute transport for the 2-layer systems (i.e. for favourable and unfavourable retention properties) with the corresponding bounding cases shows similar front sharpening and broadening, although the impact appears to be different to the cases depicted in Figure 4-19.

The observation that different F-factors give rise to different RTD sharpening and broadening effects has a strong significance for multi-path simulations reflecting a broad range of F-factors. This is what we referred to previously as secondary RTD front sharpening or

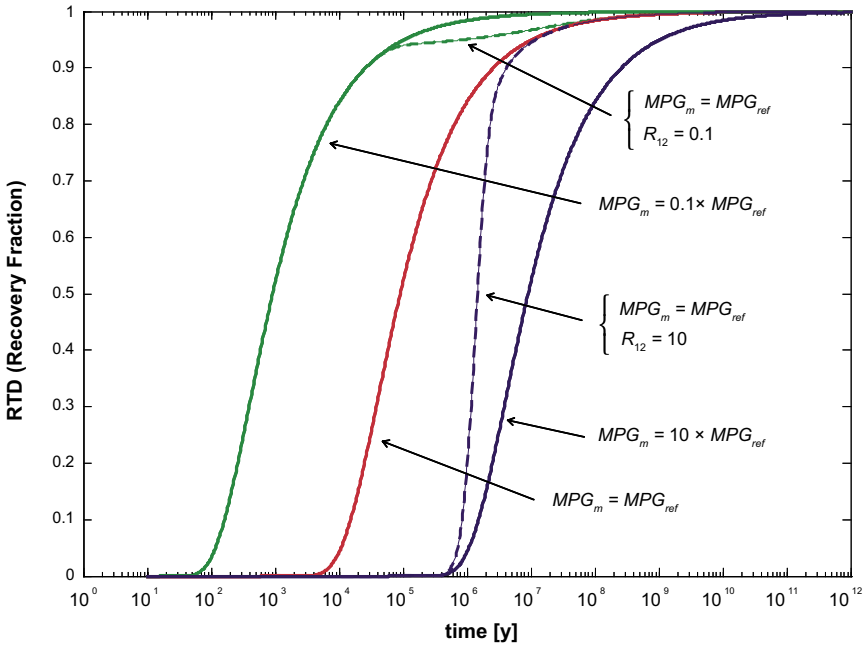

Figure 4-20. *RTD curves for different case studies of matrix microstructure parameterisation for an F-factor of 10^5 y/m and a water residence time t_w = 10 y (All RTD curves consider an infinite matrix). The broken curves correspond to a 2-layer microstructure with favourable (blue) and unfavourable (green) retention properties as indicated in the figure (MPG_m and R_{12}); green, red, and blue RTD curves represent single layer microstructure with properties as indicated (MPG_m only).*

broadening where the net effect of this phenomenon across a multitude of migration paths must be considered in the context of the distribution of F-factors.

Neglecting rock alteration layers with favourable retention properties results in solute retention being under-predicted relative to cases where a full multilayer matrix parameterisation is considered. The opposite is true for alteration layers with unfavourable retention properties. The concept of favourable and unfavourable retention properties must, however, be related to the transport scenario being considered. The inclusion or neglection of alteration layers can thereby have both positive and negative consequences for the estimated peak flux and the period of time over which a pulse source of nuclides is released to the biosphere. As already mentioned in Section 4.2.1, this also has consequences for the remobilisation of radionuclides (resulting from changes in chemical or physicochemical conditions). If altered layers are neglected in Safety Assessment calculations then the actual amount, peak load, and release timing of a radionuclide that is remobilised may be subsequently estimated incorrectly.

Although we have only considered the case of an alteration layer of 5 cm extent, we note that this is likely to be highly variable and safety analysis should ideally consider a range of possible alteration layer thicknesses, given that different alteration layer thicknesses can have different consequences for RTD front sharpening or broadening. Additionally, we note that the effect has only been demonstrated for a 2-layer system in this report. It is possible, if not highly likely, that the material properties of the rock matrix are actually best described as a gradual alteration that diminishes with depth into the rock matrix. In such cases, it is probable that the RTD front sharpening or broadening effect may be even more pronounced and this is therefore an aspect that should be investigated more thoroughly in future versions of the retardation model.

5 Conclusions and implications for further studies

The primary purpose of this background report was to use simple "first order" type models to make estimations of the F-factor for the immediate far field (10–100 m) of rock surrounding the repository within the target rock volume. A secondary goal was to combine these estimates with the *retardation model* produced within the site investigation programme for Laxemar model version 1.2 with the aim of making recommendations relating to issues of scale-up and flowpath averaging. The synthesis of the flow-related transport properties (i.e, F-factor estimates) with the retardation model has been referred to in this report and the main SDM report /SKB 2006a/ as the *integrated transport properties model*.

As has already been discussed at some length in Chapter 3, the estimation of the transport resistance, or "F-factor" is strongly dependent upon assumptions in the underlying hydrological and transport models used in its estimation. In this report, a number of different modelling concepts have been applied to the estimation of the F-factor with the stated aim of increasing transparency and reducing uncertainties.

The data in Table 3-3 which are based upon two different flow-channelling concepts, suggest a mean F-factor roughly on the order of about 10^6 y/m for a 100 m path length and typical in situ conditions, although based upon the extreme assumptions of channel length and flow channel interdependence, up to 10% of the migration paths could have an F-factor less than 10^4 y/m. Estimations of the F-factor (Table 3-4) using a stream-tube approach gives a broader range of mean values from 10^3 – 10^8 y/m depending upon the source of hydraulic data that have been used as a basis for the estimation and the borehole length over which hydraulic tests were carried out. It is intended that future work within transport modelling will include estimations of the F-factor in the immediate far-field using Hydro-DFN modelling and more sophisticated channelling models with correlated transmissivity-length relations. This should provide an improved basis for comparison of F-factors obtained by different methods and raise confidence for predictions made within Safety Assessment.

It has been noted in the evaluation of the flow related transport properties that these estimations of the F-factor and its distribution are statistical averages for the entire rock volume from which the measurement data are derived. The F-factor of relevance for Safety Assessment is therefore based upon a sub-sampling of these distributions from the aspect of migration paths intersecting individual canister deposition holes.

For the interaction between flow-related transport properties and the material properties it can be said that the uncertainty in the arrival time of a given solute is directly proportional to the uncertainty in individual retardation parameters (i.e. the individual parameters comprising the MPG). As the arrival time is proportional to the square of the F-factor, on the other hand, the same level of uncertainty in this parameter has a significantly greater impact upon the uncertainty of the arrival time. This result has been established both on theoretical grounds and quantitatively by simulation in Chapter 4. It is worth reiterating here the comment from Section 3.1 that even though the F-factor is a site characteristic and a genuine physical entity (being the flow-wetted surface to flow ratio), it is neither a directly measurable quantity nor a material property in the sense of parameters such as porosity, formation factor, or sorption K_d value. Its assessment is model dependent and subject to uncertainties stemming from modelling assumptions used in its calculation.

In general, the main uncertainties identified in the Laxemar 1.2 transport modelling are related to the absence of site-specific (and internally consistent) transport data both for the retardation model as well as the integrated transport properties model incorporating estimations of the F-factor. Furthermore, the available data are currently insufficient for establishing quantitative relation between transport parameters and other properties such as lengths, orientations and hydraulic properties of fractures and deformation zones.

Generic simulations have been made in this report detailing the impact of alteration layers adjacent to fracture surfaces on transport processes. For alteration layers with enhanced retention properties, the overall solute residence time is generally greater than if alteration layers are neglected.

The simplified, generic simulations presented in Chapter 4 for solute transport in an advective flow system with a 2-layer rock matrix microstructure have also revealed a physical phenomenon that, to the best knowledge of the author, has not been previously described in the literature in the context of solute transport in fractured rock. This residence time distribution (RTD) front sharpening or broadening effect is directly related to the parameterisation of the alteration layer relative to the unaltered rock matrix and its relationship with the F-factor.

The effect has been found to be active both on the level of individual migration paths ("primary" RTD front sharpening/broadening) and also on the level of ensemble averages that consider a multitude of possible migration paths ("secondary" RTD front sharpening/broadening). The primary effect is related to the effective penetration depth of a solute into the rock matrix that is a function of the recovery fraction at the system boundary (solute efflux location). The secondary effect relates to penetration depth of solute as a function of the F-factor (FWS/q).

The above discussion notwithstanding, we note that the status of alteration layer properties is currently unclear with respect to the unaltered rock matrix. As mentioned in previous sections, the altered layers in the previous model (i.e. Simpevarp 1.2 /SKB 2005a, Byegård et al. 2005/) were parameterised with weaker retention properties than those for the unaltered rock matrix, although this is now believed to be an artefact of the previous data import. This was essentially due to a lack of data available at the previous model version. The impact of altered layer parameterisation on Safety Assessment in the context of the above discussion, as well as the abstraction of the alteration zone into a single layer instead of a continuously variable or multi-laminar alteration zone should be scrutinised further in forthcoming transport modelling activities.

With regard to uncertainties related to spatial variability and scale, it may be noted that all measurements providing data to the retardation model are obtained in the laboratory, on a millimetre- to centimetre-scale. Some properties such as the formation factor obtained from in situ resistivity measurements give some indication of variability on a decimetre- to metre-scale. The proper mean of "upscaling" these parameters is by integrating them along flow paths in groundwater flow models /SKB 2004b/, implying that the scale of the flow model is the relevant model scale. For spatial variability in retention properties (e.g. D_e, θ_m, and $K_d^* \rho_b$), which are potentially describable as Gaussian random variables (normally or log-normally distributed) along a transport flowpath, the variance of the effective mean value for a specific rock type is expected to decrease on increasing length scales /e.g. Lake and Srnivasan 2004/. Uncertainty arising due to measurement bias and experimental artefacts have significance for the parameterisation of the retardation model, although must be handled in a different way to material properties variation as described above. It is, however, not always entirely clear how to separate these two distinct features of the input data in a rigorous fashion.

Additional uncertainties for transport processes relate to the kinds of rock and alteration types likely to be encountered by solutes along transport paths and their relation to the overall rock volume, as well as the parameterisation of alteration layers in the rock matrix. It is important that if alteration layers are to be explicitly considered in transport modelling then internally consistent sets of measurement data must be used for the material properties parameterisation. This includes not only the requirement for a "clean" set of site-specific data, but also that the properties of altered and unaltered rock are determined with consideration of possible correlations between physically adjoining altered and unaltered rock.

For the material properties of altered rock materials and fracture filling materials, it would be desirable for sampling to be carried out in a "natural" setting with respect to the conceptual retardation model in order to avoid the possibility of sampling bias when the retardation model is parameterised using pooled site data. This entails that samples of altered rock (and fracture filling materials, etc) should be paired with samples of adjoining unaltered rock materials, preferably in the vicinity of identified flow anomalies. In this way any correlations between the properties of altered rock materials and unaltered wall rock will be visible in the data, which would not be possible if data pooled from widely differing spatial locations are used to parameterise the retardation model. Managing the data in this fashion should decrease the possibility of bias relating to data pooling which could have a negative impact on the aggregate uncertainty.

No analysis of variability has been made in this report for material properties that vary along the length of a flowpath (i.e. flow-path averaging). At the present time, the differences between the various rock types are not sufficiently large that this is motivated considering the level of uncertainty associated with the data. Owing to that the material properties variability within a given rock type appears to be larger than the variability between rock types, a tentative conclusion is that a single rock material properties parameterisation can be considered a reasonable approximation for all rock types (considering both the Simpevarp and Laxemar subareas as one site). It should be emphasised, however, that this conclusion is provisional and may need to be revised when more detailed material properties data are available.

It is noted that the synthesis of flow-related transport properties with materials property parameterisation of the 3D geological model is only partly complete in this report. Owing to a lack of data, discussions relating to understanding, confidence and uncertainty have been by necessity, restricted to a generic analysis of the consequences of various material property assumptions that interact with flow-related transport properties. In future versions of the Laxemar SDM, more detailed discussions concerning these issues, their consequences for Safety Assessment and quantifications of site-specific uncertainty will be included.

6 References

Abelin H, Birgersson L, Widén H, Ågren T, Moreno L, Neretnieks I, 1994. Channeling experiments in crystalline fractured rocks, *J. Contam. Hydrol.*, 15(3), pp. 129–158.

Allard B, Kipatsi H, Rydberg J, 1977. Sorption av långlivade radionuklider i lera och berg, KBS Technical Report 55, Svensk Kärnbränslehantering AB.

Allard B, Kipatsi H, Torstenfelt B, 1978. Sorption av långlivade radionuklider i lera och berg Del 2, KBS Technical Report 98, Svensk Kärnbränslehantering AB.

Allard B, Karlsson M, Tullborg E-L, Larson S-Å, 1983. Ion exchange capacities and surface areas of some major components and common fracture filling materials of igneous rocks, SKBF Technical Report 83-64, Svensk Kärnbränslehantering AB.

Alonso U, Degueldre C, 2003. Modelling americium sorption onto colloids: effect of redox potential. *Colloids and Surfaces A: Physicochem. Eng. Aspects* 217, pp. 55–62.

Andersson J, Hermanson J, Elert M, Moreno L, Selroos J-O, 1998. Derivation and treatment of the flow-wetted surface and other geosphere parameters in the transport models FARF31 and COMP23 for use in Safety Assessment. SKB R-98-60, Svensk Kärnbränslehantering AB.

Andersson P, Byegård J, Dershowitz B, Doe T, Hermanson J, Meier P, Tullborg E-L, Winberg A, 2002a. TRUE Block Scale Project. Final report. 1. Characterisation and model development. SKB TR-02-13, Svensk Kärnbränslehantering AB.

Andersson J, Berglund J, Follin S, Hakami E, Halvarson J, Hermanson J, Laaksoharju M, Rhén I, Wahlgren C-H, 2002b. Testing the methodology for site descriptive modelling. SKB TR-02-19, Svensk Kärnbränslehantering AB.

Atkins P, 1999. Physical Chemistry, 6 ed., Oxford University Press. ISBN 0-19-850102-1.

Barker J, 1988. A generalized radial-flow model for pumping tests in fractured rock, *Water Resour. Res.*, 24(10), pp. 1796–1804.

Berglund S, Selroos J-O, 2003. Transport properties site descriptive model – Guidelines for evaluation and modelling. SKB R-03-09, Svensk Kärnbränslehantering AB.

Bertetti F, Pabalan R, Turner D, Almedarez M, 1996. Neptunium(V) sorption behaviour on clinoptilolite, quartz and montmorillonite, *Mat. Res. Soc. Symp. Proc.*, 412, pp. 631–638.

Birgersson L, Widén H, Ågren T, Neretnieks I, 1992. Tracer migration experiments in the Stripa Mine 1980-1991, SKB Stripa Project 92-25, Svensk Kärnbränslehantering AB.

Brunauer S, Emmet P, Teller E, 1938. Adsorption of gases in multimolecular layers. *J. Am. Chem. Soc.*, 60, pp 309–319.

Byegård J, Johansson H, Skålberg M, Tullborg E-L, 1998. The interaction of sorbing and non-sorbing tracers with different Äspö rock types – Sorption and diffusion experiments in the laboratory scale. SKB TR 98-18, Svensk Kärnbränslehantering AB.

Byegård J, Larsson N-Å, 2004. Metodbeskrivning för batchsorptionsmätning. SKB MD 540.002, version 1.2.

Byegård J, Gustavsson E, Tullborg E-L, 2005. Bedrock transport properties. Preliminary site description Simpevarp subarea – version 1.2. SKB R-05-05, Svensk Kärnbränslehantering AB.

Byegård J, Gustavsson E, Tullborg E-L, 2006. Bedrock transport properties. Data evaluation and retardation model. Preliminary site description Laxemar subarea – version 1.2. SKB R-06-27, Svensk Kärnbränslehantering AB.

Börjesson S, Gustavsson E, 2005. Oskarshamn site investigation. Laboratory data from the site investigation programme for the transport properties of the rock. Data delivery for data freeze Laxemar 2.1. SKB P-05-106, Svensk Kärnbränslehantering AB.

Carbol P, Engkvist I, 1997. Compilation of radionuclide sorption coefficients for performance assessment. SKB R-97-13, Svensk Kärnbränslehantering AB.

Crawford J, Moreno L, Neretnieks I, 2003. Determination of the flow-wetted surface in fractured media, *J. Contam. Hydrol.*, 61(1–4), pp. 361–369.

Crawford J, Moreno L, Neretnieks I, 2004. Harmonisation of Site Characterisation and Performance Assessment Modelling – The Relative Importance of Surface Sorption and Matrix Interaction Phenomena. In: Oversby and Werme (eds.), *Mat. Res. Soc. Symp. Proc.,* Scientific Basis for Nuclear Waste Management XXVII, 807, pp. 551–556.

Davis J, Meece D, Kohler M, Curtis G, 2004. Approaches to surface complexation modelling of Uranium(VI) adsorption on aquifer sediments. *Geochim. et Cosmochim. Acta*, 68(18), pp 3621–3641.

De Hoog F, Knight F, Stokes A, 1982. An improved method for numerical inversion of Laplace transforms, *SIAM J. Sci. Stat. Comput.*, 3, pp. 357–366.

Dershowitz W, Winberg A, Hermanson J, Byegård J, Tullborg E-L, Andersson P, Mazurek M, 2003. Äspö Hard Rock Laboratory. Äspö Task Force on modelling of groundwater flow and transport of solutes. Task 6C – A semi-synthetic model of block scale conductive structures at the Äspö HRL. SKB IPR-03-13, Svensk Kärnbränslehantering AB.

Drake H, Tullborg E-L, 2004. Oskarshamn site investigation. Fracture mineralogy and wall rock alteration. Results from drill corw KSH01A+B. SKB P-04-250, Svensk Kärnbränslehantering AB.

Drake H, Tullborg E-L, 2005. Oskarshamn site investigation. Fracture mineralogy and wall rock alteration. Results from drill cores KAS04, KA1755A and KLX02. SKB P-05-174, Svensk Kärnbränslehantering AB.

Drake H, Tullborg E-L, 2006a (in press). Mineralogical, chemical and redox features of red-staining adjacent to fractures. Results from drill cores KSH01A+B and KSH03A+B. SKB P-06-01, Svensk Kärnbränslehantering AB.

Drake H, Tullborg E-L, 2006b (in press). Mineralogical, chemical and redox features of red-staining adjacent to fractures. Results from drill core KLX04. SKB P-06-02, Svensk Kärnbränslehantering AB.

Erdal B, Aguilar R, Bayhurst B, Daniels W, Duffy C, Lawrence F, Maestas S, Oliver P, Wolfsberg K, 1979. Sorption-desorption studies on granite: 1. Initial studies of strontium, technetium, cesium, barium, cerium, europium, uranium, plutonium, and americium, Los Alamos Scientific Laboratory, Technical Report LA-7456-MS.

Gylling B, 1997. Development and applications of the channel network model for simulations of flow and solute transport in fractured rock. Ph.D. thesis, Dept. Chemical Engineering and Technology, Royal Inst. of Technology, Stockholm.

Gylling B, Birgersson L, Moreno L, Neretnieks I, 1998. Analysis of a long-term pumping and tracer test using the channel network model, *J. Contam. Hydrol.*, 32(3-4), pp. 203–222.

Hellmuth K, Siitari-Kauppi M, Lindberg A, 1993. Study of porosity and migration pathways in crystalline rock by impregnation with ^{14}C-polymethylmethacrylate. *J. Contam. Hydrol.*, 13, pp. 403–418.

Hellmuth K, Lukkarinen S, Siitari-Kauppi M, 1994. Rock matrix studies with carbon-14-polymethylmethacrylate (PMMA). Method, development and applications. *Isotopenpraxis Environ. Health Stud.*, 30, pp. 47–60.

Hermanson J, Forsberg O, Fox A, La Pointe P, 2005. Statistical model of fractures and deformation zones – Preliminary site description Laxemar subarea – version 1.2. SKB R-05-45, Svensk Kärnbränslehantering AB.

Hollenbeck K, 1998. INVLAP.M: A matlab function for numerical inversion of Laplace transforms by the de Hoog algorithm. http://www.mathtools.net/files/net/invlap.zip

Holmén J, Outters N, 2002. Theoretical study of rock mass investigation efficiency. SKB TR-02-21, Svensk Kärnbränslehantering AB.

Ikeda T, Amaya T, 1998. Model development of chemical evolution in repository. Vol. II Acquisition of nuclide migration data in near field, PNC ZJ 1281 98-003, Japan Power Reactor & Nuclear Fuel Development Corporation (JNC).

Jenne E, 1998. Adsorption of metals by geomedia – Variables, mechanisms, and model applications, Academic Press.

Laaksoharju M (ed), Smellie J, Tullborg E-L, Waber N Morales T, 2006. Hydrogeochemical Evaluation, Preliminary site description, Laxemar subarea – version 1.2. SKB R-06-12, Svensk Kärnbränslehantering AB.

Lake L W, Srinivasan S, 2004. Statistical scale-up of reservoir properties: concepts and applications, *J. Petrol. Sci. Eng.*, 44, pp. 27–39.

Ludvigson J-E, Hansson K, Rouhiainen P, 2002. Methodology study of Posiva difference flowmeter in borehole KLX02 at Laxemar. SKB R-01-52, Svensk Kärnbränslehantering AB.

Ludvigson J-E, Levén J, Källgården J, Jönsson S, 2004. Oskarshamn site investigation. Single-hole injection tests in borehole KSH02. SKB P-04-247, Svensk Kärnbränslehantering AB.

Löfgren M, Neretnieks I, 2003. Formation factor logging by electrical methods. Comparison of formation factor logs obtained in situ and in the laboratory. *J. Contam. Hydrol.*, 61**,** pp. 107–115.

Löfgren M, 2004. Diffusive properties of granitic rock as measured by in-situ electrical methods, Ph.D. Thesis, Department of Chemical Engineering and Technology, Royal Inst. of Technology, Stockholm.

Löfgren M, Neretnieks I, 2005. Oskarshamn site investigation. Formation factor logging in-situ and in the laboratory by electrical methods in KLX03 and KLX04. SKB P-05-105, Svensk Kärnbränslehantering AB.

Löfgren M, Neretnieks I, 2006 (in press). Through-electromigration: A new method of investigating pore connectivity and obtaining formation factors *J. Contam. Hydrol.*, xx**,** pp. xx–xx.

Moreno L, Tsang Y, Tsang C, Hale F, Neretnieks I, 1988. Flow and tracer transport in a single fracture: A stochastic model and its relation to some field observations, *Water Resour. Res.*, 24(12), pp. 2033–3048.

Moreno L, Neretnieks I, 1989. Channelling in fractured zones and its potential impact on the transport of radionuclides, In: Lutze W., and Ewing, R. C. (eds.), *Mat. Res. Soc. Symp. Proc.,* Scientific Basis for Nuclear Waste Management XII, Vol. 127, pp. 779–786.

Moreno L, Neretnieks I, 1993. Fluid flow and solute transport in a network of fractures, *J. Contam. Hydrol.*, **14**(3–4), pp. 163–192.

Nakayama S, Moriyama H, Arimoto H, Higashi K, 1986. Distribution coefficients of Americium, Neptunium and Protoactinium for selected rocks. *The Memoirs of the Faculty of Engineering*, Kyoto University, 48(3), pp. 275–283.

Neretnieks I, 1980. Diffusion in the rock matrix: An important factor in radionuclide migration, *J. Geophys. Res.*, 85, pp. 4379–4397.

Neretnieks I, Rasmuson A, 1984. An approach to modelling radionuclide migration in a medium with strongly varying velocity and block sizes along the flowpath, *Water Resour. Res.*, 20(12), pp. 1823–1836.

Neretnieks I, 2002. A stochastic multi channel model for solute transport – analysis of tracer tests in fractured rock, *J. Contam. Hydrol.*, 55(3–4), pp. 175–211.

Neretnieks I, 2006 (manuscript in preparation). Channelling with diffusion into stagnant water and into matrix in series, Department of Chemical Engineering and Technology, Royal Inst. of Technology, Stockholm.

Norman S, Kjellbert N, 1990. FARF31 – A far field radionuclide migration code for use with the PROPER package. SKB TR-90-01, Svensk Kärnbränslehantering AB.

Ohlsson Y, Neretnieks I, 1995. Literature survey of matrix diffusion theory and of experiments and data including natural analogues. SKB TR-95-12, Svensk Kärnbränslehantering AB.

Ohlsson Y, Neretnieks I, 1997. Diffusion data in granite – Recommended values. SKB TR-97-20, Svensk Kärnbränslehantering AB.

Pinnioja T, Jaakkola T, Miettinen J, 1984. Comparison of batch and autoradiographic methods in sorption studies of radionuclides in rock and mineral samples, Nuclear Waste Commission of Finnish Power Companies, Report YJT-87-17.

Poteri A, Billaux D, Cvetkovic V, Dershowitz B, Gómez-Hernández J-J, Hautojärvi A, Holton D, Medina A, Winberg A, 2002. TRUE Block Scale Project. Final Report – 3. Modelling of flow and transport. SKB TR-02-15, Svensk Kärnbränslehantering AB.

Prikryl J, Jain A, Turner D, Pabalan R, 2001. Uranium(VI) sorption behaviour on silicate minerals mixtures. *J. Cont. Hydrol.*, 47, pp. 241–253.

Pöllänen J, Sokolnicki M, 2004. Oskarshamn site investigation: Difference flow logging of borehole KAV04A and KAV04B. SKB P-04-216, Svensk Kärnbränslehantering AB.

Rahm N, Enachescu C, 2004a. Oskarshamn site investigation: Hydraulic testing of percussion drilled lineament boreholes on Ävrö and Simpevarp, 2004. SKB P-04-287, Svensk Kärnbränslehantering AB.

Rahm N, Enachescu C, 2004b. Oskarshamn site investigation: Hydraulic injection tests in borehole KLX02, 2003. SKB P-04-288, Svensk Kärnbränslehantering AB.

Rahm N, Enachescu C, 2004c. Oskarshamn site investigation: Hydraulic injection tests in borehole KSH01A, 2003/2004. SKB P-04-289, Svensk Kärnbränslehantering AB.

Rahm N, Enachescu C, 2004d. Oskarshamn site investigation: Hydraulic injection tests in borehole KSH03A, 2004. SKB P-04-290, Svensk Kärnbränslehantering AB.

Rahm N, Enachescu C, 2004e. Oskarshamn site investigation: Hydraulic injection tests in borehole KAV04A, 2004. SKB P-04-291, Svensk Kärnbränslehantering AB.

Rahm N, Enachescu C, 2004f. Oskarshamn site investigation: Hydraulic injection tests in borehole KLX04, 2004. SKB P-04-292, Svensk Kärnbränslehantering AB.

Rahm N, Enachescu C, 2005a. Oskarshamn site investigation: Pumping tests and water sampling in KLX04, 2004. SKB P-05-16, Svensk Kärnbränslehantering AB.

Rahm N, Enachescu C, 2005b. Oskarshamn site investigation: Pumping tests and water sampling in KLX06, 2004. SKB P-05-184, Svensk Kärnbränslehantering AB.

Rhén I, Forsmark T, Forsman I, Zetterlund M, 2006a. Hydrogeological single-hole interpretation of KSH01, KSH02, KSH03, KAV01, KLX02 and HSH01-03. Simpevarp subarea – version 1.2. SKB R-06-20, Svensk Kärnbränslehantering AB.

Rhén I, Forsmark T, Forsman I, Zetterlund M, 2006b. Hydrogeological single-hole interpretation of KLX02, KLX03, KLX04, KAV04A,B, HAV09-10 and 6 HLXxx-boreholes. Laxemar subarea – version 1.2. SKB R-06-21, Svensk Kärnbränslehantering AB.

Robinson P, 1984. Connectivity, flow and transport in network models of fractured media, Ph.D. thesis, St. Catherine's College, Oxford University, Ref. TP 1072.

Rouhiainen P, 2000. Difference flow measurements in borehole KLX02 at Laxemar. SKB IPR-01-06, Svensk Kärnbränslehantering AB.

Rouhiainen P, Pöllänen J, Sokolnicki M, 2005. Oskarshamn site investigation: Difference flow logging of borehole KLX03 – Subarea Laxemar. SKB P-05-67, Svensk Kärnbränslehantering AB.

Rouhiainen P, Sokolnicki M, 2005. Oskarshamn site investigation: Difference flow logging of borehole KLX04 – Subarea Laxemar. SKB P-05-68, Svensk Kärnbränslehantering AB.

SKB, 1999. Deep repository for spent nuclear fuel, SR 97 – Post-closure safety. SKB TR-99-06, Svensk Kärnbränslehantering AB.

SKB, 2004a. Hydrogeochemical evaluation for Simpevarp model version 1.2. Preliminary site description of the Simpevarp area. SKB R-04-74, Svensk Kärnbränslehantering AB.

SKB, 2004b. RETROCK Project: Treatment of geosphere retention phenomena in Safety Assessments – Scientific basis of retention processes and their implementation in Safety Assessment models (WP2). SKB R-04-48, Svensk Kärnbränslehantering AB.

SKB, 2005a. Preliminary site description, Simpevarp subarea – version 1.2. SKB R-05-08, Svensk Kärnbränslehantering AB.

SKB, 2005b. Preliminary safety evaluation for the Forsmark area. Based on data and site descriptions after the initial site investigation stage. SKB TR-05-16, Svensk Kärnbränslehantering AB.

SKB, 2006a. Preliminary site description, Laxemar subarea – version 1.2. SKB R-06-10, Svensk Kärnbränslehantering AB.

SKB, 2006b (in prep.), Long-term safety for KBS-3 repositories at Forsmark and Laxemar – a first evaluation. Main report of the SR-Can project. SKB TR-06-XX, Svensk Kärnbränslehantering AB.

Sokolnicki M, Rouhiainen P, 2005. Oskarshamn site investigation: Difference flow logging of borehole KLX06 – Subarea Laxemar. SKB P-05-74, Svensk Kärnbränslehantering AB.

Tang G, Frind E, Sudicky E, 1981. Contaiminat transport in fractured porous media. An analytical solution for a single fracture, *Water Resour. Res.*, 177, pp. 555.

Thunehed H, 2005. Oskarshamn site investigation: resistivity measurements and determination of formation factors on samples from KLX04 and KSH02. SKB P-05-75, Svensk Kärnbränslehantering AB.

Vieno T, Hautojärvi A, Koskinen L, Nordman H, 1992. TVO-92 Safety Assessment of Spent Fuel Disposal. Nuclear Waste Commission of Finnish Power Companies, Report YJT-92-33E.

Walker D, Roberts R, 2003. Flow dimensions corresponding to hydrogeologic conditions, Water Resour. Res, 39(12), pp. 1349.

Widestrand H, Byegård J, Ohlsson Y, Tullborg E-L, 2003. Strategy for the use of laboratory methods in the site investigations programme for the transport properties of the rock. SKB R-03-20, Svensk Kärnbränslehantering AB.

Winberg A, Andersson P, Hermansson J, Byegård J, Cvetkovic V, Birgersson L, 2000. Äspö Hard Rock Laboratory. Final report of the first stage of the Tracer Retention Understanding Experiments. SKB TR-00-07, Svensk Kärnbränslehantering AB.

Öhberg A, Rouhiainen P, 2000. Posiva groundwater flow measuring techniques. POSIVA Report 2000-12.

Appendix A

Groundwater compositions representative of site specific conditions

Table A-1. Chemical composition of the groundwater types used in the diffusivity and sorption measurements for the Simpevarp and Laxemar sub areas and the Forsmark site /Byegård et al. 2005/. Concentrations are given in mg/l.

	Type I (HSH02 0–200 m) Fresh water	Type II (KFM02A 509–516 m) Groundwater with marine character	Type III (KSH01A 558–565 m) Present ground-water at repository level	Type IV (KLX02 1,383–1,392 m) Brine type water of very high salinity
Li^+	0.016	0.051	0.58	4.85
Na^+	127	2,120	3,230	7,450
K^+	2.16	33.3	12.4	32.6
Rb^+	(0.0252)[A]	0.0628	0.0424	0.178
Cs^+	(0.00117)[A]	0.00179	0.00137	0.0186
NH_4^+	(0.0947)[A]	0.04	0.04	0.56
Mg^{2+}	1.43	232	44.7	1.2
Ca^{2+}	5.21	934	2,190	14,800
Sr^{2+}	0.0695	7.95	32.3	253
Ba^{2+}	(1.29)[A]	0.188	0.188	0.024
Fe^{2+}	(0.364)[C]	1.20	0.686	3.45
Mn^{2+}	0.02	2.12	0.46	1.11
F^-	3.03	0.9	0.967	(1.6)[D]
Cl^-	21.5	5,150	8,800	36,800
Br^-	(0.2)[B]	22	71	509
SO_4^{2-}	8.56	510	221	1,210
Si(tot)	6.56	5.2	4.7	2.6
HCO_3^-	252	124	12	42
S^{2-}	(0.01)[B]	0.05	0.05	0.05
pH	8.58	7.1	7.45	6.8
Approximate Ionic Strength	5.86×10^{-3}	1.88×10^{-1}	3.16×10^{-1}	1.44

A) No measurements available, data imported from KSH01 #5263.

B) Based on detection limit.

C) Based on the Fe-tot measurement.

D) No measurements available, data imported from KLX02 #2731.

Appendix B

Generic calculations using the channel network model

The hydrologic flow problem is solved by way of analogy with electric networks (i.e. Kirchoff's current law) where a simple boundary condition consisting of a fixed head differential between opposite boundary planes of the network is assumed. The absolute value of the conductance used in the simulations is not important as the resulting head and flow distributions can be scaled to arbitrary conditions. It is important, however, to specify the variance of the transmissivity distribution as this strongly influences flow channelling in the network. Simulations were carried out for a number of different transmissivity standard deviations, σ_T in the range 0.5–2.25 ($\log_{10}$ units).

Based upon the steady state hydrologic solution, particle tracking calculations were then made. In the current version of the model, 1,000 tracer particles were injected in a square window of 5×5 nodes centred on the upstream boundary plane. The fraction of particles injected at each node in the window was calculated to be proportional to the flow at that node, thereby simulating a constant concentration boundary condition. The set of 5×5 tracer particle release nodes was arbitrary, although chosen so that poorly conductive channels near the release point would not overly influence the transport predictions.

The trajectories of individual particles travelling through the channel network are calculated using a particle-following technique /Robinson 1984, Moreno et al. 1988/. Many particles are introduced, one at a time, into the known flow field at one or more locations. Particles arriving at an intersection are distributed in the outlet channel members with a probability proportional to their flow rates. This is equivalent to assuming total mixing at the intersections. Although an assumption in the present numerical implementation of the model, full mixing is not an essential feature of the model and other partial-mixing or non-mixing assumptions can be envisioned. The question of whether full diffusive mixing actually occurs at channel intersections is not assured under Safety Assessment conditions as it is dependent upon the geometry of contact of different channels and their contact residence time. For sufficiently low flowrates and representative flow channel contact geometries, however, it can be shown that it is not an unreasonable assumption /SKB 2004b/. At present this is a customary assumption in transport models, although should be revisited in the future owing to its relevance for solute transport channelling.

Each individual particle is followed through the network. The water residence time in a given channel is determined by the flow through the channel member and by its volume. To calculate the water residence time also requires knowledge about fracture apertures or, at least the overall flow porosity of the system. It has been shown, however, that over SA timescales the water residence time and thus the fracture aperture has little, or no importance for the estimation of solute residence times when matrix interaction effects are dominating /Crawford et al. 2004/. This may even be true in certain situations for non-sorbing solutes if the matrix diffusion effect is sufficiently strong.

The particle tracking results are shown in Figure B-1 below for a typical channel network realisation and different transmissivity variances:

It is interesting to note that the large transverse spread of particles in the channel network is reminiscent of a Gaussian plume, suggesting that a highly connected channel network gives results that are similar to those for a homogeneous porous medium. Particle trajectories resulting from these simulations were then used as the basis for calculating the transport resistance distribution in the channel network.

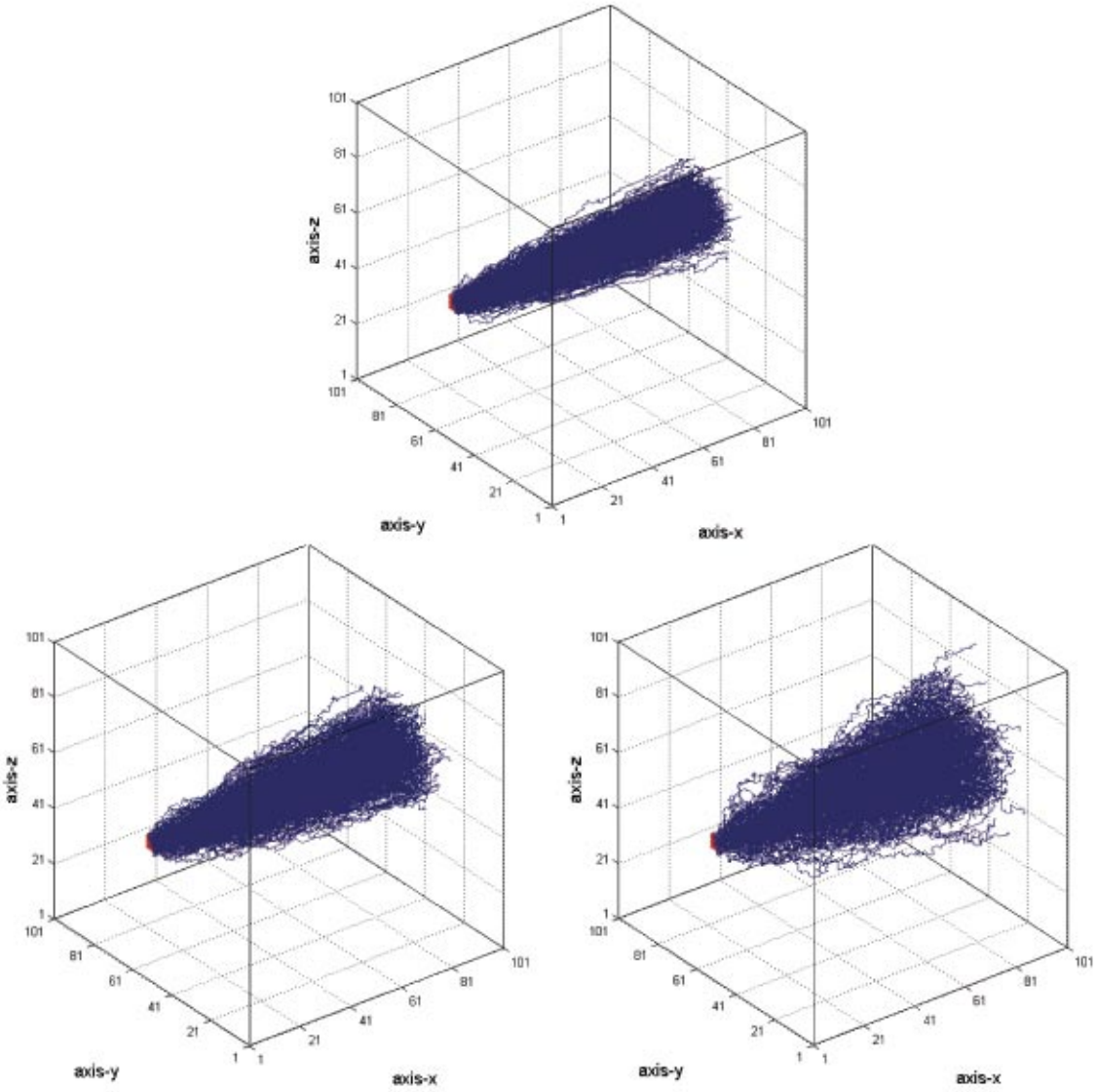

Figure B-1. *Visualisation of particle tracking data for a typical realisation of tracer injection in a 5×5 node window centred on the upstream boundary plane. Top centre image corresponds to transmissivity standard deviation,* $\sigma_T = 0.5$. *Lower left hand image corresponds to* $\sigma_T = 1.0$ *while lower right hand image corresponds to* $\sigma_T = 2.0$.

For a given mean transmissivity T (m^2/y), channel width W_c (m), and a hydraulic gradient i_x (m/m) applied parallel to the x-axis, the total flow across the simulation volume is:

$$Q = n^2 T W_c i_x \qquad \text{(B-1)}$$

Where n^2 is the total number of nodes comprising the flow boundary. The flow-wetted surface in an individual channel (where L_c (m) is the channel length) is:

$$fws_c = 2 W_c L_c \qquad \text{(B-2)}$$

Here, we use the term fws_c to denote the flow-wetted surface of an individual channel in order to distinguish it from the flow-wetted surface for an entire transport flowpath, *FWS*. In the hydrologic simulations, the total boundary flow is normalised to 1.0 m^3/y. The individual

channel flows calculated in the simulation can thereby be transformed to arbitrary channel dimensions and hydraulic boundary conditions by combining Equation B-1 and B-2 to get the following scaling relation:

$$\frac{fws_c}{q_c} = f_c \times \frac{1}{q_{c_0,i}} \tag{B-3}$$

Where, q_c is the rescaled flow in each channel, q_{c0} is the flow determined in the original simulation, and the scaling factor f_c is given by:

$$f_c = \frac{2L_c}{n^2 T i_x} \tag{B-4}$$

For a path length comprising m individual channels in sequence, the total transport resistance is given by:

$$F = f_c \times \sum_{i=1}^{m} \frac{1}{q_{c_0,i}} \tag{B-5}$$

Each particle released into the channel network traces out an individual path thereby giving a transport resistance distribution.

Implicit in the derivation given above is that flow paths in the fractured rock can be represented as a network of channel members having identical lengths and widths. In reality, it is likely that a variety of channel lengths and widths will exist. It is almost certainly the case that channel width and aperture can be expected to vary more or less continuously along a flowpath. It has been shown, however, that it is the total or path-integrated flow-wetted surface along a streamline, irrespective of its variation, that can be used to account for the interaction of a solute with the rock matrix /Neretnieks and Rasmuson 1984/. This means it is not necessary to consider the detailed variation of width and aperture along a flowpath in order to calculate the solute residence time distribution for that path /SKB 2004b/.

It is interesting to note that if flowpaths are short and highly interconnected, then the calculated F-factor over a distance of, say, 100 m will reflect the average transmissivity of the conductive members within the rock volume and not be strongly influenced by the presence of a smaller number of individual conductors with high transmissivity. If, however, the transmissivity is positively correlated with the length of conductive features the transport resistance may be dominated by a small number of features that have high transmissivity. In DFN models, it is commonly assumed that the transmissivity of conductive fractures is correlated with size by way of a power law relation of some kind.

The existence of a transmissivity-channel length relation does not invalidate the use of channels of fixed length and width in a transport model as multiple channels of similar transmissivity could potentially be connected in series to replicate the same effect. Poor network connectivity can also be simulated by removing flow channels from the network, or by setting their transmissivities to arbitrarily low values. In these simulations, however, we have chosen the limiting case where the channels are equidimensional and highly interconnected.

When considering the distribution of the transport resistance amongst different flowpaths, an important assumption is that the "*measured flowrates represent unknown, but equally large areas of a fracture*" /SKB 2004b/ in hydraulic tests carried out between packed-off sections in a borehole (i.e. it is assumed that all sampled flow channels have the same length and width, although differing hydraulic apertures). This assumption is implicit in the formulation outlined above and is generally consistent with the method used for derivation of transmissivity data from PFL measurements, although it has not been tested rigorously.

It means that the measured flowrate distribution is also directly related to the distribution of flowrate to flow-wetted surface. Consequently, it is not necessary to know what surface area the measurements actually represent as the total specific flow-wetted surface, a_R obtainable from borehole statistics can be distributed equally amongst the different flow channels.

It is worth noting that another possible assumption is that the flow-wetted surface of individual flow channels is proportional to the flowrate. This would be the case if all flow channels were to have identical lengths and hydraulic apertures, although different widths. It also implies a constant channel transmissivity regardless of flowrate. It can be shown, however, that this gives trivial results as the calculated F-factor will then be a constant and independent of the flowrate /Neretnieks 2006 *(manuscript in preparation)*/.

To calculate the F-factor for individual channels in the CNM it is necessary to specify the channel length, L_c in Equation B-4 in addition to the simulation volume dimensions, mean transmissivity and hydraulic gradient. From the form of Equation B-4 it appears that the choice of channel width should not have a direct influence upon the calculated F-factor. We note, however, that the choice of channel length does have an influence upon the calculated F-factor distribution by way of altering the total number of channel lengths and mixing nodes that need to be traversed to cover a given distance thereby influencing the dispersion of particles in the channel network. As fewer mixing nodes are encountered for transport over a given distance with longer channel lengths, the variance of the calculated F-factor varies with channel length. This is illustrated below in Figure B-2:

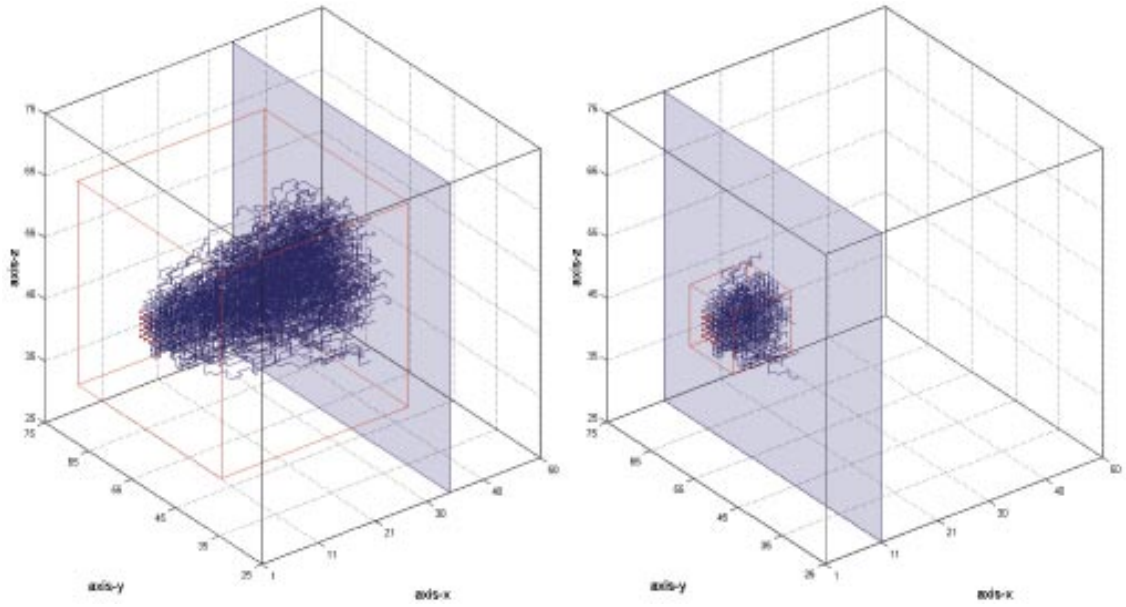

Figure B-2. *Visualisation of particle tracking data from a typical realisation (σ_T = 1.0) using the channel network model indicating transport paths for L_c = 3 m (left) and L_c = 10 m (right). The total straight line distance travelled is the same in both cases (L_p = 100 m, indicated by the blue-shaded plane), although the number of channels traversed differs owing to differing channel lengths. The red cube outlines in the figure indicate a volume with dimensions 100 m×100 m×100 m. Note that the axis markings correspond to integer channel segments rather than actual length units.*

This effect will also occur if we fix the channel width at some arbitrary value and calculate an appropriate channel length in order to preserve the overall specific flow-wetted surface in the system. In this case, the calculated F-factor distribution will differ slightly depending upon the choice of channel width, W_c as it is related to the channel length, L_c by way of the requirement that the overall flow-wetted surface in the system is of some specified value. This, however, can be considered to be a secondary effect of flowpath connectivity that is not directly related to the impact that channel width has upon the F-factor.

To distinguish between the actual length of individual migration paths (which typically follow a meandering route through the channel network) from the straight line travel distance, L_p we refer to the latter as the "nominal" path length in the following sections.

In the channel network model, it is assumed that all particles arriving at the recovery location (in this case a downstream plane) are mixed. From the estimated transport resistance for each particle track, a residence time distribution (RTD) can be calculated for an arbitrary radionuclide concentration boundary condition at the release point if we additionally specify the transport aperture of the flow channels (or water residence time). The RTD of the recovered tracer in the mixed effluent is then equal to the ensemble average of all flowpaths. Under SA conditions, however, it is generally not necessary to specify the transport aperture as the water residence time is usually very small in comparison to the rock matrix retention time /e.g. Crawford et al. 2004/.

The site specific data typically has a transmissivity variance that differs from that used in the generic simulations. The transmissivity distribution for KLX02 derived from PFL-s data, for example, has a standard deviation of $\sigma_T = 1.27$. The generic simulations, on the other hand, were carried out with transmissivity standard deviations of $\sigma_T = 1.25$ and 1.50. In order to obtain estimates of the F-factor and its distribution without having to make detailed CNM simulations for each individual case, an interpolation technique was employed using the σ_T values as a correlating variable. It was found that a simple cubic polynomial could fit the data well, thereby obviating the need for extensive case specific hydrological simulations. An example of the data interpolation is shown in Figure B-3 and Figure B-4 below.

It was generally not possible to obtain a convergent numerical solution to the hydrological problem using the simple CNM model for σ_T greater than about 2.25 (an iterative solver using the bi-conjugate gradient method with incomplete LU-preconditioning was used). For this reason F-factor estimations corresponding to transmissivity data with $\sigma_T > 2.25$ had to be extrapolated. This was only an issue for transmissivity data interpreted from 5 m-scale PSS measurements in KLX02 where σ_T was found to be on the order of 2.5.

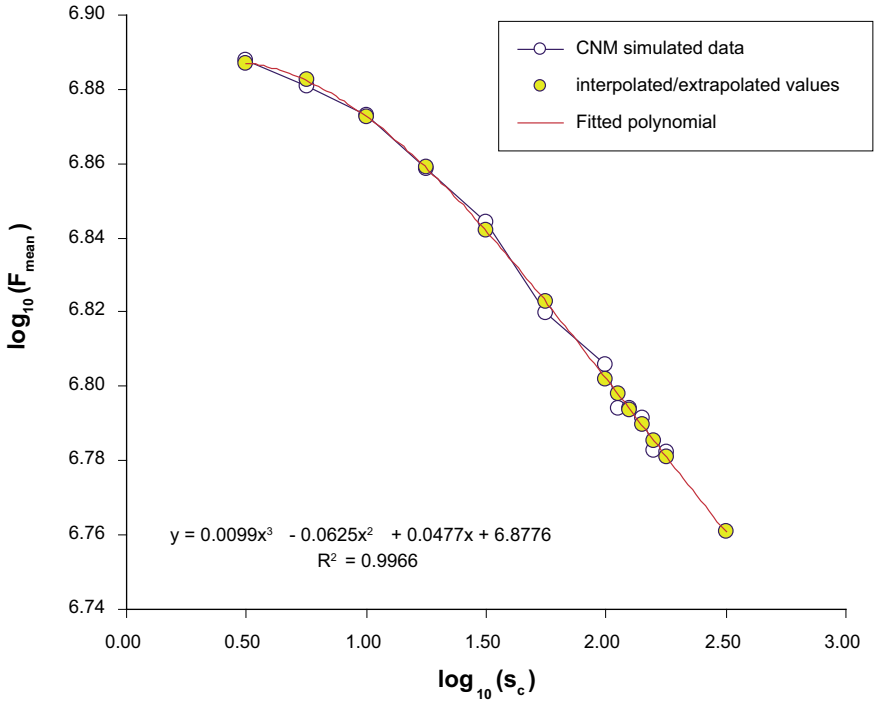

Figure B-3. *Mean F-factor (20-run averages) calculated using CNM simulated data as a function of channel conductance standard deviation, s_c (equivalent to σ_T) for a channel length, L_c = 1.0 m and nominal path length, L_p = 100 m. The data trend is fitted using a simple cubic polynomial.*

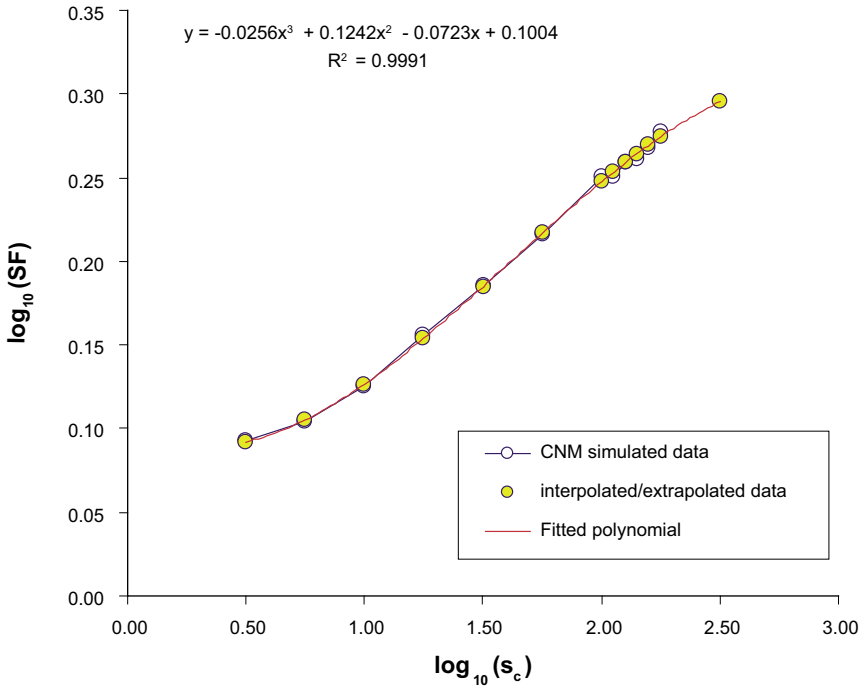

Figure B-4. *F-factor standard deviation, s_F (20-run averages) calculated using CNM simulated data as a function of channel conductance standard deviation, s_c (equivalent to σ_T) for a channel length, L_c = 1.0 m and nominal path length, L_p = 100 m. The data trend is fitted using a simple cubic polynomial.*

Appendix C

Flow channel intersection frequency for a canister emplacement

The relation between frequency of flow channel intersection for a canister emplacement and that of a borehole can be addressed by a simple ray-tracing simulation. Here, we consider infinitely long channels with random orientation in space and a finite width. The intersection of such a channel with a vertical, cylindrical control volume (i.e. a borehole or canister emplacement hole) depends only on the strike component of its orientation regardless of dip. We can therefore reduce the three-dimensional problem to a simpler two-dimensional representation without any loss of generality.

To generate a set of rays with random strike it is sufficient to generate a set of random angle pairs (θ_1, θ_2) corresponding to chord endpoints $P_1\langle x_1, y_1\rangle$, $P_2\langle x_2, y_2\rangle$ located on the perimeter of a large circle. The equation of the line connecting these points then defines the trajectory of the ray. If we take the centre of the circle to be at the origin, we can then inscribe two additional, although smaller concentric circles with radii corresponding to that of the hypothetical borehole and the canister hole.

Any point, P on the line connecting the chord endpoints is defined by (in vector form):

$$P = P_1 + u\,(P_2 - P_1) \qquad \text{(C-1)}$$

For each coordinate this gives:

$$x = x_1 + u\,(x_2 - x_1) \qquad \text{(C-2)}$$

$$y = y_1 + u\,(y_2 - y_1) \qquad \text{(C-3)}$$

A circle centred at the origin with a radius, R has the equation:

$$x^2 + y^2 = R \qquad \text{(C-4)}$$

Substituting Equation C-2 and C-3 into C-4 gives the quadratic equation:

$$au^2 + bu + c = 0 \qquad \text{(C-5)}$$

Where the parameters a, b, and c are defined as:

$$a = (x_2 - x_1)^2 + (y_2 - y_1)^2 \qquad \text{(C-6)}$$

$$b = 2\left((x_2 - x_1)x_1 + (y_2 - y_1)\,y_1\right) \qquad \text{(C-7)}$$

$$c = x_1^2 + y_1^2 - R^2 \qquad \text{(C-8)}$$

Whether, or not a randomly oriented ray intersects a circle of radius, R depends upon the discriminant of the quadratic equation.

The value of the discriminant ($b^2 - 4ac$) gives the following information:

$b^2 - 4ac < 0$ the ray does not intersect the circle

$b^2 - 4ac = 0$ the ray touches the circle at a tangent

$b^2 - 4ac > 0$ the ray intersects the circle

If the outer circle is sufficiently larger than the inner circles describing the canister hole and the borehole (to avoid window biasing), the ratio of P_{10can}/P_{10bh} for infinitely thin channels can be calculated directly from circle intersection statistics if a sufficiently large number of random oriented rays are simulated. Figure C-1 below shows a typical simulation result for this type of ray-tracing calculation.

For channels of finite width (W_c), it is necessary to consider the bounds of the channel when performing the ray tracing calculation. To achieve this, the initial chord as defined previously is extended to include an upper and lower bound as depicted in Figure C-2 below.

To test whether a channel of finite width intersects the canister emplacement hole or borehole, the same procedure is used as for an infinitely thin channel described previously, although this time both the lower and upper bounds of the channel are tested. If either bounding ray intersects a circle then the channel is assumed to intersect the appropriate hole. For channel widths larger than the borehole (or canister hole) diameter it is also possible for the bounding rays to straddle the hole. This situation is identified by a simple algebraic sign test.

For a borehole with diameter, d_{bh} = 0.076 m and a canister emplacement hole with diameter, d_{can} = 1.5 m, the ratio P_{10can}/P_{10bh} can be calculated for a range of channel widths. These results are given in Table C-1 below.

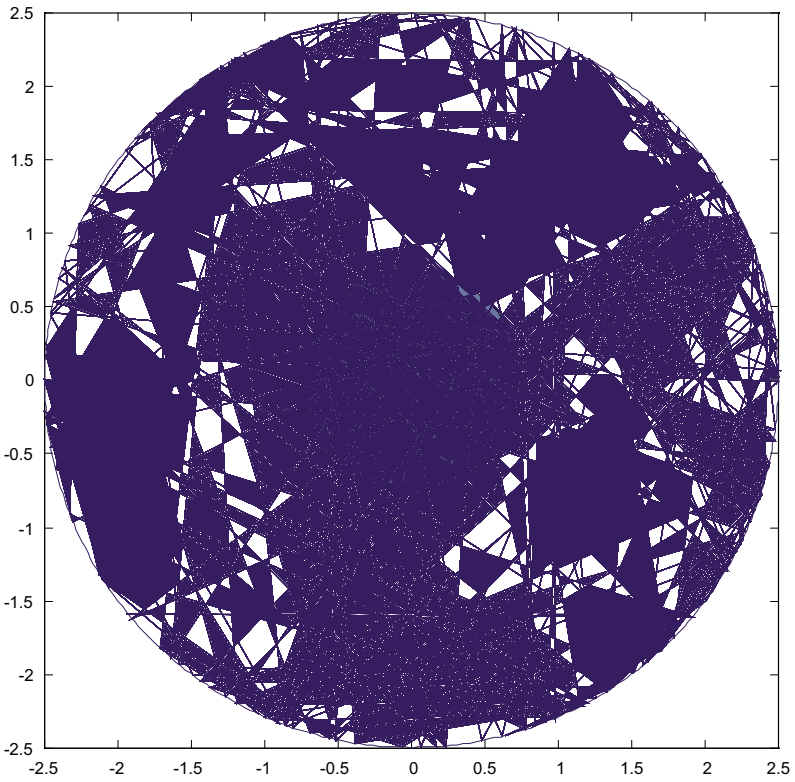

Figure C-1. *Visualisation of 100 random rays shown together with canister emplacement hole (large dark disc) and borehole (small central disc).*

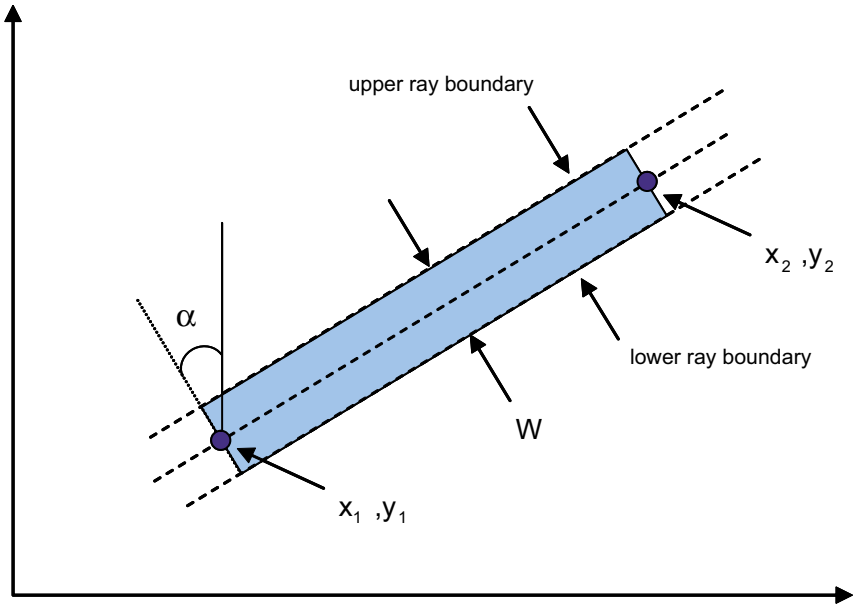

Figure C-2. *Visualisation of channel of finite width where upper and lower bounding rays are defined relative to initially defined, central ray.*

Table C-1. Ratio of flow channel intersection frequencies for a canister emplacement hole and borehole for various channel widths. The results are based upon stochastic ray tracing simulation of 10^6 randomly oriented channels.

Channel Width, W_c (m)	P_{10can}/P_{10bh}
0	20
0.05	12.9
0.1	10.3
0.2	8.4
0.3	7.3
0.4	6.6
0.5	6.1
1.0	4.4

Appendix D

Equivalence of stream-tube and multi channel representations for F-factor estimation

Here, we consider a stream tube such as that in the Figure D-1 below.

To predict the residence time distribution of a transported solute, we need to calculate the *FWS/q* ratio. For a stream tube this is given by:

$$\frac{FWS}{q} = \frac{V_p a_R}{q} \qquad \text{(D-1)}$$

Where, V_p (m^3) is the volume of the stream tube, a_R (m^2/m^3) is the (volumetric) specific flow-wetted surface, and q (m^3/y) is the flowrate. If the stream tube has some average cross-sectional area A_{xs} (m^2) and a length, L_p (m) then the *FWS/q* ratio can be written as:

$$\frac{FWS}{q} = \frac{A_{xs} L_p a_R}{\mathrm{K} A_{xs} i_x} = \frac{L_p a_R}{\mathrm{K} i_x} \qquad \text{(D-2)}$$

The variable K (m/y) is the hydraulic conductivity of the stream tube, and i_x (m/m) is the hydraulic gradient over the length of the stream tube.

Although the actual shape of the stream tube is not important for the analysis, we will now consider a stream tube in the form of a rectangular prism in order to facilitate comparisons between the stream tube and channelling models that can be used for transport modelling:

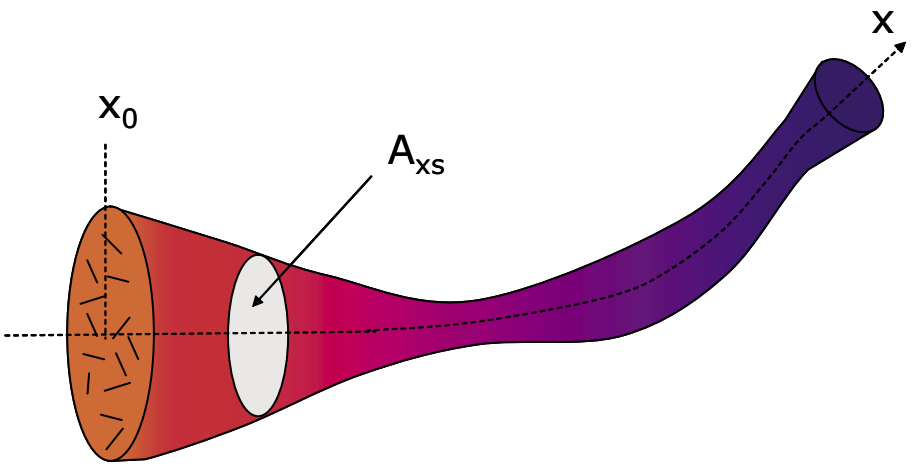

Figure D-1. *Equivalent stream tube for solute transport in fractured rock. A bundle of discrete flow channels is approximated as a porous medium where channels do not cross stream tube walls.*

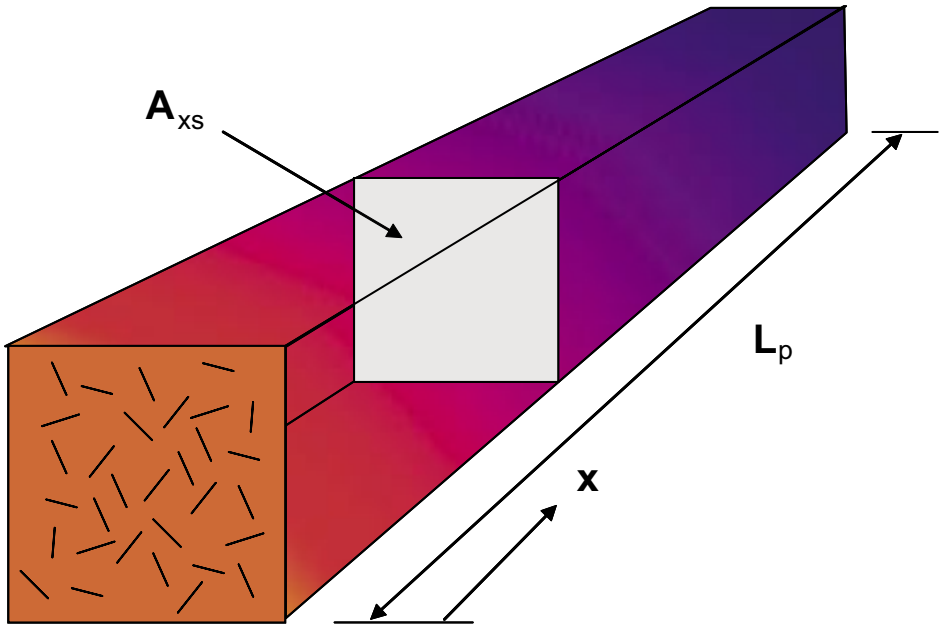

Figure D-2. *Equivalent stream tube for solute transport in fractured rock visualised as a simple rectangular prism. A "bundle" of discrete flow channels is approximated as a porous medium where channels do not cross stream tube walls.*

If we consider the case of n independent (although otherwise identical) flow channels, the hydraulic conductivity of the stream tube can be given in terms of the individual flow channel transmissivities, T (m^2/y) (assumed to be identical for all channels) as:

$$K = \frac{n T W_c}{A_{xs}} \qquad \text{(D-3)}$$

The concept of transmissivity here, however, can be misleading as we have to be very clear how it is defined in order to calculate the flow correctly. To illustrate this point, we use the cubic law for viscous flow to calculate the transmissivity of the flow channels from first principles.

Assuming the cubic law for laminar fluid flow in a rectangular slit and neglecting viscous end effects, the hydraulic conductivity of the stream tube is defined as:

$$K = \frac{n \alpha W_c}{\tau_p A_{xs}} \qquad \text{(D-4)}$$

Where, the variable τ_p is the flowpath tortuosity, W_c (m) is the channel width, and the constant α is defined as:

$$\alpha = \frac{\rho_w g \delta^n}{12 \mu} \quad (n = 3 \text{ for cubic law for flow}) \qquad \text{(D-5)}$$

In this equation g (m/s^2) is the gravitational constant, μ (Ns/m^2) is the dynamic viscosity of water, ρ_w (kg/m^3) is the density of water, and δ (m) is the fracture hydraulic aperture (noting that the units of α must be altered to give agreement with a flow, q given in m^3/y).

The individual channel transmissivity is then given by:

$$T = \frac{\alpha}{\tau_p} \qquad \text{(D-6)}$$

The flowpath tortuosity is defined as the ratio of the actual flowpath length (L_s) and the nominal length of the stream tube (L_p). For a linear flow field this would be equal to the actual flowpath length divided by the "straight line" transport distance. This accounts for the fact that the flow channels do not necessarily have to be linear with respect to the overall flow direction and can follow a convoluted path through the medium that is longer than the nominal flowpath length.

We note here that the assumption of a cubic law is not absolutely essential for the outcome of the analysis and the same result can be obtained by using other power law exponents. If, for example, the flow resistance arises largely due the presence of fine particles in the fracture it may behave more like a porous medium in which case the exponent would be $n = 1$. If, on the other hand, the flow resistance is due to flow restrictions randomly located in the fracture, the exponent would be $n = 0$. For a more detailed discussion concerning the power law exponent for viscous flow in fractures, the reader is directed to the paper by /Neretnieks 2002/. For the current analysis, however, we shall assume the term α as defined in Equation D-5.

Using Equation D-4 the flowrate can be given as:

$$q = \mathrm{K} A_{xs} i_x = \left(\frac{n \alpha W_c}{\tau_p} \right) i_x \qquad \text{(D-7)}$$

The specific flow-wetted surface (a_R) is:

$$a_R = \frac{2 n W_c L_p \tau_p}{A_{xs} L_p} = \frac{2 n W_c \tau_p}{A_{xs}} \qquad \text{(D-8)}$$

The product $L_p\tau_p$ is, of course, the actual path length, L_s of a channel accounting for flow-path tortuosity (here we assume for simplicity that all flow channels have equal tortuosity):

$$L_s = \tau_p L_p \qquad \text{(D-9)}$$

Using Equation D-2, the *FWS/q* ratio can then be written as:

$$\frac{FWS}{q} = \frac{L_p a_R}{\mathrm{K} i_x} = \frac{L_p \left(\frac{2 n W_c \tau_p}{A_{xs}} \right)}{\left(\frac{n \alpha W_c}{\tau_p A_{xs}} \right) i_x} = \frac{2 L_p \tau_p^2}{\alpha\, i_x} \qquad \text{(D-10)}$$

Notionally, the value of *FWS/q* is independent of both the number of flowpaths, *n* and the flowpath width, W_c, although it is quadratically related to the flowpath tortuosity, τ_p. It should be remembered in this analysis that the extent to which the flowpath tortuosity influences the flowrate depends upon whether a global hydraulic gradient or a local hydraulic gradient is specified (i.e. a gradient over the length of the stream tube, or relative to specific internal flowpaths or fractures).

If we were to consider a bundle of straight, independent flow channels (i.e. a multi channel model, or MCM) instead of the stream tube with hypothetically tortuous flow channels, the *FWS/q* ratio would then be given by:

$$\left.\begin{array}{l} FWS = n\left(2 W_c L_p\right) \\ q = n T W_c i_x \end{array}\right\} \frac{FWS}{q} = \frac{2 L_p}{T\, i_x} \qquad \text{(D-11)}$$

This is identical to Equation D-10 for the case $\tau_p = 1.0$ (i.e. straight flow channels).

As can be seen from the above equations, changing the channel width, W_c has an influence on both the specific flow-wetted surface (a_R) and the flowrate (q). This is only true, however, for situations where the flowrate is proportional to the flow channel width and it is easy to imagine scenarios where the flow is restricted in such a way that it is independent of the flow channel width (e.g. a flow annulus or "bottleneck"). It can also be seen that for a bundle of essentially identical flow channels it makes no difference for the estimate of *FWS/q* how many channels there are as the variable n appears both in the definition of a_R and q thereby cancelling each other. For a bundle of tubes that have identical transmissivities, this is a trivial result as the *FWS/q* ratio for any individual channel is the same as the ensemble *FWS/q* regardless of how many channels there are. If we double the fracture intensity thereby doubling the number of channels, we double the flow-wetted surface, but we also double the overall flow for the ensemble of channels.

This means that it is quite feasible for a system with many flowpaths and a high specific flow-wetted surface to have the same *FWS/q* ratio as a system with very few flowpaths and consequently a low specific flow-wetted surface.

Additionally, including the possibility of tortuous flowpaths in the system also illustrates a feature of viscous flow in a multi channel representation that would not otherwise be obvious. As can be seen from the above equations, changing the flowpath tortuosity will also change the numerical value of both the specific flow-wetted surface and hydraulic conductivity. In this case, however, a doubling in the flowpath tortuosity results in a doubling of flow-wetted surface and a halving of the flowrate thereby giving a four-fold increase in the *FWS/q* ratio.

We also note that for a fixed flowrate, a change in the specific flow-wetted surface gives a corresponding change in the *FWS/q* ratio. If the specific flow-wetted surface is halved, then the length of the stream tube must be doubled in order to accumulate the same *FWS/q* for the same flow.

As the above discussion implies, the specific flow-wetted surface therefore does not uniquely describe the transport properties of the system and must always be put in the context of flow to make predictions of the transport resistance. Notwithstanding this, however, we note that in systems where diffusive exchange with the rock matrix dominates the solute residence time distribution, the magnitude of the surface area over which matrix diffusion takes place is a key entity governing transport. The magnitude of the specific flow-wetted surface is therefore an indicator of the potential for solute-rock matrix interaction for a given flow system and has a strong qualitative significance for site understanding in this respect.

Appendix E

Estimation of the specific flow-wetted surface in fractured rock

The flow-wetted surface is estimated from geometrical-statistical considerations, based upon the number of hydraulically conductive fractures (channels) intersected by a borehole drilled in the rock mass. We consider a rock volume with a number of channels randomly oriented in space. In this rock volume we also consider that the channels have some mean length (L_c), width (W_c), and area (A_c).

A borehole drilled through the rock mass will intersect a channel, on average, every H metres. To estimate the flow-wetted surface, we want to be able to relate the frequency with which channels are intersected by the borehole with the number of channels in a given volume of rock. We do not know a priori what the average dimensions (L_c and W_c) of the channels are. The only details we know are the borehole diameter (D_{bh}) and the average distance between conductive fractures in the rock (H) obtained from hydraulic packer tests.

Given that the channels are randomly distributed in space they can be oriented parallel, perpendicular, or at some oblique angle relative to the borehole. Channels that are perpendicular, or nearly so, to the borehole are more likely to be intersected than those having sharply oblique inclinations. For this reason, we consider the average area of the channels projected onto the plane perpendicular to the borehole rather than the actual average area of the channels.

As we are interested in the "average" properties of the rock volume, the projected areas are then redistributed over this plane with a separation between them equal to the borehole diameter. The separation between the projected channel areas is equal to the borehole diameter, as the borehole only has to touch the edge of a channel for a hydraulic test to indicate a conductive feature. This concept is illustrated in Figure E-1 below where the variables W_p and L_p represent the average projected dimensions corresponding to the actual channel length and width.

It should be noted that the average projected area is not equal to the product of the projected length and width, as would be the case for a rectangular shape such as that depicted above. This is because the projected areas are not necessarily rectangular and are actually parallelograms. The perimeter of the projected area, however, is the same regardless of whether it is in the form of a rectangle or a parallelogram.

If we visualise a single channel of length L_c and width W_c, with centre fixed at the Cartesian origin, we can pivot the channel in any direction and it will trace out a spherical surface as shown in Figure E-2 below.

If a large number of channels are randomly oriented in this fashion, the extremities of these channels should be randomly distributed over the surface of the sphere as shown in the diagram on the right-hand side of Figure E-2. The projected length of the channel will be equal to the length vector projected onto the x-y plane and is dependent upon the inclination of the channel relative to the borehole axis (θ). As the channels are evenly distributed with reference to the surface of the sphere, this suggests that the average projected length should be calculated based upon the first moment of the projected length with respect to the spherical surface.

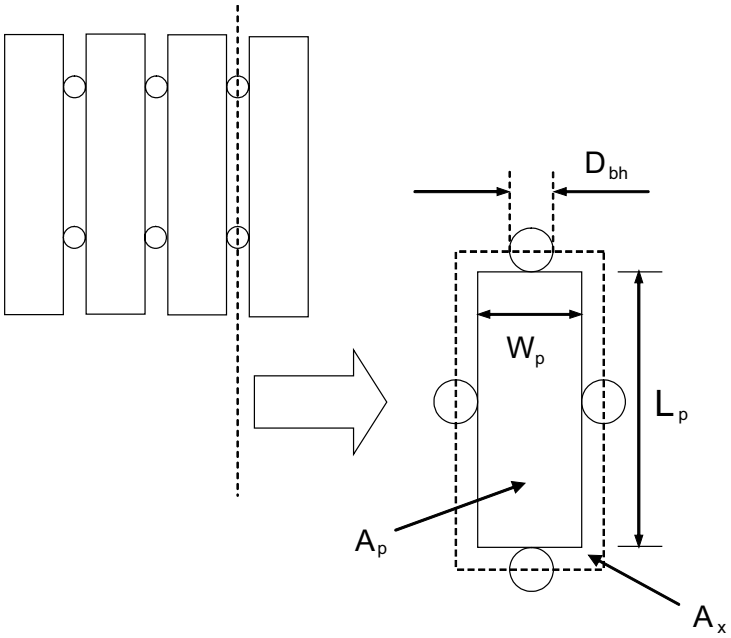

Figure E-1. *Schematic diagram showing projected channel areas (**A_p**) distributed over the plane perpendicular to the borehole axis. The projected channels have length **L_p** and width **W_p** and are separated by a distance equal to the borehole diameter, **D_{bh}**. **A_x** is the area comprising the spaces between the channels. (Note that the projected areas are actually parallelograms and are not necessarily rectangular as shown in the figure).*

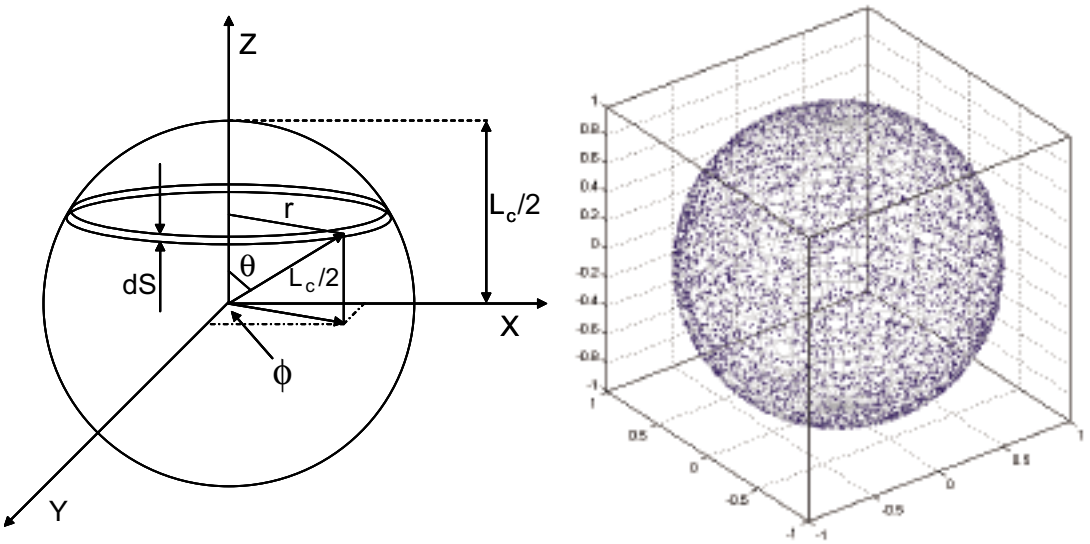

Figure E-2. *Schematic diagram of a channel with centre fixed at the origin. The channel can be pivoted in any direction and it will trace out a spherical surface with diameter equal to the channel length (**L_c**). The **z**-axis corresponds to the axial direction of the borehole; **x-y** axis is the plane perpendicular to the borehole. The figure on the right-hand side shows the distribution of 4,500 randomly oriented channels touching the surface of the sphere.*

From geometrical considerations, the differential area variable (dS) is given by:

$$dS = 2\pi r(L_c/2)d\theta = 2\pi(L_c/2)\sin\theta(L_c/2)d\theta \quad \text{(E-1)}$$

The length sum over all possible angles is then:

$$L_{sum} = 2\int_0^{\frac{\pi}{2}} r\, dS = \frac{\pi}{2} L_c^3 \int_0^{\frac{\pi}{2}} \sin^2\theta\, d\theta$$

$$= \frac{\pi}{2} L_c^3 \int_0^{\frac{\pi}{2}} 1-\cos 2\theta\, d\theta = \frac{\pi}{2} L_c^3 \left[\frac{\theta}{2} - \frac{\sin 2\theta}{4}\right]_0^{\frac{\pi}{2}} = \frac{\pi^2}{8} L_c^3 \quad \text{(E-2)}$$

The average projected length, L_p is then obtained by:

$$L_p = \frac{\frac{\pi}{2}\int_0^{\frac{\pi}{2}} r\, dS}{\frac{\pi}{2}\int_0^{\frac{\pi}{2}} dS} = \frac{L_c^3 \int_0^{\frac{\pi}{2}} \sin^2\theta\, d\theta}{L_c^2 \int_0^{\frac{\pi}{2}} \sin\theta\, d\theta} = L_c \frac{\pi}{4} \quad \text{(E-3)}$$

In the same fashion, the average projected width of the channel is found to be:

$$W_p = W_c \frac{\pi}{4} \quad \text{(E-4)}$$

The average projected perimeter is the same regardless of whether the projected shape is a rectangle or a parallelogram and is equal to twice the sum of W_p and L_p.

The projected area is obtained by taking the inner product of the area vector (perpendicular to the length vector) and the unit vector of the projection plane (the unit vector in the direction of the z-axis). Once again, we take the first moment of the projected area with respect to the spherical surface to find the average projected area (A_p). The area sum over all possible angles is then:

$$A_{sum} = 2\int_0^{\frac{\pi}{2}} A_c\, dS = \frac{\pi}{2} A_c L_c^2 \int_0^{\frac{\pi}{2}} \cos\theta \sin\theta\, d\theta$$

$$= \frac{\pi}{2} A_c L_c^2 \int_0^{\frac{\pi}{2}} \frac{\sin 2\theta}{2}\, d\theta = \frac{\pi}{4} A_c L_c^2 \left[-\cos 2\theta\right]_0^{\frac{\pi}{2}} = \frac{\pi}{4} A_c L_c^2 \quad \text{(E-5)}$$

The average projected area, A_p is then obtained by:

$$A_p = \frac{\frac{\pi}{2}\int_0^{\frac{\pi}{2}} A_c \cos\theta\, dS}{\frac{\pi}{2}\int_0^{\frac{\pi}{2}} dS} = \frac{A_c L_c^2 \int_0^{\frac{\pi}{2}} \cos\theta \sin\theta\, d\theta}{L^2 \int_0^{\frac{\pi}{2}} \sin\theta\, d\theta} = \frac{A_c}{2} = \frac{L_c W_c}{2} \quad \text{(E-6)}$$

The average projected area, A_0 required for a channel to be intersected by a borehole is equal to the average projected area of the channel (A_p) plus the area comprising the space between the channels (A_x) as illustrated in Figure E-1. The area A_0 is given by:

$$A_0 = A_p + A_x \approx \frac{L_c W_c}{2} + D_{bh}\left(L_p + W_p\right) + D_{bh}^2$$

$$= \frac{L_c W_c}{2} + \frac{\pi}{4} D_{bh}\left(L_c + W_c\right) + D_{bh}^2 \quad \text{(E-7)}$$

If the average distance between channels intersected by the borehole is H, then the average rock volume containing one channel is equal to HA_0. The specific flow-wetted surface area, a_R (m^2/m^3) is the actual surface area of the channel ($2A_c$) divided by the rock volume HA_0. The specific flow-wetted surface is thus:

$$a_R = \frac{2A_c}{HA_0} = \frac{2L_cW_c}{H\left(\frac{L_cW_c}{2} + \frac{\pi}{4}D_{bh}\left(W_c + L_c\right) + D_{bh}^2\right)} \quad \text{(E-8)}$$

If the borehole diameter is sufficiently small in relation to the channel dimensions (L_c and W_c), we denote the specific flow-wetted surface as a_{R0} and Equation E-8 simplifies to:

$$a_{R0} \approx \frac{4}{H} = 4P_{10c} \quad \text{(E-9)}$$

It should be noted from Equation E-9 that the inverse of the average flow channel spacing, H (m) is the conductive fracture frequency, or P_{10c} (m^{-1}) as referred to in various SKB reports and documents /e.g. Holmén and Outters 2002/.

If the borehole diameter is not negligible in comparison with the flow channel dimensions, an error is introduced by using the approximation given in Equation E-9. The ratio between the specific flow wetted surface given by Equation E-8 and that given by the simplified Equation E-9 is:

$$\frac{a_R}{a_{R0}} = \frac{L_cW_c}{2\left(\frac{L_cW_c}{2} + \frac{\pi}{4}D_{bh}\left(W_c + L_c\right) + D_{bh}^2\right)} \quad \text{(E-10)}$$

For a borehole with diameter, D_{bh} = 0.076 m, the ratio a_R/a_{R0} calculated using Equation E-10 is roughly in the range 0.3–1.0 for channel widths of 0.1–1.0 m and large channel aspect ratios (i.e. L/W ≫1). If we consider flow channels where the aspect ratio is greater than unity and the average width of the flow channels is at least equal to the borehole diameter, it appears that the aspect ratio only has a minor influence on the calculated a_R (see Table E-1 below).

Table E-1. Relative specific flow-wetted surface (a_R/a_{R0}) for various channel widths and channel L/W aspect ratios.

Aspect Ratio (L/W)	1	5	10	100	∞
W (m)	a_R/a_{R0}				
0.01	0.01	0.03	0.04	0.07	0.08
0.1	0.22	0.38	0.41	0.45	0.46
0.25	0.47	0.62	0.65	0.67	0.68
0.5	0.66	0.77	0.79	0.81	0.81
0.75	0.75	0.84	0.85	0.86	0.86
1	0.80	0.87	0.88	0.89	0.89
10	0.98	0.99	0.99	0.99	0.99

If the exact number of conductive fractures in the rock is known, the value of H is equal to the borehole depth divided by the number of conductive fractures. For a hydraulic test using packed off borehole sections (or otherwise binned data) the Poisson frequency, λ (fractures/ packer section) is equal to the packer spacing, L_s, divided by the average distance between fractures:

$$\lambda = L_s / H \tag{E-11}$$

The specific flow-wetted surface can therefore be written as:

$$a_{R0} = 4\lambda / L_s \tag{E-12}$$

If the distribution of fractures in a homogeneous rock mass can be assumed to be random and non-correlated in space, any hydraulic measurements performed to identify the locations of the fractures can be described with Poisson statistics for a sufficiently large number of measurements. This may not always be a valid assumption owing to trends of changing fracture frequency with depth, non-random fracture orientations, possible non-Poissonian fracture clustering, etc. If we consider as a working hypothesis, however, that the fractures are randomly distributed, the probability of finding a given number, x of flowing (i.e. hydraulically conductive) fractures within a random packer section is then given by:

$$P(\lambda, x) = \frac{\lambda^x}{x!} e^{-\lambda} \tag{E-13}$$

It cannot be determined, on the basis of hydraulic measurements using packed-off borehole sections, whether a conductive interval contains only one fracture or multiple fractures. This means that if hydraulic measurements are used to estimate the frequency of open (and flowing) fractures in a borehole, the result will tend to underestimate the actual number.

Statistically, the fraction of undetected flowing fractures, f_u is given by:

$$f_u = \frac{\lambda - \left(1 - P\left[\lambda, 0\right]\right)}{\lambda} = 1 - \frac{\left(1 - e^{-\lambda}\right)}{\lambda} \tag{E-14}$$

The probability of finding multiple conductive fractures in a given packer section as well as the statistical fraction of undetected conductive fractures is shown in Figure E-3 as a function of the normalised conductive fracture frequency, λ.

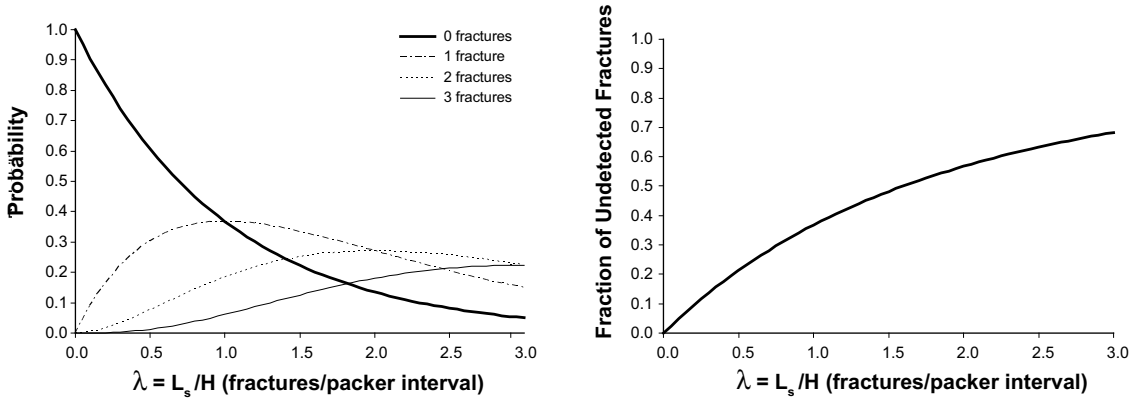

Figure E-3. *Probability of finding multiple conductive fractures in a given packer section as well as the statistical fraction of undetected conducted fractures as a function of fracture Poisson frequency.*

The results indicate that for a packer distance of roughly the same size as the average conductive fracture spacing ($\lambda = 1$), up to 40% of the conductive fractures will remain undetected. The fraction of undetected conductive fractures increases with increasing λ and the packer spacing used for measurements should preferably be smaller than, and certainly not larger than, the average conductive fracture spacing.

In order to address the uncertainty of estimating the true number of conductive fractures, the Poisson distribution can be used to estimate the "actual" conductive fracture frequency from the proportion of non-conductive sections measured in hydraulic tests. The actual conductive fracture frequency is estimated by:

$$\lambda = -\ln (P_0) \qquad \text{(E-15)}$$

An estimate of the actual specific flow-wetted surface, a_{R0} (m^2/m^3) is therefore given by:

$$a_{R0} \approx -\frac{4}{L_s} \ln \left(P_0 \right) \qquad \text{(E-16)}$$

Where P_0 is the probability of finding a non-conductive packer section during the borehole test. This is equal to the number of non-conductive sections identified, divided by the total number of sections tested. The estimated fracture Poisson frequency, λ is plotted in Figure E-4 as a function of the fraction of non-conductive packer intervals.

From Figure E-4 it can be seen that the most reliable estimate of a_{R0} will be obtained in the approximately linear portion of the curve when the fraction of non-conducting intervals is at least 20% and less than about 80%. As the fraction of non-conducting packer intervals is only an estimate of the true probability of finding a non-conducting interval, a confidence interval may be constructed for the estimated a_{R0}. For a finite sample size, n the probability of finding a non-conductive interval is given by the binomial distribution.

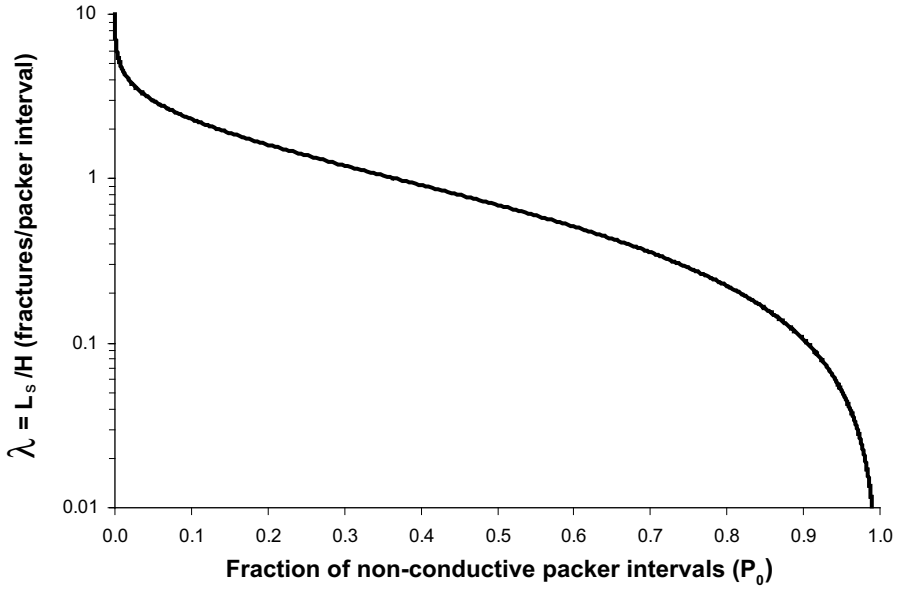

Figure E-4. *Estimated fracture Poisson frequency as a function of the fraction of non-conductive intervals in a hydraulic packer test.*

The standard error of the estimated conductive fracture frequency is given by:

$$\sigma_\lambda = \frac{1}{P_0}\sigma_{P_0} = \sigma_{P_0}^{rel} \tag{E-17}$$

As the conductive fracture frequency is directly proportional to the specific flow-wetted surface, the relative standard error of the estimated a_{R0} is:

$$\sigma_{a_{R0}}^{rel} = \sigma_\lambda^{rel} = \frac{1}{\lambda}\sigma_{P_0}^{rel} \tag{E-18}$$

To estimate the relative standard error of the probability, P_0 we need to use the binomial distribution. The binomial distribution is appropriate in this case as P_0 is the probability of finding a non-conductive section in a finite set of measurements where there are only two possible outcomes for a given section; conductive, or non-conductive.

Assuming binomial probabilities, the standard error of P_0 is then given by:

$$\sigma_{P_0} = \sqrt{\frac{P_0\left(1-P_0\right)}{n}} \tag{E-19}$$

The relative error is thus:

$$\sigma_{P_0}^{rel} = \frac{1}{P_0}\sqrt{\frac{P_0\left(1-P_0\right)}{n}} = \sqrt{\frac{\left(1-P_0\right)}{nP_0}} \tag{E-20}$$

The relative error of the estimated specific flow-wetted surface, a_{R0} is therefore:

$$\sigma_{a_{R0}}^{rel} = \frac{1}{\lambda}\sigma_{P_0}^{rel} = \frac{-1}{\ln\left(P_0\right)}\sqrt{\frac{\left(1-P_0\right)}{nP_0}} \tag{E-21}$$

Using Equation E-16, we can write for the absolute error:

$$\sigma_{a_{R0}} = \frac{4}{L_s}\sqrt{\frac{\left(1-P_0\right)}{nP_0}} \tag{E-22}$$

The 100(l–α)% binomial confidence interval for the estimated a_{R0} may be calculated with the following expression:

$$-\frac{4}{L}\ln\left(P_U\right) \le a_{R0} \le -\frac{4}{L}\ln\left(P_L\right) \tag{E-23}$$

For a data set consisting of n measurements, the two-sided confidence limits (P_U and P_L) are determined by solving the associated cumulative binomial probability equations:

$$\sum_{k=0}^{nP_0}\binom{n}{k}P_U^k\left(1-P_U\right)^{n-k} = \alpha/2 \tag{E-24}$$

$$\sum_{k=0}^{nP_0-1}\binom{n}{k}P_L^k\left(1-P_L\right)^{n-k} = 1-\alpha/2 \tag{E-25}$$

It should be noted that the confidence interval calculated in this manner is not symmetric about the estimated a_{R0} given by Equation E-16 unless the sample size is large.

For sufficiently large sample sizes, the normal approximation to the binomial distribution may be used to define the 100(l–α)% confidence interval for a_{R0}:

$$-\frac{4}{L_s}\ln\left(P_0 + z_{\frac{\alpha}{2}}\sqrt{\frac{P_0(1-P_0)}{n}}\right) \le a_{R0} \le -\frac{4}{L_s}\ln\left(P_0 - z_{\frac{\alpha}{2}}\sqrt{\frac{P_0(1-P_0)}{n}}\right) \quad \text{(E-26)}$$

For large n, the distribution can also be approximated by:

$$-\frac{4}{L_s}\ln(P_0) - z_{\frac{\alpha}{2}}\frac{4}{L_s}\sqrt{\frac{(1-P_0)}{nP_0}} \le a_{R0} \le -\frac{4}{L_s}\ln(P_0) + z_{\frac{\alpha}{2}}\frac{4}{L_s}\sqrt{\frac{(1-P_0)}{nP_0}} \quad \text{(E-27)}$$

Figure E-5 below shows an example confidence interval (95%) for the estimated a_{R0} given a hypothetical packer fracture frequency of 0.33 fractures/packer interval and varying sample sizes.

The confidence intervals calculated using Equation E-23 or E-27 only consider the possibility that the Poisson frequency may be incorrectly estimated from a limited number of measurement data points. The evaluation assumes that the hydraulic measurements are accurate (i.e. that they can detect low flow-rates, that individual fractures do not overlap adjacent packer sections, that leaky packers do not corrupt the measurements) and that the measurements are representative for the rock volume being sampled.

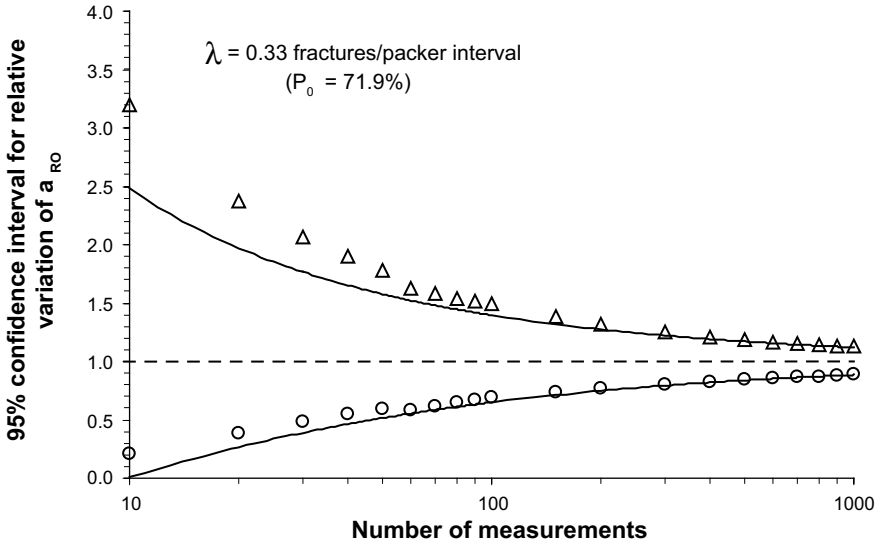

Figure E-5. *95% confidence interval for the relative variation of specific flow-wetted surface (a_{R0}) as a function of sample size with a fracture Poisson frequency, λ = 0.33 fractures/interval. Symbols indicate "exactly" calculated binomial confidence limits. Unbroken lines indicate confidence limits based upon the normal approximation to the binomial distribution.*

If the method used to detect water flow within the packed-off section is not sufficiently sensitive, many flowing features may remain undetected and thus lead to a significant underestimation of the flow-wetted surface. Under field conditions, some or all of the above mentioned factors would reduce the accuracy of the estimation to some degree. For this reason, the confidence intervals calculated should be considered as the minimum degree of variation that can be expected to arise from purely statistical consideration of the conductive fracture frequency. It should also be remembered that conductive fractures identified using borehole tests might not be hydraulically conductive under natural conditions with different hydraulic gradients and boundary conditions.

The probability that a fracture with a random orientation will overlap adjacent packer sections increases with decreasing packer separation. Consequently, there is a lower limit to the practical size of a packer interval that can be used in a hydraulic test. This problem can be reduced somewhat by using longer packers, although there is also a practical limit to the dimensions of the packers that can be used efficiently.

Mechanically eroded borehole walls and loose debris can also cause problems by preventing the establishment of a tight seal over the packed-off section. This can also lead to short-circuiting of the packers and an overestimation of the flow-wetted surface.

In addition to the binomial uncertainty discussed here, there is also the question of finite channel dimensions influencing the estimation of specific flow-wetted surface. As shown in Table E-1, the value of a_R (as estimated by a_{R0}) may be too large by a factor of as much as ≈ 3 owing to finite channel length and width relative to the investigatory borehole diameter (at least for flow channels with $W_c \geq 0.1$ m and reasonably large aspect ratios).

To evaluate the combined impact of finite channel dimensions and binomial uncertainties on the estimated a_R, we have made Monte-Carlo type simulations using random sampling from P_0 and W_c distributions assuming a large L_c/W_c aspect ratio. This was carried out using the following procedure:

1) Generate an $n \times 2$ list of random normal deviates R

2) Calculate a vector of random $P_{0,i}$ values assuming normally distributed P_0 (i.e. the normal approximation to the binomial distribution):
   $P_{0,i} = \mu_{P_0} + R_{(1:n,1)} \times \sigma_{P_0}$

3) Calculate a vector of $W_{c,i}$ values assuming a log-normal distribution of channel widths:
   $\log_{10} W_{c,i} = \mu_{W_c} + R_{(1:n,2)} \times \sigma_{W_c}$

4) For an assumed flow channel aspect ratio, $f_{L/W}$ calculate the corresponding vector of channel lengths:
   $L_{c,i} = f_{L/W} \times W_{c,i}$

5) Using the $P_{0,i}$ data calculate the vector of H_i values for the average flow channel separation given the known packer distance, L_s used in the PFL data acquisition:
   $H_i = -L_s / \ln (P_{0,i})$

6) Calculate a_R using Equation E-8.

Table E-2 below summarises some data taken from PFL measurements carried out in the Laxemar sub-region for KLX02, KLX03, KLX04, and KLX06 /Ludvigson et al. 2002, Rouhiainen et al. 2005, Rouhiainen and Sokolnicki 2005, Sokolnicki and Rouhiainen 2005/.

The data include the number of measured borehole sections (n) the number of flowing sections (N_{fl}), the fraction of non-flowing sections identified (P_0), the average distance between adjacent flowing features (H, derived using Equation E-11), the approximately estimated specific flow-wetted surface (a_{R0}), and the upper and lower confidence intervals (95%-level) for the distribution considering binomial probabilities (Equation E-23):

Table E-2. PFL data for some boreholes in the Laxemar sub area. Sections residing within deformation zones have been excluded for data sets KLX02_NDZ, KLX03_NDZ and KLX04_NDZ. Borehole KLX02 has DZ regions extending from 704–1,107 m. For borehole KLX03 there is only one DZ in the lower part of the borehole (770–960 m). KLX04 has five smaller DZ regions in the upper 450 m and one large DZ in the lower part of the borehole (873–973 m).

Borehole	n	N_{fl}	P_0	H (m)	a_{R0} (m^2/m^3)	a_{RL} (m^2/m^3)	a_{RU} (m^2/m^3)
	Data for entire borehole (100–1,000m)						
KLX02_NDZ [1)]	n/a	n/a	0.667	22.2	0.540	n/a	n/a
KLX03	178	36	0.798	22.1	0.181	0.126	0.250
KLX03_NDZ	161	29	0.820	25.2	0.159	0.106	0.228
KLX04	177	67	0.616	10.3	0.388	0.299	0.493
KLX04_NDZ	148	49	0.662	12.1	0.330	0.250	0.446
KLX06	178	72	0.596	9.7	0.412	0.322	0.524
	Data for depth < 450m						
KLX02_NDZ [2)]	68	43	0.368	3.0	1.334	0.942	1.828
KLX03	70	23	0.671	12.6	0.319	0.213	0.502
KLX04	70	38	0.443	6.1	0.652	0.454	0.901
KLX04_NDZ	60	30	0.483	6.9	0.582	0.409	0.871
KLX06	71	51	0.282	4.0	1.008	0.731	1.366

1) Data taken from /Andersson et al. 2002b/ for depth 186–704 m and transmissivity cut-off of 10^{-10} m^2/s
2) Data taken from /Crawford et al. 2003/ for depth 204–405 m and a flow cut-off of 6 ml/min

For the following calculation, we have elected to use the data from borehole KLX03 (i.e. KLX03_NDZ 100–1,000 m). The choice is arbitrary, although partly motivated by the fact that KLX03 has the lowest frequency of conductive fractures and consequently gives the lowest specific flow-wetted surface amongst the data for the different boreholes.

If we were to consider as a base case, a single fracture with very large dimensions relative to the borehole diameter, we obtain a distribution for a_R that is only dependent upon binomial uncertainty. This case is illustrated in Figure E-6 below (10^6 stochastic realisations) to confirm that the distribution calculated using the Monte-Carlo technique is consistent with the bounds for a_{RL} and a_{RU} given by Equation E-23 (data are based upon PFL measurements made in KLX03).

We do not know a priori what the average dimensions of a typical flow channel will be. If we assume an average flow channel width, W_c = 0.5 m (i.e. a single-value), we obtain the distribution for a_R illustrated in Figure E-7.

For a channel width, W_c = 0.1 m, the deviation is even more pronounced as can be seen in Figure E-8.

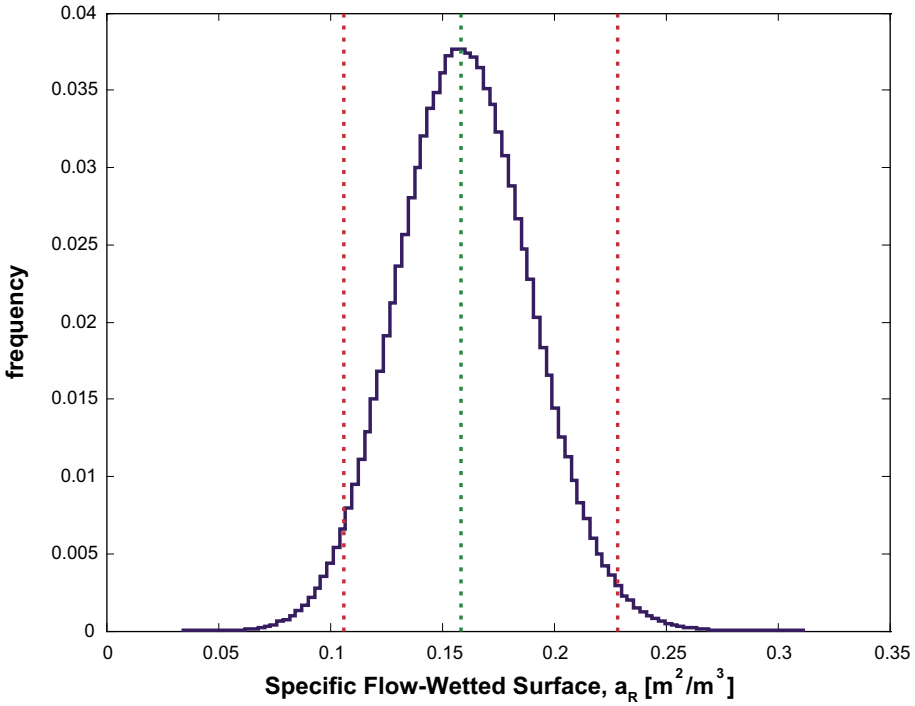

Figure E-6. *Uncertainty distribution of "true" specific flow-wetted surface, a_R (m^2/m^3) owing to binomial probability for fractures with very large dimensions (W_c and L_c) relative to the borehole diameter (E_{bh}). The vertical lines in the figure illustrate the central value of the estimate (a_{R0}) as well as the lower (a_{RL}) and upper (a_{RU}) bounds defining the 95% confidence interval for a_{R0}.*

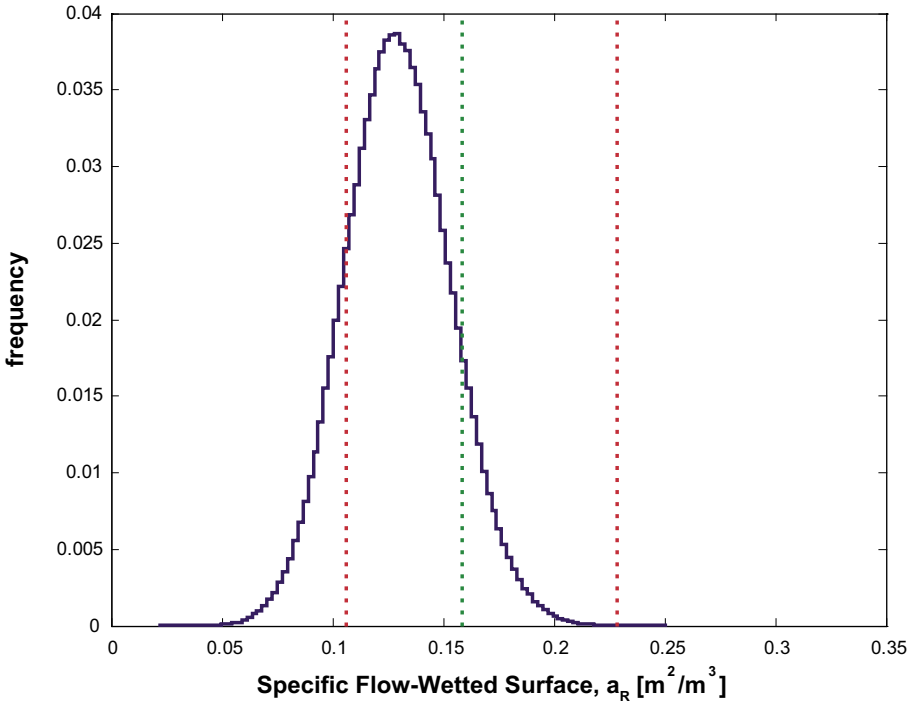

Figure E-7. *Uncertainty distribution of "true" specific flow-wetted surface, a_R (m^2/m^3) owing to binomial probability for an average flow channel width of W_c = 0.5 m and aspect ratio, $L_c/W_c = \infty$ for a borehole diameter, D_{bh} = 0.076 m. The vertical lines in the figure illustrate the central value of the estimate (a_{R0}) as well as the lower (a_{RL}) and upper (a_{RU}) bounds defining the 95% confidence interval for a_{R0}.*

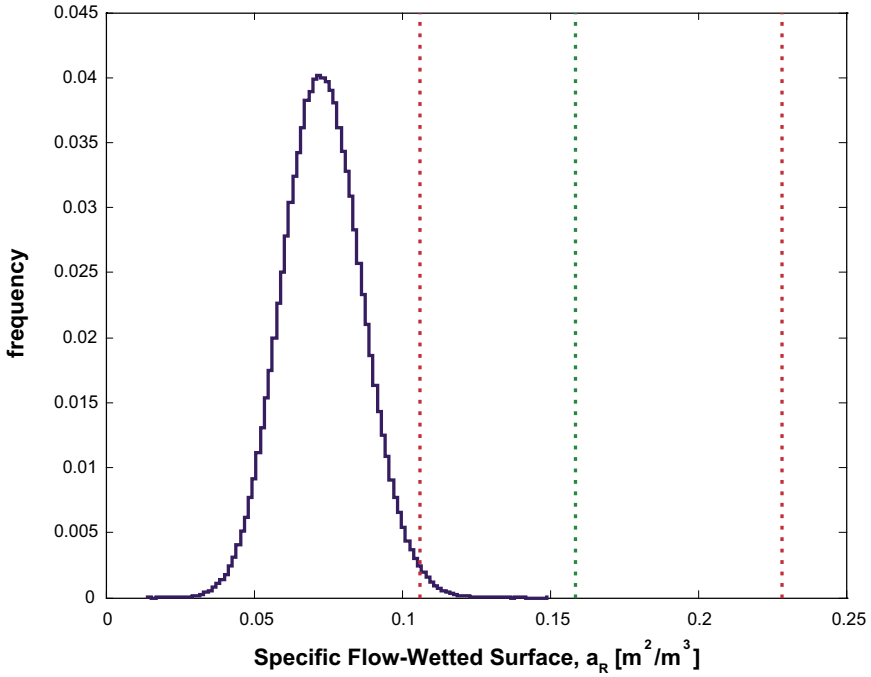

Figure E-8. *Uncertainty distribution of "true" specific flow-wetted surface, a_R (m^2/m^3) owing to binomial probability for an average flow channel width of W_c = 0.1 m and aspect ratio, $L_c/W_c = \infty$ for a borehole diameter, D_{bh} = 0.076 m. The vertical lines in the figure illustrate the central value of the estimate (a_{R0}) as well as the lower (a_{RL}) and upper (a_{RU}) bounds defining the 95% confidence interval for a_{R0}.*

As can be seen from the figures above, the distribution of a_R for finite channel dimensions is likely to be significantly lower than the estimated confidence interval for a_{R0} would otherwise indicate. For a channel width of 0.1 m, the estimated specific flow-wetted surface, a_{R0} is some 2.4 times larger than the value estimated when considering a finite channel width (a_R). For a channel width of 0.5 m, a_{R0} is roughly 1.3 times larger.

If we were to consider a distribution of channel widths (such as a probability function reflecting our uncertainty concerning W_c), the uncertainty distribution for a_R will be broader than indicated in the figures above.

As discussed previously, it has been speculated from field observations that flow channel widths are likely to be on the order of a few cm up to perhaps 0.5–1.0 m wide /e.g. Abelin et al. 1994, Birgersson et al. 1992, SKB, 2005b/. Based upon observations in the Bolmen and Kymmen tunnels in Sweden it is thought that there possibly are very few flow channels with widths larger than about 0.2 m /Moreno and Neretnieks 1989/ in fractured rock typical of Swedish conditions.

Taking these figures as a rough guide, we assume the following log-normal distribution as the basis for a scoping calculation for the impact of flow channel width uncertainty:

$$\log_{10} W_{c,i} = \log_{10} (0.1) + R_{(1:n,2)} \times 0.3 \qquad \text{(E-28)}$$

Although this is an arbitrary distribution it approximately covers the range of values suggested in the previous discussion as can be seen in Figure E-9.

The resulting uncertainty distribution calculated for a_R is shown in Figure E-10.

The central estimate for a_{R0} in this case is some 2.4–2.7 times higher than the central moment of the uncertainty distribution for a_R depending upon whether we compare with the arithmetic or logarithmic mean of the resulting distribution for a_R shown.

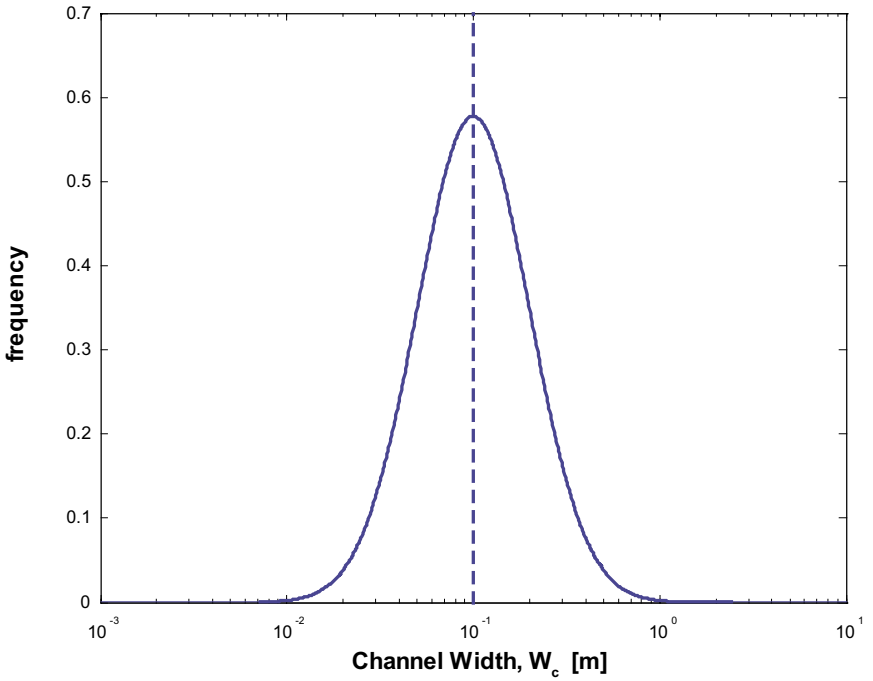

Figure E-9. *Uncertainty distribution of flow channel width assuming a central value of 0.1 m, a log-normal distribution and a standard deviation of 0.3 (log_{10}-units).*

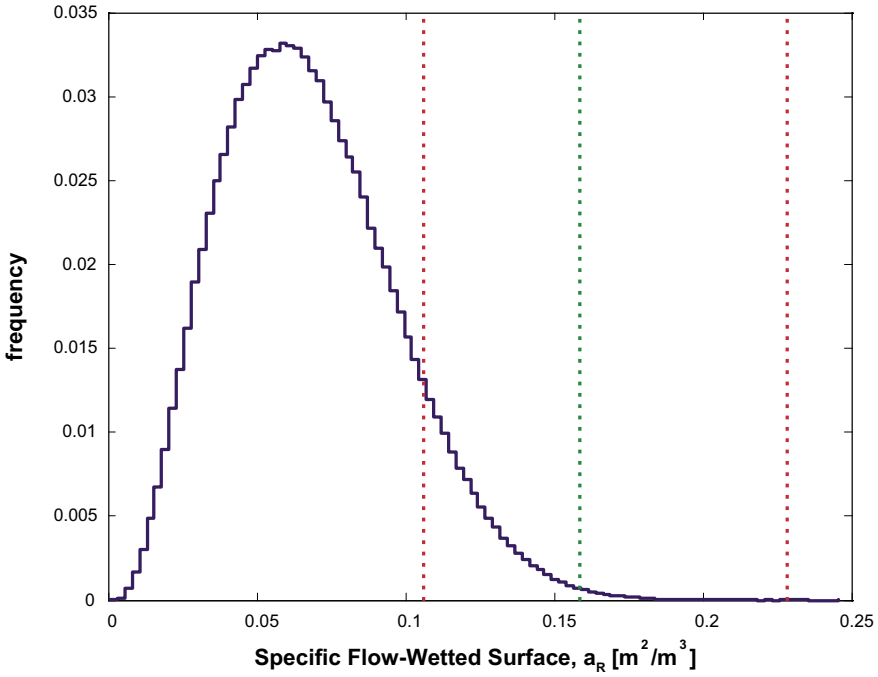

Figure E-10. *Uncertainty distribution of "true" specific flow-wetted surface, a_R (m^2/m^3) owing to binomial probability and channel width uncertainty (assuming the distribution of W_c given by Equation E-28) for an aspect ratio, $L_c/W_c = \infty$ and borehole diameter, $D_{bh} = 0.076$ m. The vertical lines in the figure illustrate the central value of the estimate (a_{R0}) as well as the lower (a_{RL}) and upper (a_{RU}) bounds defining the 95% confidence interval for a_{R0}.*

Appendix F

Development of transport model

Advective flow and transport in a single channel with matrix uptake

The transport model considers advective flow and transport along a flowpath where solute can diffuse into and sorb upon micro-surfaces in the rock matrix. The rock matrix adjacent to the fracture flowpath may consist of multiple layers of rock with differing sorptive and diffusive properties. Additionally, the model considers the existence of stagnant zones lying in the plane of the fracture. Solute may diffuse into these stagnant zones and then subsequently also diffuse and sorb within the rock matrix.

The model assumes that flow is fully mixed across the width of the flowpath and that hydrodynamic dispersive mixing can be neglected. This last assumption is reliant upon the observation that hydrodynamic dispersion is generally dominated by the difference in residence times of solutes transported along different advective flowpaths and therefore does not need to be treated on the level of individual flow channels /Gylling 1997/. The geometry of the flow system is illustrated in Figure F-1 below.

The rock matrix adjacent to the flow channel is discretised into a number of distinct layers with differing material properties as shown in Figure F-2:

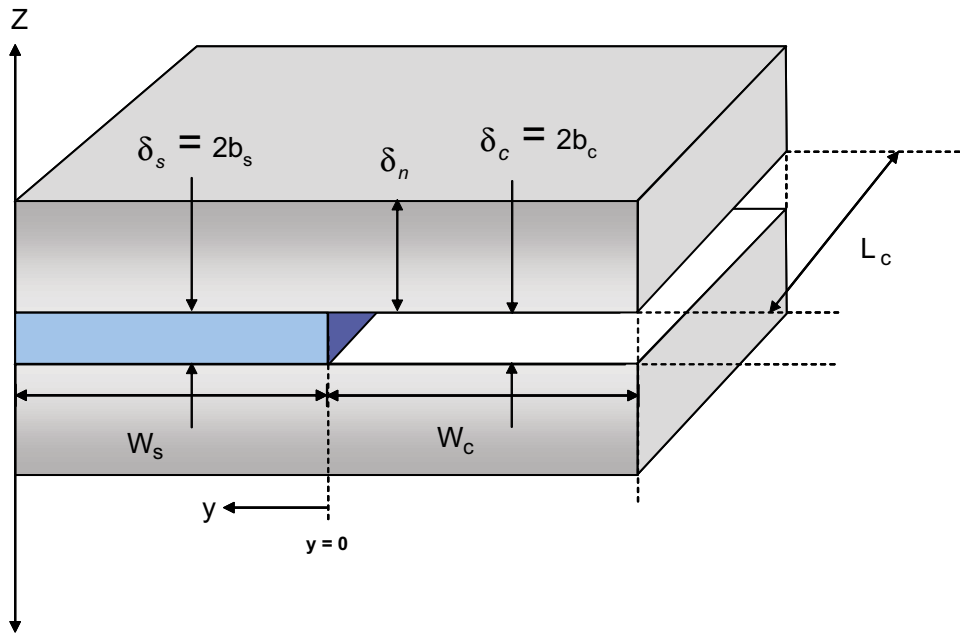

Figure F-1. *Schematic diagram showing layout of flow channel and adjacent stagnant zone. Matrix diffusion can occur in both the mobile and stagnant zones.*

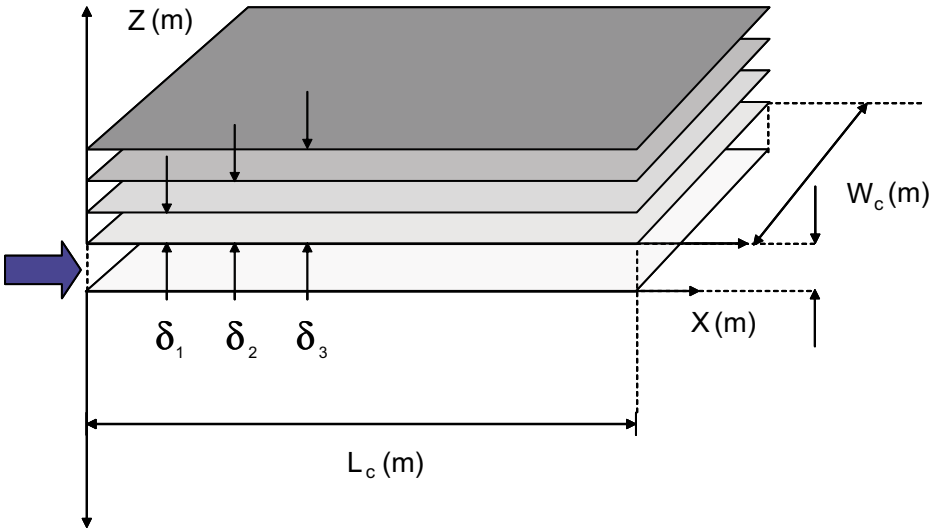

Figure F-2. *Conceptualisation of rock matrix as a composite system with layers possessing differing material properties.*

In the derivation of the mass balance equations for solute transport we assume that the solute concentration is fully mixed across the width of the flow channel. Furthermore, we neglect two- or three-dimensional interactions as may occur, for example, at the boundary between the mobile and stagnant water volumes. The solute fluxes in the rock matrix are thereby modelled as a set of parallel coupled, one-dimensional fluxes. This approximation is valid for flow channel with width significantly greater than the channel transport aperture (i.e. $W_c \gg \delta_c$), although this may not be accurate for very narrow flow channels or those that are cylindrical or tube-shaped. The model does not consider diffusive stagnant volumes perpendicular to the plane of the flow channel (i.e. abutting or crossing fractures containing stagnant water).

Assuming a Dirac $\delta(t)$ pulse concentration boundary condition and a finite concentration for $x \rightarrow \infty$, the Laplace-space solution (ϕ is the Laplace-space variable) for the solute concentration in the fracture is:

$$\bar{C}_f = \frac{M}{q}\exp\left(-t_w\phi\right)\exp\left(-\frac{FWS_c}{q}\left(\psi_{mf} + R_s\psi_s\right)\right) \qquad \text{(F-1)}$$

Where, M is the released solute mass, t_w is the water residence time and FWS_c/q is the wetted surface to flow ratio for a channel. The terms ψ_{mf} and ψ_s are the Laplace-space fluxes to the rock matrix and stagnant zones, while the term R_s is simply the ratio of the different mass transfer surface areas at the mobile/stagnant zone boundary:

$$R_s = \frac{FWS_s}{FWS_c} = \frac{b_s f_c}{W_c} \qquad \text{(F-2)}$$

The variable f_c accounts for any constrictions at the boundary between the mobile and stagnant water zone and can also be used to account for symmetric diffusion into stagnant zones on either side of the flow channel (i.e. by setting $f_c \approx 2$).

The flux term for mass transfer from the flowing water to the rock matrix is given by:

$$\psi_{mf} = -MPG_{mf}\sqrt{\phi} \quad \text{(for an infinite, simple matrix)} \qquad \text{(F-3)}$$

$$\psi_{mf} = -MPG_{mf}\sqrt{\phi}\tanh\left(A_{mf}\delta_{mf}\sqrt{\phi}\right) \quad \text{(for a limited, simple matrix)} \qquad \text{(F-4)}$$

$$\psi_{mf} = -MPG_{mf(1)}\sqrt{\phi}\left(1-\frac{2}{1+\frac{w_{mf}}{p_{mf}}}\right) \quad \text{(for a limited, complex matrix)} \qquad \text{(F-5)}$$

The variables w_{mf} and p_{mf} are recursive terms that are derived later. The flux term for mass transfer from the flowing water to the stagnant zone (including subsequent diffusion to the rock matrix) is:

$$\psi_s = \sqrt{D_w T_s}\tanh\left(W_s\sqrt{\frac{T_s}{D_w}}\right) \quad \text{(for a limited stagnant zone width)} \qquad \text{(F-6)}$$

or,

$$\psi_s = \sqrt{D_w T_s} \quad \text{(for an infinite stagnant zone width)} \qquad \text{(F-7)}$$

The variable T_s in Equation F-6 and F-7 is defined as:

$$T_s = \phi + \frac{MPG_{ms}}{b_s}\sqrt{\phi} \quad \text{(for an infinite, simple matrix)} \qquad \text{(F-8)}$$

$$T_s = \phi + \frac{MPG_{ms}}{b_s}\sqrt{\phi}\tanh\left(A_{ms}\delta_{ms}\sqrt{\phi}\right) \quad \text{(for a limited, simple matrix)} \qquad \text{(F-9)}$$

$$T_s = \phi + \frac{MPG_{ms(1)}}{b_s}\sqrt{\phi}\left(1-\frac{2}{1+\frac{w_{ms}}{p_{ms}}}\right) \quad \text{(for a limited, complex matrix)} \qquad \text{(F-10)}$$

We note here that the subscripts *mf* and *ms* refer to the rock matrix adjacent to the flow channel and that adjacent to the stagnant zone, respectively to allow the possibility of defining differing matrix properties in these zones.

The effective diffusivity, bulk rock density, and bulk solute partitioning coefficient are combined to give a materials property group for each rock type in the system:

$$MPG = \sqrt{D_e K_d^* \rho_b} = \sqrt{D_e\left(\varepsilon_p + K_d\rho_b\right)} \qquad \text{(F-11)}$$

Where, D_e (m^2/s) is the effective diffusivity, ε_p (–) is the rock matrix storage porosity, and ρ_b (kg/m^3) is the bulk density of the rock. The variables K_d^* (m^3/kg) and K_d (m^3/kg) are the bulk and solid partitioning coefficients respectively (noting that the former term accounts for the storage capacity of the water filled porosity).

If the material properties of the rock matrix and stagnant zone and the flow-wetted surface to flow ratio vary along the length of the flowpath this must be accounted for. The flowpath integrated version of Equation F-1 is:

$$\bar{C}_f = \frac{M}{q}\exp\left(-t_w\phi\right)\exp\left(-\int_0^{L_p}\frac{2W(x)}{q(x)}\psi_{mf}(x)\,dx\right)\exp\left(-\int_0^{L_p}\frac{2W(x)}{q(x)}R_s(x)\psi_s(x)dx\right) \quad \text{(F-12)}$$

If the flowpath is discretised into n channels of length, L_c, Equation F-12 can be given as:

$$\bar{C}_f = \frac{M}{q}\exp\left(-\phi\sum_{i=1}^{n}t_{w_i}\right)\exp\left(-\sum_{i=1}^{n}\psi_{mf_i}\frac{FWS_i}{q_i}\right)\exp\left(-\sum_{i=1}^{n}R_{s_i}\psi_{s_i}\frac{FWS_i}{q_i}\right) \quad \text{(F-13)}$$

We note that this is the same result as would be obtained by multiplication of individual flow channel transfer functions along a flow path.

In the case where there are constant material properties and R_s along a flowpath of length L_p, Equation F-12 can be simplified to:

$$\bar{C}_f = \frac{M}{q}\exp\left(-t_w\phi\right)\exp\left(-\left(\psi_{mf}+R_s\psi_s\right)\int_0^{L_p}\frac{2W(x)}{q(x)}\,dx\right) \quad \text{(F-14)}$$

Once again, if the flowpath is discretised into n channels of length, L, we can write Equation F-14 as:

$$\bar{C}_f = \frac{M}{q}\exp\left(-\phi\sum_{i=1}^{n}t_{w_i}\right)\exp\left(-\left(\psi_{mf}+R_s\psi_s\right)\sum_{i=1}^{n}\frac{FWS_i}{q_i}\right) \quad \text{(F-15)}$$

For the case where there is asymmetry in the properties of the stagnant zones, we can write:

$$\bar{C}_f = \frac{M}{q}\exp\left(-t_w\phi\right)\exp\left(-\frac{FWS_c}{q}\left(\psi_{mf}+R_{sA}\psi_{sA}+R_{sB}\psi_{sB}\right)\right) \quad \text{(F-16)}$$

Where, the subscripts A and B refer to each stagnant zone individually.

In a similar fashion, it is also possible to include additional terms to account for the presence of fault gouge, etc. How this is done, of course, depends upon how the fault gouge is conceptualised to occur in the fracture. Below, we consider two limiting cases that may be relevant for solute transport in fractured rock. In the first case (fracture infill scenario 1), the fault gouge is conceptualised to be a separate entity to the rock matrix as indicated in Figure F-3. In the second case (fracture infill scenario 2), the fault gouge lies flush with the fracture surface to one side of the flowpath and can be considered to be part of the rock matrix as shown in Figure F-4. In this case, the two sides of the fracture surface may have asymmetrical matrix properties.

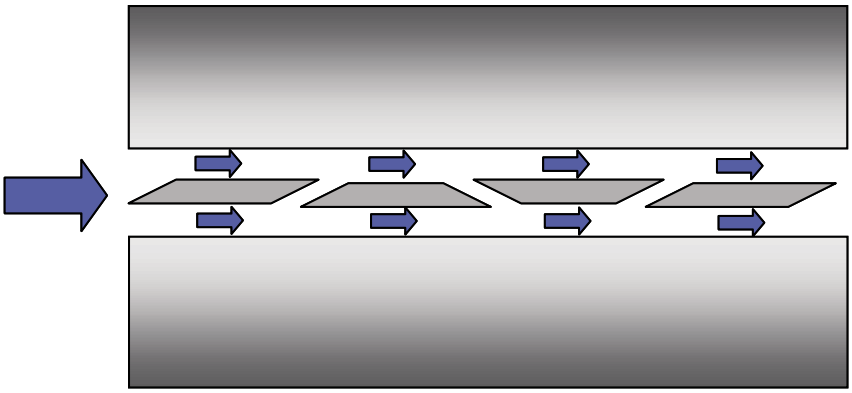

Figure F-3. *Fault gouge lies within flow channel in such a way that flowing water has direct contact with the fracture surface on either side of the rock fracture. The physical description of this system is referred to as fracture infill scenario 1.*

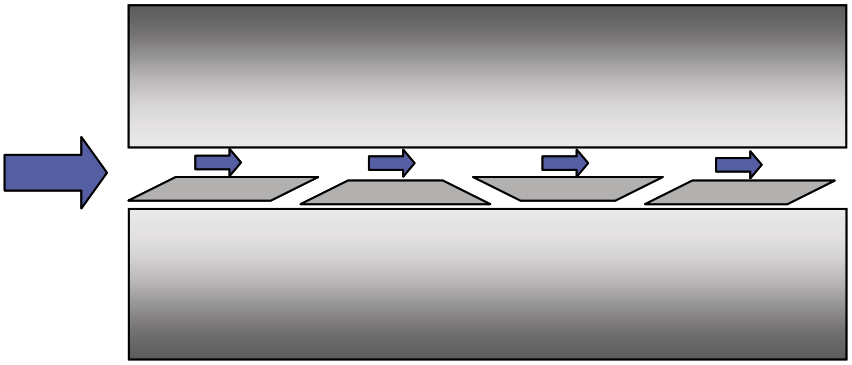

Figure F-4. *Fault gouge lies flush with the rock matrix on one side of the rock fracture. Although shown to cover the entire lower surface of the fracture in the figure, it is not necessary for this to be the case and it is possible for the gouge material to obstruct only a fractional amount of the available flow-wetted surface bounding the rock matrix. The physical description of this system is referred to as fracture infill scenario 2.*

Fracture Infill Scenario 1

For scenario 1, the fault gouge behaves as an extra solute sink and, assuming a slab shape for the gouge, can be included as an additional flux term in Equation F-1:

$$\bar{C}_f = \frac{M}{q}\exp\left(-t_w\phi\right)\exp\left(-\frac{FWS_c}{q}\left(\psi_{mf} + R_s\psi_s + R_g\psi_g\right)\right) \qquad \text{(F-17)}$$

The variable ψ_g is defined by analogy with Equations F-3 to F-5, which for a simple structure of limited extent would give:

$$\psi_g = -MPG_g\sqrt{\phi}\tanh\left(A_g\frac{\delta_g}{2}\sqrt{\phi}\right) \qquad \text{(F-18)}$$

Here, it should be noted that since diffusion is conceptualised to occur from both sides of the gouge pieces simultaneously, the diffusion thickness (i.e. matrix depth) of the gouge slabs is half their geometrical thickness. Although Equation F-18 assumes a simple matrix, it is possible to include a microstructure of arbitrary complexity in the gouge slab using Equation F-5.

By analogy with Equation F-2, the variable R_g is defined as the ratio of gouge flow-wetted surface to the rock matrix flow-wetted surface:

$$R_g = \frac{FWS_g}{FWS_c} \tag{F-19}$$

For sufficiently long residence times, the gouge will become saturated and behave as an equilibrium sink for transported solute. In these cases Equation F-17 can be simplified to:

$$\overline{C}_f = \frac{M}{q}\exp\left(-R_b t_w \phi\right)\exp\left(-\frac{FWS_c}{q}\left(\psi_{mf} + R_s\psi_s\right)\right) \tag{F-20}$$

Where the retardation term, R_b is given by:

$$R_b = 1 + K^*_{dg}\rho_{bg}\left(\frac{\beta_g}{1-\beta_g}\right) \tag{F-21}$$

The parameter, β_g is the void fraction occupied by gouge material in the flow channel volume, while $K^*_{dg}\,\rho_{bg}$ is the dimensionless sorption coefficient for the gouge material (including pore water storage capacity).

In the same way, if the outermost layer of altered rock in the fracture (i.e. the "fracture skin") can also be considered to be in equilibrium, the layer can be relegated to an additional equilibrium retardation term provided the matrix flux term, ψ_{mf} is simultaneously adjusted to reflect this simplification:

$$R_b = 1 + K^*_{dg}\rho_{bg}\left(\frac{\beta_g}{1-\beta_g}\right) + K^*_{dfs}\rho_{bfs}\frac{2\delta_{fs}}{\delta_c} \tag{F-22}$$

Here, the fracture skin thickness is given as δ_{fs}, and $K^*_{dfs}\,\rho_{bfs}$ is the corresponding dimensionless sorption coefficient for the geological material comprising the fracture skin (including pore water storage capacity).

Fracture Infill Scenario 2

For fracture infill scenario 2, we adjust Equation F-1 to get:

$$\overline{C}_f = \frac{M}{q}\exp\left(-t_w\phi\right)\exp\left(-\frac{FWS}{q}\left(\left(1-R_g\right)\psi_{mf} + R_s\psi_s + R_g\psi_{mfg}\right)\right) \tag{F-23}$$

In this case, the term R_g represents the fraction of flow-wetted surface that is occluded by the gouge material. Instead of the term ψ_g describing the gouge material properties, we define instead a function ψ_{mfg} describing the material properties of the rock-matrix with additional layers having the properties of fault gouge. In this case, because diffusion is conceptualised to occur from only one surface of the gouge material, its diffusion thickness is equal to the full geometric thickness of the gouge slabs.

Numerical inversion of the Laplace-space solution

There are a number of different algorithms that can be used for numerical inversion of Laplace-space solutions to obtain a solution in the time domain. In the transport modelling work carried out as part the Laxemar 1.2 site descriptive modelling, the MATLAB programming environment has been used for calculations of solute residence time distribution (RTD's) using code based upon the equations developed in this report. For numerical inversion of the Laplace-space solutions, the algorithm described by /de Hoog et al. 1982/ and implemented in the public domain MATLAB function "invlap.m" /Hollenbeck 1998/ was used.

Derivation of mass transfer flux equations for complex rock matrix microstructures

Given a complex rock matrix microstructure of the kind illustrated in Figure F-2, the mass balance describing instationary diffusion in the rock matrix ($z > 0$, $x > 0$) is:

$$K_d^i \rho_b^i \frac{\partial C_{p(i)}}{\partial t} = D_e^i \frac{\partial^2 C_{p(i)}}{\partial z^2} - \lambda K_d^i \rho_b^i C_{p(i)} \qquad \text{(F-24)}$$

The index i signifies a number of discrete zones ($1 \le i \le n$) with differing material properties making up the rock matrix. The variable λ is the first order decay constant of the transported radionuclide.

The unsteady, differential mass balance equation for the tracer concentration in the channel ($z = 0$, $x > 0$) is given by:

$$2W_c b_c \frac{\partial C_f}{\partial t} + q \frac{\partial C_f}{\partial x} = 2W_c F_{mf} - 2W_c b_c \lambda C_f \qquad \text{(F-25)}$$

For reasons of transparency we do not include a term for uptake into stagnant zones as we intend to simply derive a Laplace-space expression for the matrix flux term, F_{mf}. The corresponding flux term, F_{ms} for uptake from the stagnant zones into the rock matrix can then be derived by analogy. The mass flux from the flow channel into the rock matrix is:

$$F_{mf} = D_e^{(1)} \left. \frac{\partial C_{p(1)}}{\partial z} \right|_{z=0} \qquad \text{(F-26)}$$

Where the effective diffusivity of the matrix layer ($i = 1$) immediately adjacent to the fracture surface is designated $D_e^{(1)}$.

Applying the Laplace transform to Equation F-24 gives:

$$\frac{D_e^i}{K_d^i \rho_b^i} \frac{d^2 \overline{C}_{p(i)}}{dz^2} - (s + \lambda) \overline{C}_{p(i)} + C_{p(i)}^0 = 0 \qquad \text{(F-27)}$$

Similarly, for Equation F-25 we can write:

$$-\frac{q}{2W_c b_c} \frac{\partial \overline{C}_f}{\partial x} + \frac{\overline{F}_{mf}}{b_c} + (s + \lambda) \overline{C}_f + C_f^0 = 0 \qquad \text{(F-28)}$$

The initial conditions of the system are defined to be:

IC1: $C_f = 0$ (z = 0, x > 0, t = 0) (F-29)

IC2: $C_{p(i)} = C^0_{p(i)} = 0$ ($0 < z < \delta_n$, x > 0, t = 0) (F-30)

The boundary conditions for a Dirac δ(t) pulse tracer input are given by:

BC1: $C_f = \frac{M}{q}\delta(t)$ (z = 0, x = 0, t > 0) (F-31)

BC2: $C_{p(1)} = C_f$ (z = 0, x > 0, t > 0) (F-32)

BC3: $C_f = finite$ (z = 0, x = ∞, t > 0) (F-33)

BC4: $C_{p(i)} = C_{p(i+1)}$ ($z = \delta_i$, x > 0, t > 0, ($i < n$)) (F-34)

BC5: $D_e^i \left.\frac{\partial C_{p(i)}}{\partial z}\right|_{\delta_i} = D_e^{i+1} \left.\frac{\partial C_{p(i+1)}}{\partial z}\right|_{\delta_i}$ ($z = \delta_i$, x > 0, t > 0, ($i < n$)) (F-35)

For a matrix of finite depth we have:

BC6A: $D_e^n \left.\frac{\partial C_{p(n)}}{\partial z}\right|_{\delta_m} = 0$ ($z = \delta_n$, x > 0, t > 0) (F-36)

If, on the other hand, the matrix is considered to be infinite we find instead:

BC6B: $C_{p(n)}\Big|_{z=\infty} = 0$ (z = ∞, x > 0, t > 0) (F-37)

The Laplace transforms of the boundary conditions are:

BC1: $\overline{C}_f = \frac{M}{q}$ (z = 0, x = 0) (F-38)

BC2: $\overline{C}_{p(1)} = \overline{C}_f$ (z = 0, x > 0) (F-39)

BC3: $\overline{C}_f = \text{finite}$ (z = 0, x = ∞) (F-40)

BC4: $\overline{C}_{p(i)} = \overline{C}_{p(i+1)}$ ($z = \delta_j$, x > 0, ($i < n$)) (F-41)

BC5: $D_e^i \left.\frac{\partial \overline{C}_{p(i)}}{\partial z}\right|_{\delta_i} = D_e^{i+1} \left.\frac{\partial \overline{C}_{p(i+1)}}{\partial z}\right|_{\delta_i}$ ($z = \delta_i$, x > 0, ($i < n$)) (F-42)

BC6A: $D_e^n \left.\frac{\partial \overline{C}_{p(n)}}{\partial z}\right|_{\delta_m} = 0$ ($z = \delta_n$, x > 0) (F-43)

BC6B: $\overline{C}_{p(n)}\Big|_{z=\infty} = 0$ (z = ∞, x > 0) (F-44)

The general solution to Equation F-27 is:

$$\bar{C}_{p(i)} = \alpha_{1(i)} \exp\left(m_{1(i)} z\right) + \alpha_{2(i)} \exp\left(m_{2(i)} z\right) \tag{F-45}$$

$\alpha_{1(i)}$ and $\alpha_{2(i)}$ are constants of integration and $m_{1(i)}$ and $m_{2(i)}$ are the roots of the eigenvalue equation:

$$m^2 - A_i^2 \left(s + \lambda\right) = 0 \tag{F-46}$$

Where, the variable A_i is defined:

$$A_i = \sqrt{\frac{K_d^i \rho_b^i}{D_e^i}} \tag{F-47}$$

The roots of Equation F-46 are:

$$m = \pm A_i \sqrt{s + \lambda} \tag{F-48}$$

Equation F-45 can thus be written as:

$$\bar{C}_{p(i)} = \alpha_{1(i)} \exp\left(A_i z \sqrt{s + \lambda}\right) + \alpha_{2(i)} \exp\left(-A_i z \sqrt{s + \lambda}\right) \tag{F-49}$$

In order to simplify the problem, we initially assume a limited number of layers and then extend the result to arbitrary n. We also define a materials property group (MPG_i):

$$MPG_i = \sqrt{D_e^i K_d^i \rho_b^i} = D_e^i A_i \tag{F-50}$$

Furthermore, to simplify equations we define:

$$\phi = s + \lambda \tag{F-51}$$

The Laplace transformed flux at the fracture surface is:

$$\bar{F}_{mf} = D_e^{(1)} \left. \frac{\partial \bar{C}_{p(1)}}{\partial z} \right|_{z=0} \tag{F-52}$$

In general, for any number of layers, we can write the flux as:

$$\bar{F}_{mf} = -MPG_1 \sqrt{\phi} \left(\bar{C}_f - 2\alpha_{1(1)}\right) \tag{F-53}$$

We will subsequently also show that the flux can also be given in the form:

$$\bar{F}_{mf} = \psi_{mf} \bar{C}_f \tag{F-54}$$

Using IC1, we can therefore write for the mass balance (Equation F-28) in the mobile water:

$$\frac{\partial \bar{C}_f}{\partial x} = -\frac{2 W_c b_c}{q} \left(\phi + \frac{\Psi_{mf}}{b_c}\right) \bar{C}_f \tag{F-55}$$

This is a first-order, variables separable ODE and (with the help of BC1 and BC3) can be shown to have the solution:

$$\bar{C}_f = \frac{M}{q} \exp\left(-\frac{2 W_c b_c x}{q} \left(\phi + \frac{\psi_{mf}}{b_c}\right)\right) \tag{F-56}$$

Equation F-56 may also be written in terms of the water residence time, t_w and the flow-wetted surface to flow ratio, FWS/q for a flow channel of length L_c:

$$\bar{C}_f = \frac{M}{q}\exp\left(-t_w\phi\right)\exp\left(-\frac{FWS_c}{q}\psi_{mf}\right) \tag{F-58}$$

Where,

$$\frac{FWS_c}{q} = \frac{2W_cL_c}{q} \tag{F-59}$$

$$t_w = \frac{2W_cL_cb_c}{q} \tag{F-60}$$

Mass flux for a single rock matrix layer

Using Equation F-49 we can write in the case of a single rock matrix layer:

$$\bar{C}_{p(1)} = \alpha_{1(1)}\exp\left(A_1z\sqrt{\phi}\right)+\alpha_{2(1)}\exp\left(-A_1z\sqrt{\phi}\right) \tag{F-61}$$

For the boundary at the fracture surface, we have from BC2:

$$\bar{C}_{p(1)}\Big|_{z=0} = \bar{C}_f \tag{F-62}$$

This gives:

$$\bar{C}_f = \alpha_{1(1)} + \alpha_{2(1)} \tag{F-63}$$

For a matrix of limited extent, we have from BC6A:

$$\alpha_{2(1)} = \alpha_{1(1)}\exp\left(2A_1\delta_1\sqrt{\phi}\right) \tag{F-64}$$

Substituting Equation F-63 into F-64 gives:

$$\alpha_{1(1)} = \bar{C}_f\Big/\left(1+\exp\left(2A_1\delta_1\sqrt{\phi}\right)\right) \tag{F-65}$$

Substituting Equation F-64 and F-65 into F-61 gives (with some rearrangement):

$$\bar{C}_{p(1)} = \bar{C}_f\left(\frac{\exp\left(A_1z\sqrt{\phi}\right)+\exp\left(2A_1\delta_1\sqrt{\phi}\right)\exp\left(-A_1z\sqrt{\phi}\right)}{1+\exp\left(2A_1\delta_1\sqrt{\phi}\right)}\right) \tag{F-66}$$

For a matrix of infinite depth, we instead have from BC6B:

$$\alpha_{1(1)} = 0 \tag{F-67}$$

Substituting Equation F-63 and F-67 into F-61 then gives:

$$\bar{C}_{p(1)} = \bar{C}_f\exp\left(-A_1z\sqrt{\phi}\right) \tag{F-68}$$

The flux at the fracture surface is given by:

$$\overline{F}_{mf} = D_e^{(1)} \left. \frac{\partial \overline{C}_{p(1)}}{\partial z} \right|_{z=0} \tag{F-69}$$

The flux is then given by:

$$\overline{F}_{mf} = -\overline{C}_f \psi_{mf} \tag{F-70}$$

Where, for a matrix of finite extent we have:

$$\psi_{mf} = MPG_1 \sqrt{\phi} \tanh\left(A_1 \delta_1 \sqrt{\phi}\right) \tag{F-71}$$

For an infinite matrix, we have instead:

$$\psi_{mf} = MPG_1 \sqrt{\phi} \tag{F-72}$$

It should be noted that Equation F-71 and F-72 are equal in the limit $\delta_1 \rightarrow \infty$.

Mass flux for an arbitrary number of discrete rock matrix layers

For the general case of *n* distinct layers, we can write:

$$\overline{C}_{p(n)} = \alpha_{1(n)} \exp\left(A_n z \sqrt{\phi}\right) + \alpha_{2(4)} \exp\left(-A_n z \sqrt{\phi}\right) \tag{F-73}$$

……

$$\overline{C}_{p(i)} = \alpha_{1(i)} \exp\left(A_i z \sqrt{\phi}\right) + \alpha_{2(i)} \exp\left(-A_i z \sqrt{\phi}\right) \tag{F-74}$$

……

$$\overline{C}_{p(1)} = \alpha_{1(1)} \exp\left(A_1 z \sqrt{\phi}\right) + \alpha_{2(1)} \exp\left(-A_1 z \sqrt{\phi}\right) \tag{F-75}$$

For the given boundary conditions, the problem of finding the coefficients $\alpha_{i(j)}$ to the above system of equations can be formulated in abbreviated array form as:

$$\begin{pmatrix} E_{n,n} & -1 & 0 & . & . & 0 \\ . & . & . & . & . & . \\ . & (1+R_{i,i-1})\sqrt{E_{i,i-1}} & (1-R_{i,i-1})/\sqrt{E_{i,i-1}} & -2\sqrt{E_{i-1,i-1}} & 0 & . \\ . & (1-R_{i,i-1})\sqrt{E_{i,i-1}} & (1+R_{i,i-1})/\sqrt{E_{i,i-1}} & 0 & -2/\sqrt{E_{i-1,i-1}} & . \\ . & . & . & . & . & . \\ 0 & . & . & 0 & 1 & 1 \end{pmatrix} \begin{pmatrix} \alpha_{1,n} \\ \alpha_{2,n} \\ . \\ . \\ \alpha_{11} \\ \alpha_{21} \end{pmatrix} = \begin{pmatrix} 0 \\ 0 \\ . \\ . \\ 0 \\ \overline{C}_f \end{pmatrix} \tag{F-76}$$

Where,

$$R_{ij} = \frac{MPG_i}{MPG_j} \tag{F-77}$$

$$E_{ij} = \exp\left(2 A_i \delta_j \sqrt{\phi}\right) \tag{F-78}$$

The solution for $\alpha_{1(1)}$ is given by a recursive expression. The general solution for a limited matrix can be shown to be:

$$\alpha_{11} = \frac{\bar{C}_f}{1 + \frac{w}{p}} \tag{F-79}$$

Where,

$$\chi_{n,A} = E_{n,n-1}\,(1 + R_{n,n-1}) + E_{n,n}\,(1 - R_{n,n-1}) \tag{F-80}$$

$$\chi_{n,B} = E_{n,n-1}\,(1 - R_{n,n-1}) + E_{n,n}\,(1 + R_{n,n-1}) \tag{F-81}$$

……

$$\chi_{i,A} = E_{i,i-1}\,(1 + R_{i,i-1})\,\chi_{i+1,A} + E_{i,i}\,(1 - R_{i,i-1})\,\chi_{i+1,B} \qquad (2 \le i \le n-1) \tag{F-82}$$

$$\chi_{i,B} = E_{i,i-1}\,(1 - R_{i,i-1})\,\chi_{i+1,A} + E_{i,i}\,(1 + R_{i,i-1})\,\chi_{i+1,B} \qquad (2 \le i \le n-1) \tag{F-83}$$

……

$$w = E_{11}\chi_{2,B} \tag{F-84}$$

and

$$p = \chi_{2,A} \tag{F-85}$$

For the case of an infinite matrix, the corresponding generalised array equation is:

$$\begin{pmatrix}
(1-R_{n,n-1})/\sqrt{E_{n,n-1}} & -2\sqrt{E_{n-1,n-1}} & 0 & . & . & . & 0 & 0 \\
(1+R_{n,n-1})/\sqrt{E_{n,n-1}} & 0 & -2/\sqrt{E_{n-1,n-1}} & 0 & . & . & . & . \\
. & . & . & . & . & . & . & . \\
. & (1+R_{i,i-1})\sqrt{E_{i,i-1}} & (1-R_{i,i-1})/\sqrt{E_{i,i-1}} & -2\sqrt{E_{i-1,i-1}} & 0 & . & . & . \\
. & (1-R_{i,i-1})\sqrt{E_{i,i-1}} & (1+R_{i,i-1})/\sqrt{E_{i,i-1}} & 0 & -2/\sqrt{E_{i-1,i-1}} & . & . & . \\
. & . & . & . & . & . & . & . \\
. & . & . & . & . & . & . & . \\
0 & . & . & . & . & 0 & 1 & 1
\end{pmatrix}
\begin{pmatrix} \alpha_{1,n} \\ \alpha_{2,n} \\ . \\ \alpha_{1,i} \\ \alpha_{2,i} \\ . \\ \alpha_{1,1} \\ \alpha_{2,1} \end{pmatrix}
=
\begin{pmatrix} 0 \\ 0 \\ . \\ 0 \\ 0 \\ . \\ 0 \\ \bar{C}_f \end{pmatrix} \tag{F-86}$$

In a similar fashion, the solution for $\alpha_{1(1)}$ is given by a recursive expression. The general solution for an infinite matrix can be shown to be:

$$\alpha_{11} = \frac{\bar{C}_f}{1 + \frac{w}{p}} \tag{F-87}$$

Where,

$$\chi_{n-1,A} = E_{n-1,n-2}\,(1 + R_{n-1,n-2})\,(1 - \mathrm{R}_{n,n-1}) + E_{n-1,n-1}\,(1 - R_{n-1,n-2})\,(1 + R_{n,n-1}) \tag{F-88}$$

$$\chi_{n-1,A} = E_{n-1,n-2}\,(1 - R_{n-1,n-2})\,(1 - \mathrm{R}_{n,n-1}) + E_{n-1,n-1}\,(1 + R_{n-1,n-2})\,(1 + R_{n,n-1}) \tag{F-89}$$

……

$$\chi_{i,A} = E_{i,i-1}\,(1 + R_{i,i-1})\,\chi_{i+1,A} + E_{i,i}\,(1 + R_{i,i-1})\,\chi_{i+1,B} \qquad (2 \le i \le n-2) \tag{F-90}$$

$$\chi_{i,A} = E_{i,i-1}\,(1 - R_{i,i-1})\,\chi_{i+1,A} + E_{i,i}\,(1 - R_{i,i-1})\,\chi_{i+1,B} \qquad (2 \le i \le n-2) \tag{F-91}$$

……

$$w = E_{11}\chi_{2,B} \tag{F-92}$$

and

$$p = \chi_{2,A} \tag{F-93}$$

For both matrix boundary conditions, the flux is given by:

$$\bar{F}_{mf} = -\bar{C}_f \psi_{mf} \tag{F-94}$$

Where,

$$\psi_{mf} = MPG_1\sqrt{\phi}\left(1 - \frac{1}{1+\frac{w}{p}}\right) \tag{F-95}$$